TECHNISCHE UNIVERSITÄT DARMSTADT

Nek1 - developmental involvement in DNA repair and role as a target in radiotherapy

vom Fachbereich Biologie

der Technischen Universität Darmstadt

zur Erlangung des akademischen Grades eines

Doctor rerum naturalium

(Dr. rer. nat.)

Dissertation von

M. Sc. Isabel Freund

Erstgutachten: Prof. Dr. Markus Löbrich

Zweitgutachten: Prof. Dr. Franz Rödel

Tag der Einreichung: 19.04.2022

Tag der mündlichen Prüfung: 10.06.2022

Darmstadt 2022

Für Papa

Ehrenwörtliche Erklärung

Ich erkläre hiermit ehrenwörtlich, dass ich die vorliegende Arbeit entsprechend den Regeln guter wissenschaftlicher Praxis selbstständig und ohne unzulässige Hilfe Dritter angefertigt habe. Sämtliche aus fremden Quellen direkt oder indirekt übernommenen Gedanken sowie sämtliche von Anderen direkt oder indirekt übernommenen Daten, Techniken und Materialien sind als solche kenntlich gemacht. Die Arbeit wurde bisher bei keiner anderen Hochschule zu Prüfungszwecken eingereicht. Die eingereichte elektronische Version stimmt mit der schriftlichen Version überein.

Darmstadt, den 19.04.2022

Isabel Freund

Zusammenfassung

Organismen sind unweigerlich ionisierender Strahlung (engl. *Ionizing Radiation*, IR) ausgesetzt, die von verschiedenen natürlichen Quellen wie beispielsweise zerfallenden Radionukliden emittiert wird. Seit ihrer Entdeckung im 19. Jahrhundert ist die IR vor allem in der Medizin für diagnostische und therapeutische Verfahren zu einem äußerst wichtigen Instrument geworden. Ihre Eigenschaft, chemische Strukturen und Bindungen in der bestrahlten Materie aufzubrechen, bedroht jedoch die Integrität eines besonderen Moleküls, das die Grundvoraussetzung für die Lebensfähigkeit eines jeden Organismus darstellt, die DNA. Eine Strahlenexposition der DNA führt zu verschiedenen Arten von Schäden, von denen der Doppelstrangbruch (DSB) die schwerwiegendste Läsion darstellt. Da DSBs auch als Folge verschiedener endogener Prozesse entstehen können, haben Zellen verschiedene Mechanismen entwickelt, um die schädlichen Auswirkungen dieser Läsion auf ihre genomische Integrität zu minimieren. Diese DNA-Schadensantwort (engl. *DNA damage response*, DDR) besteht aus koordinierten Signalwegen, die Schadenserkennung, Unterbrechung des Zellzyklus und Reparatur der DNA ermöglichen.

Die Mitglieder der *never in mitosis-gene A (NIMA) related kinase* (Nek)-Familie wurden ursprünglich für ihre Beteiligung in der Ciliogenese, der Zentrosomenorganisation und der Mitose untersucht, rücken jedoch zunehmend in den Fokus der DDR-Forschung, da fast alle eine Schlüsselrolle in entsprechenden Prozessen spielen. Ein Mitglied, Nek1, sticht in diesem Zusammenhang aufgrund seiner multifunktionalen Aufgaben in der DDR (Regulierung von Zellzyklus-Checkpoints, Apoptose und DNA-Reparatur) hervor. In der folgenden Arbeit werden die Ergebnisse zweier Projekte vorgestellt, die jeweils einen anderen Aspekt von Nek1 als wichtige Kinase der DNA-Schadensantwort beleuchten.

Das erste Projekt basiert auf Forschungsarbeiten der AG Löbrich, in denen Nek1 als Regulator eines Faktors identifiziert wurde, der für die erfolgreiche Durchführung des DSB-Reparatur-weges "Homologe Rekombination" (HR) essentiell ist, Rad54. Nachfolgende *in vivo* Studien ergaben das überraschende Ergebnis, dass Nek1 zwar für die HR in adulten Mäusen von Bedeutung ist, nicht aber für Embryonen, die trotz Knock-Out-Mutation im Nek1-Gen ein normales Reparaturverhalten aufweisen. Das Hauptziel dieses Teilprojekts der vorgelegten Arbeit war es daher, die offensichtlich unterschiedliche Regulierung der HR während der murinen Entwicklung weiter zu charakterisieren. Zu diesem Zweck wurden embryonale und adulte Fibroblastenlinien aus verschiedenen Mausstämmen isoliert und im Hinblick auf DSB-Reparatur sowie Genexpression analysiert. Die gesammelten Daten deuten darauf hin, dass sich die Kinasen, die für die Aktivierung von Rad54 erforderlich sind, tatsächlich in Abhängigkeit vom Entwicklungsstadium eines Organismus ändern: Nek1 kontrolliert die Aktivierung von Rad54 ausschließlich in adulten Zellen, während Nek3 und Nek5 Rad54 in embryonalen Zellen redundant aktivieren können. Diese Studie konsolidiert also nicht nur

frühere Ergebnisse der AG Löbrich, sondern ist vielmehr die erste, die über eine entwicklungsbedingte Veränderung in der Regulierung der HR berichtet und Nek3 sowie Nek5 mit der DNA-Reparatur in Verbindung bringt.

In Anbetracht seiner Multifunktionalität in der DDR besitzt die pharmakologische Inaktivierung von Nek1 das Potenzial, die Behandlung von Krebs durch z.B. eine Strahlentherapie deutlich zu verbessern. Die AG Rödel bestätigte diese Annahme, indem sie nachwies, dass die Depletion von Nek1 zwei verschiedene Krebszelllinien signifikant für Einzeldosenbestrahlung sensibilisiert, was sich in einer verminderten Fähigkeit zur Koloniebildung äußerte. Da weitere Experimente zeigten, dass Nek1-depletierte Krebszellen einen funktionsfähigen G2/M-Kontrollpunkt induzieren können, untersuchte das zweite Projekt dieser Arbeit, inwiefern eine fraktionierte Bestrahlung die Strahlen-sensitivierende Wirkung eines Nek1-Verlusts verstärken kann. Krebszellen wurden daher drei fraktionierten Bestrahlungsschemata unterzogen, bei denen eine Gesamtdosis von 6 Gy in drei kleinen Fraktionen entweder alle 2 h, 6 h oder 24 h verabreicht wurde. Die Analyse des Zellzyklusverhalten und des klonogenen Überlebens ergab, dass das 6 h Intervall tatsächlich die Radiosensitivität von Nek1-depletierten Zellen über das bei Einzeldosen beobachtete Maß hinaus erhöhte, während Nek1-profiziente Zellen weniger betroffen waren. Dieses Ergebnis konnte in *in vivo* Xenotransplantationsstudien zusätzlich bestätigt werden. Insgesamt konsolidiert dieses Teilprojekt Nek1 als vielversprechendes Ziel in der Krebstherapie. Sie zeigt darüber hinaus, dass die Wirksamkeit einer fraktionierten Strahlentherapie deutlich erhöht werden kann, wenn das verwendete Bestrahlungsintervall an die Zyklusrate der Krebszellen angepasst ist und die zellzyklusabhängige Funktion von Nek1 als HR-Faktor berücksichtigt wird.

Summary

Organisms are inevitably exposed to ionizing radiation (IR) which is emitted by various natural sources such as decaying radionuclides. Since its discovery in the 19th century, IR has become a highly relevant tool, especially in the field of medicine where it is used for diagnostic procedures and the treatment of tumors. However, its property to alter the structure of the exposed matter by breaking chemical bonds threatens the integrity of an important molecule that presents the fundamental prerequisite of life, namely DNA. Exposing DNA to IR results in different types of lesions of which the DNA double-strand break (DSB) represents the most detrimental. Since DSBs can also result from several endogenous processes, cells evolved certain mechanisms to minimize the harmful impact of this lesion on their genomic integrity, collectively termed DNA damage response (DDR). The DDR consists of highly coordinated signaling pathways that allow for damage detection, cell cycle arrest, and damage repair.

While originally studied for their involvement in ciliogenesis, centrosome organization, and mitosis, the members of the never-in mitosis-gene A (NIMA) related kinase (Nek) family increasingly move into the focus of DDR research as nearly all have functions in related processes. However, one member, Nek1, stands out in this context due to its multifunctional role in the DDR, including the regulation of cell cycle checkpoints, apoptosis, and DNA repair. In the following work, the results of two projects are presented, each highlighting a different aspect of Nek1 as an important kinase of the DNA damage response.

The first project is based on research conducted by the Löbrich lab, which identified Nek1 as a regulator of a factor required for the successful execution of the DSB repair pathway "Homologous Recombination" (HR), namely Rad54. Subsequent *in vivo* studies surprisingly revealed that Nek1 is important for HR in adult mice but not in embryos, which exhibit a normal repair behavior despite a Knock-Out mutation in the Nek1 gene. The objective of this project was therefore to further characterize the apparent differential regulation of HR during development. To this end, embryonic and adult fibroblast lines were isolated from different mice strains and analyzed for DSB repair and differences in gene expression. The collected data suggest that the kinases required for the activation of Rad54 indeed change in response to an organism’s developmental stage: Nek1 exclusively controls Rad54’s activation in adult cells whereas Nek3 and Nek5 can redundantly activate Rad54 in embryonic cells. Thus, this study not only consolidates previous findings of the Löbrich lab but is also the first to report a developmental change in the regulation of HR and to associate Nek3 and Nek5 with DNA repair.

Considering its multifunctionality in the DDR, pharmacological inactivation of Nek1 has the potential to significantly improve the treatment of cancer by e.g. radiotherapy. The Rödel lab confirmed this assumption by demonstrating that depleting Nek1 significantly sensitizes two different cancer cell lines to single-dose irradiation as shown by their reduced ability to form

colonies. Since further experiments revealed that Nek1-depleted cancer cells are still capable of inducing a functional G2/M checkpoint, the second project of this work investigated the extent to which fractionated irradiation can enhance the radiosensitizing effect of Nek1 depletion. Cancer cells were therefore subjected to three fractionation regimes, in which a total radiation dose of 6 Gy was applied in three small fractions either every 2 h, 6 h, or 24 h, and evaluated for cell cycle behavior as well as colony-forming ability. Indeed, the 6 h interval tremendously increases the radiosensitivity of Nek1-depleted cells beyond the level observed for single-dose irradiations while Nek1-proficient cells are less affected. This finding has been additionally strengthened in *in vivo* xenograft studies. Taken together, this work strengthens Nek1 as a promising target in cancer therapy. It further demonstrates that the efficacy of fractionated radiotherapy can be significantly increased if the employed regime is adapted to the cycle rate of cancer cells and takes the cell cycle-dependent function of Nek1 as an HR factor into account.

Table of Contents

1 Introduction

1.1 Ionizing Radiation: friend and foe

Organisms are inevitably exposed to ionizing radiation (IR), which is emitted by various natural sources including the sun, outer space, and decaying terrestrial radionuclides such as uranium-238 or radon-222.[1,2] It generally comprises any form of electromagnetic waves (γ-, X-rays) or particles (α- and β- particles, neutrons, heavy ions, etc.) that have energies high enough to release electrons from atoms and, thus, ionize molecules.[3] The consequent loss of electrons in the exposed matter results in chemical alterations and irreversible damages.

In organisms, the most important molecule threatened by IR exposure is the DNA.[4] By providing the genetic code for the production of thousands of different proteins that interact with each other and the environment, it is the fundamental prerequisite for the development and functionality of organisms.[5] IR can damage DNA either indirectly, e.g., through the radiolysis of cellular water yielding reactive oxygen species (ROS), or directly through the ionization of atoms in the DNA (Fig. 1). 1 Gy of X-rays, for example, induces thousand DNA lesions ranging from base oxidization to breakages of the DNA backbone.[4,6] The accumulation of such damages can eventually cause mutations and chromosomal rearrangements leading to malignancies or cell death.[3,7]

Since its discovery in the late 19th century, radiation became exploitable for human purposes and advanced into a highly relevant tool, especially in the field of medicine.[8,9] Low doses of IR are frequently applied to patients during diagnostic procedures, e.g., CT scans, and range from 15 mGy for an abdominal to 60 mGy for a head image.[10] While the DNA damaging properties of radiation make the use of IR-related diagnostics potentially risky for patients, they provide the basis for highly effective treatment of almost all types of solid tumors using radiotherapy.[11,12] Depending on the entity, tumors are typically irradiated with doses of 40-70 Gy which are applied in small, daily fractions of 1-3 Gy over several weeks to minimize IR-mediated complications in normal, tumor-surrounding tissues while facilitating tumor DNA disruption and consequential cell death.[12–14]

1.2 The DNA damage response

In terms of mutation induction and lethality, the DNA double-strand break (DSB) constitutes the most serious consequence of exposure to IR. DSBs can also be caused by numerous chemical agents, e.g., chemotherapeutics (camptothecin, doxorubicin, etc.) and pollutants present in car exhaust gases or cigarette smoke (furan, benzene, etc.).[15,16]

In addition to these exogenous factors, a variety of endogenous, hence physiological processes contributes to the formation of DSBs including the general cellular metabolism, which often produces DNA-modifying byproducts such as ROS, aldehydes, or alkylating metabolites. The majority of endogenous DSBs, however, arise during genome replication,

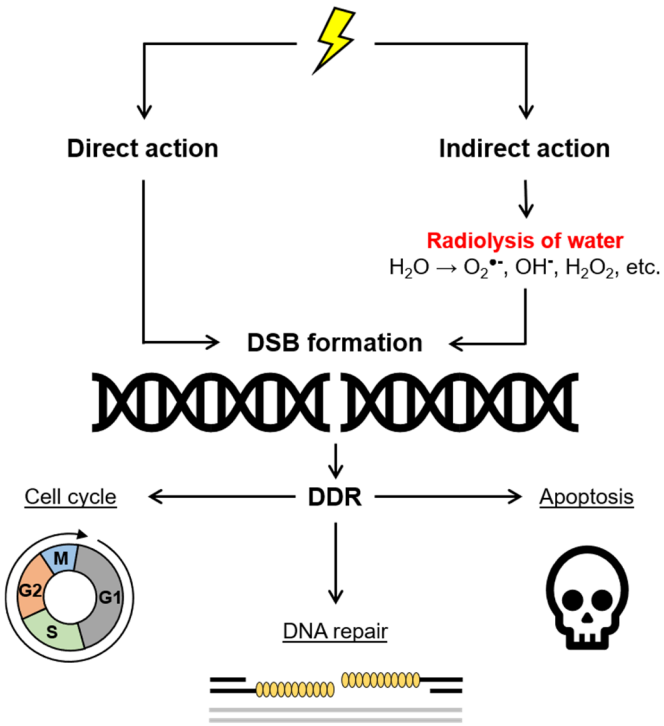

Fig. 1 Schematic representation of IR-mediated DSB induction and the compartments of the DNA damage response. IR (yellow flash) induces double-strand breaks (DSB) either directly (left) or indirectly by the production of reactive oxygen species (right) such as superoxide anions ($O_2^{\bullet-}$), hydroxyl ions (OH^-) or hydrogen peroxide (H_2O_2). The DNA damage response (DDR) subsequently reacts to this lesion by activating cell cycle checkpoints, DNA repair and, if necessary, cellular death by apoptosis. Modified according to [17].

when for example pre-existing DNA modifications (e.g., oxidized bases), lesions (e.g., single-strand breaks), or transcription complexes collide with the replication machinery (referred to as 'replicative stress') and eventually cause it to collapse.[17] Moreover, DSBs can be transiently induced for example by topoisomerase IIb to unwind or "smooth" the topological structure of DNA ahead of the replication machinery.[18] Other factors involved e.g., in meiosis or the V(D)J recombination purposely induce DSBs to enable genome or antibody diversification, respectively.[19,20]

Due to the persistent confrontation with DSBs, cells evolved various mechanisms to minimize the harmful impact of this lesion on the DNA and, thus, sustain their genomic integrity. This so-called DNA damage response (DDR) consists of highly coordinated processes allowing for damage detection, cell cycle arrest, and damage repair (Fig. 1).[20,21] When damages remain unrepaired and consequently accumulate, cells can induce their death in a controlled manner by activating caspases via intrinsic (p53-mediated) or extrinsic (death receptor-mediated) apoptosis pathways.[22,23]

1.2.1 From DSB detection to cell cycle arrest

Once generated, DSBs are immediately recognized by the MRN protein complex consisting of Mre11, Rad50, and Nbs1. The MRN complex captures the free ends of the DSB, recruits the

serine/threonine kinase ATM to the break site, and facilitates its activation through autophosphorylation.[24,25] ATM subsequently transduces the DSB-induced signaling to effector proteins also responsible for cell cycle regulation. The cell cycle consists of four distinct phases in which a proliferating cell accumulates nutrients (G1 phase), replicates its DNA (S phase), prepares for division (G2 phase), and eventually divides into two daughter cells (mitosis).[26] When experiencing DSBs, cells can stop their cell cycle progression by the induction of so-called checkpoints at the G1/S or G2/M transitions. This is not only important to prevent DSBs from interfering with replication during S-phase or chromosomal segregation in mitosis but also to provide a sufficient time window for DSB repair.[27] The process of cell cycle arrest is initiated by ATM phosphorylating both, Chk2 and the transcription factor p53.[26]

To halt cellular proliferation at the G1/S checkpoint, activated Chk2 mediates the translocation of the phosphatase Cdc25a to the cytoplasm and, thus, prevents the activation of the cyclin E/Cdk2 complex by Cdc25a-dependent dephosphorylation in the nucleus.[28] At the same time, p53 increases the production of the Cdk inhibitor p21 which binds to the protein complexes CyclinD/Cdk4/6 and eventually suppresses their activity.[29]

The G2/M checkpoint is initiated quite similarly through Chk2-dependent transport of Cdc25c, which prevents CyclinB1/Cdk1 activation, and through p53-mediated production of p21 inhibiting CyclinB1/Cdk1.[28,29]

In response to a high accumulation of DSBs, cells may additionally slow down or even stop the replication process in S phase to avoid collisions of the replication machinery with lesion sites and consequential DNA damages due to increased replication stress.[30] This intra-S checkpoint is induced independently of the MRN complex and depends on the sensing properties of ATRIP. In detail, when the replication machinery encounters a DSB site, the associated polymerase is forced to stop while involved helicases continue to unwind the DNA ahead of the DSB leading to long stretches of single-stranded DNA. These areas are subsequently bound by RPA to prevent their nucleolytic degradation and then recognized by ATRIP which recruits the serine/threonine kinase ATR and facilitates its activation. ATR eventually forwards the signaling to Chk1 that inhibits the Cdc25a-dependent activation of the cyclin E/Cdk2 complex.[31]

1.2.2 DSB repair

The elimination of DSBs is initiated by ATM-dependent phosphorylation of the histone variant H2AX forming the so-called γH2AX. γH2AX is subsequently bound by Mdc1 thereby inducing a positive feedback loop.[32] This triggers the extension of H2AX phosphorylation to a region of several Mbp around the break site through the repeated recruitment of the MRN complex and ATM. In this way, γH2AX labels the break site and promotes the precise recruitment of numerous repair factors.[33,34]

The subsequent repair of DSBs is accomplished by two pathways: Non-Homologous End-

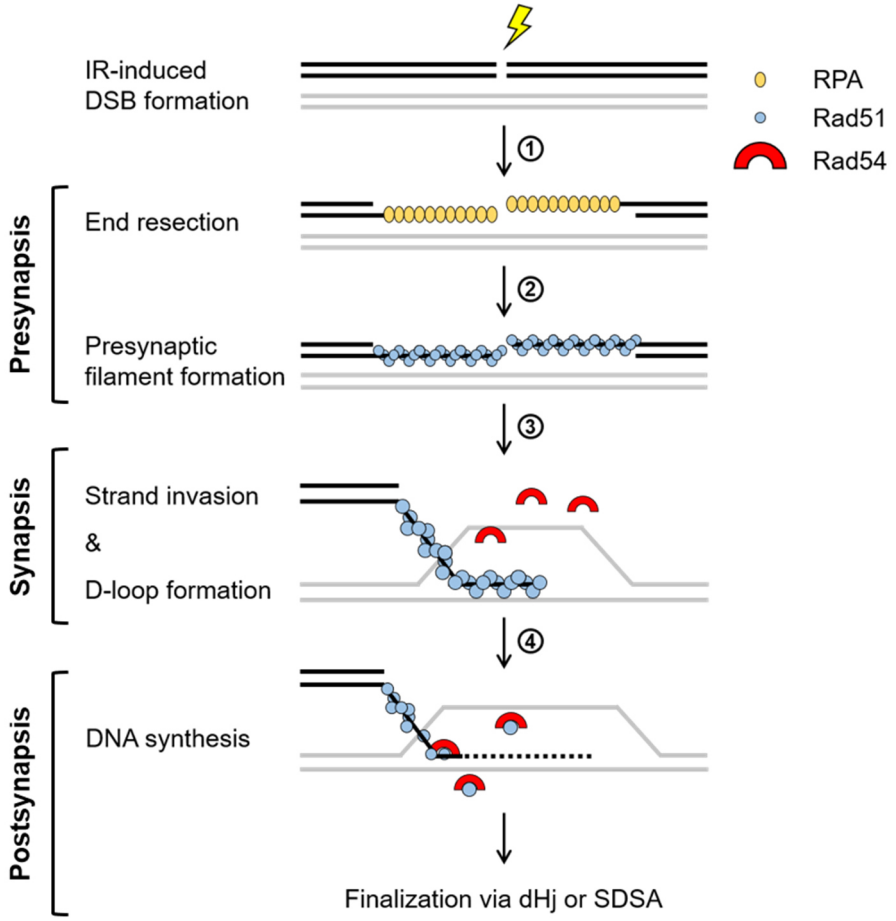

Fig. 2 Simplified overview of the early steps of the Homologous Recombination (HR) pathway. 1 Following IR-induced DSB formation, break ends are resected and the resulting single-stranded overhangs are coated with RPA to prevent nucleolytic degradation. **2** RPA is then replaced by Rad51 forming the presynaptic filament which searches for homologous regions on the sister chromatid (grey). **3** The identification of respective regions triggers strand invasion and the formation of a D-loop structure in the invaded strand. **4** With the successful alignment of homologous sequences in the invading and the invaded strands, Rad51 is removed from the DNA by Rad54 allowing for DNA synthesis. HR is then finalized either through the double Holliday junction subpathway (dHj) or through synthesis-dependent strand annealing (SDSA). Modified according to [33].

Joining or Homologous Recombination (HR).[35]

NHEJ is the most prominent DSB repair pathway in mammalian cells and responsible for the elimination of around 80% of X-ray-induced DSBs. It facilitates a fast DSB repair in all cell cycle phases and comprises only a few reactions that eventually mediate the direct re-ligation of the DSB ends.[36] The mechanism relies on several factors including Ku70/80 and DNA-PKcs protecting and tethering the break ends, nucleases such as CtIP or Artemis for the resection of uneven break ends, and the Xrcc4/LigIV complex that finally joins the break ends.[37] Due to the combination of end processing and ligation, NHEJ may contribute to the loss of genetic material and is therefore considered error-prone.

Of more interest for the following studies, however, is the DSB repair by HR (Fig. 2). This pathway depends on the availability of a sister chromatid that allows for the accurate retrieval

of the damaged region at the DSB site from a homologous sequence.[38] Unlike NHEJ, it is therefore only applicable in the late S and G2 phase when the DNA has already been duplicated and a sister chromatid is available.[39] The HR mechanism provides a high-fidelity process for the error-free repair of DSBs and consists of three steps, namely presynapsis, synapsis, and postsynapsis.[40] During presynapsis, the 3' ends of the DSB are processed by MRN-CtIP-Brca1-mediated nucleolytic degradation.[41] This resection process is then accelerated by Exo1, Blm, and DNA2 generating long single-stranded DNA (ssDNA) overhangs of more than 1000 bps.[42] These 3' ssDNA regions are immediately coated by RPA to avoid nucleolytic degradation or the formation of secondary structures.[43] Subsequently, Rad52, and Brca2 mediate the formation of the presynaptic nucleoprotein filament by replacing RPA with Rad51 and, thus, initiate the synapsis step of the HR pathway.[44] Once generated, the nucleoprotein filament searches for homologous regions on the undamaged sister chromatid and, when found, invades the respective DNA strand while promoting the formation of a D-loop structure in the invaded strand.[45] The resulting synaptic complex is stabilized by Rad54, an ATPase with translocase activity, which associates with Rad51 and ensures the correct alignment of nucleoprotein filament and sister strand by preventing base mispairing. Following proper alignment to the homologous sequence, Rad54 dissociates, and concurrently removes Rad51 from the DNA thereby transforming the synaptic complex into a joint heteroduplex DNA molecule.[46–50] During the postsynaptic stage of HR, PCNA is loaded onto the heteroduplex DNA molecule and recruits DNA polymerase δ that, supported by the helicase Pif1, drives DNA synthesis and amplifies the invading DNA strand using the invaded sequence as template.[51,52]

The process of HR can then be finalized by two mechanistically different subpathways, namely the double Holliday junction (dHj) model or synthesis-dependent strand annealing.[53]

The dHj model is characterized by a process mainly referred to as 'second end capture' in which the second DSB end is annealed to the invading strand within the D-loop. The resulting DNA intermediate is joined by two Holliday junctions and eventually resolved by nuclease-mediated incisions that can occur along or across the direction of DNA synthesis leading to non-crossover products or crossover recombinants, respectively.[54]

During SDSA, however, the elongated invading strand is simply displaced from the D-loop by specific helicases and reannealed with its complementary end at the DSB. Since, in contrast to the dHj model, no cleavable DNA intermediates are formed, this mechanism strictly results in non-crossover products.[55]

1.3 The Nek kinase family

The initiation and progression of DDR pathways strongly depend on the function of protein kinases, which transduce stressor-induced signals to effector proteins and thus not only coordinate but also specify the nature of the cellular response to damaged DNA.[56] Next to

already established kinase families such as the phosphatidylinositol 3-kinase-related kinases (PIKKs, e.g., ATM or ATR) and Cdks, the never in mitosis-gene A (NIMA) related kinase (Nek)-family currently emerges as modulators of various DDR processes.

1.3.1 Structure and function

The mammalian Nek family of serine/threonine kinases comprises a total of 11 genes, named *nek1-nek11*, and has been founded based on their homology to the NIMA gene of the fungus *Aspergillus nidulans*.[57,58] Although *nimA* has been widely considered the "ancestral" gene version of the mammalian *neks*, an extensive phylogenetic analysis performed by Parker *et al*. suggests otherwise.[59] The authors propose that, although there is orthology to *nimA*, the Nek genes rather evolved from five distinct genes expressed in the last common ancestor of all metazoan species and, through expansion, diversified in mammals into five subfamilies of paralogs: *nek1*/*3*/*5*, *nek2*, *nek4*/*11*, *nek6*/*7* and *nek8*/*9*. The overall sequence homology between the corresponding kinases is therefore relatively low.[60]

While the N-terminally, in the case of Nek10 more centrally, located kinase domains are highly conserved, Neks strongly differ in the structural composition of their C-termini (Fig. 3).[58] Nek1, 2, 9, 10, and 11 harbor both, coiled-coil domains for protein interactions and PEST sequences for proteasomal degradation. Although equipped with a long C-terminus, none of the aforementioned motifs exist in Nek4. Unique features are present in the sequences of Nek5 (DEAD-box helicase-like domain), Nek8 and Nek9 (Rcc1-like domain), as well as Nek10 (N-terminally located armadillo repeats). Nek6 and Nek7 miss a complex C-terminal region and instead have an N-terminally located short unfolded interaction segment probably needed for protein-protein interaction.[61,62]

Given their structural diversity and complexity, it is not surprising that the Nek family members play a predominant role in more than one cellular process. Although only a few direct substrates have been identified so far, all Neks are involved to some extent in primary cilia formation, cell cycle regulation, microtubule/centrosome organization, and/or mitosis.[63] More importantly though, evidence for the dependency of several DDR processes on the activity of Nek kinases, e.g., checkpoint induction, DNA repair, or apoptosis, has been growing in recent years.[56,64] For example, Nek4 has been described to function in the DNA repair pathway NHEJ as scaffold protein stabilizing the DNA-PKcs/Ku70/89 complex, and Nek11 seems to stop the cellular progression at the G1/S checkpoint like Chk2 by inducing the transport of Cdc25a to the cytoplasm in response to genotoxic stress.[65,66] As a consequence of their extensive functions, deregulated Nek variants are connected to various ciliopathies, degenerative diseases, and cancers.[67] Table 1 provides an overview of the established functions of Nek2 - Nek11 and diseases associated with deregulated Nek variants. As the main topic of this thesis, Nek1 will be introduced in more detail in the next section.

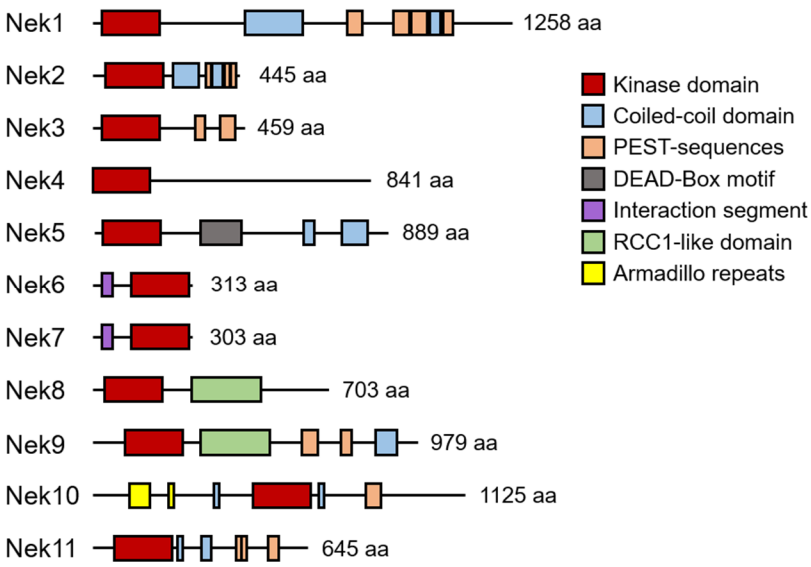

Fig. 3 Schematic presentation of the Nek family members. Nek kinases are characterized by their heterogenous composition, especially regarding their C-terminus. Although the kinase domain (Red) is conserved, Neks display coiled-coil domains (Blue) or interaction segments (Purple) or Armadillo repeats (Yellow) for protein interaction, PEST-sequences (Orange) for degradation, DEAD-Box motifs (Grey) for RNA interaction and RCC1-like domains (Green) for chromatin binding to varying degrees. Modified according to [59].

1.3.2 Nek1

As the name implies, Nek1 is the first identified mammalian NIMA ortholog and was discovered in 1992 by Letwin *et al*. during a mouse cDNA library screen.[68] Its structure stands out through an increased accumulation of C-terminal coiled-coil domains and PEST sequences, making Nek1 the largest representative of the Nek family.[69] Based on its homology to NIMA, which is indispensable for mitosis in *A. nidulans*, initial functional studies focused on the possible participation of Nek1 in the regulation of the cell cycle.[57,70] However, the current state of research summarized below suggests that Nek1, like the other Neks, exerts functions far beyond those described for NIMA.

1.3.2.1 Nek1 is essential for early development

Soon after the discovery of Nek1, researchers at The Jackson Laboratory reported the appearance of a C57/B6 mouse strain with a severe pleiotropic phenotype manifesting around 14 days after birth.[72] High-resolution mapping and sequencing techniques eventually identified a spontaneous single-base insertion in the Nek1 gene on chromosome 8 that triggers a frameshift mutation and, thus, the formation of a premature stop codon.[72,73] The resulting Nek1 deficiency in these so-called kat2j mice is associated with male sterility, female fertility reduction, and premature lethality caused by numerous developmental disorders including hydrocephalus, dwarfism, facial dysmorphia, anemia, and polycystic kidney disease (PKD).[72,74] A complete loss of Nek1 in humans is considered embryonic lethal and has only been observed

Tab. 1 Interactors, functions and associated diseases of Nek2-Nek11[58,60,64,67,71]

	Interactors; pathways	Functions	Diseases
Nek2	EHZ2, USP7, CDK4, TRF1, PP1, p53; PP1/AKT/ NFκB pathway, WNT pathway	Maintaining centrosome and chromosome integrity, cell cycle control, regulation of apoptosis, putative role in RNA splicing processes	Left-right (LR) asymmetry, retinis pigmentosa, multiple cancer entities
Nek3	SNAP29, VAV2, PRLR, RhoGDI2, putative interactions with PCNA and other proteins functioning in transcription, DNA repair, RNA processing, proliferation, invasiveness, and metastasis*; Prolactin signaling pathway	Regulation of myogenic differentiation, regulation of microtubule organization	Muscular phosphorylase kinase deficiency, glycogen storage disease, breast, and gastric cancer
Nek4	RPGRIP1, RPGRIP1L, DNA-PKcs/KU70/80, putative interactions with PCNA and other proteins functioning in NHEJ or HR processes*; TRAIL apoptotic pathway	Ciliogenesis, stabilization of microtubule, regulation of apoptosis, DNA repair (NHEJ), putative role in RNA splicing processes	Ciliopathy, Rhyns Syndrome, lung, colon, and colorectal cancer
Nek5	TOPOIIβ, BCLAF1, Cyclin A2, Cyclin B1, Caspase-3	Regulation of myogenic differentiation, maintenance of centrosome integrity, protection from replication stress, cell cycle control, regulation of apoptosis	Amyotrophic lateral sclerosis, primary autosomal recessive microcephaly, breast and prostate cancer
Nek6	ACD, CDK7, DDR1, HSP70, KIF20A, NMDAR1, NUP98, p70S6K, Rb-like 2, SGK1, STAT3, NEK9, CHK1, CHK2, CDC42, SMAD4, HIF-1α, RAD26L, TRIP4; TGF-β pathway	Cell cycle control, regulation of apoptosis, putative driver of invasion and angiogenesis	Ulcerative colitis, retinoblastoma, and multiple other cancer entities
Nek7	KIF7/EG5, KIF14, NEK9, TRF1, RAD50, RGS2, WHSC1, UNC45A, NLRP3	Maintaining telomere integrity, organization of microtubule and centrosomes, regulation of neuronal differentiation,	NLRP3-related diseases, e.g., systemic lupus erythematosus and another inflammatory, autoimmune or neuronal disorders, multiple cancers
Nek8	ATR/ATRIP, CDK, RAD51, ANKS6; HIF pathway	Ciliogenesis, protection from replication stress, cell cycle control, regulation of apoptosis	Antenatal cystic kidney disease, nephronophthisis, Renal-Hepatic-Pancreatic dysplasia hypertrophic cardiomyopathy, gastric cancer
Nek9	NEDD1, NEK6, NEK7, CHK1, putative interactions with RFC3 and other proteins functioning in DNA repair or replication*	Cell cycle control, organization of microtubules, centrosomes, and the mitotic spindle	Skeletal dysplasia, Nevus Comedonicus, multiple cancer entities
Nek10	RAF1, MEK1/2, ERK1/2, PKA, PCM1, p53, putative interactions with ATRX and other proteins functioning in DDR pathways*; cAMP pathway	Ciliogenesis, cell cycle control, regulation of apoptosis, DNA repair (NHEJ)	Primary ciliary dyskinesia, melanoma, and breast cancer
Nek11	CDC25A, CHK1; p53 apoptotic pathway	Cell cycle control, regulation of apoptosis	Ketotic hypoglycemia, colorectal and ovarian cancer

* Putative interactors have been identified using yeast two-hybrid assays.

in aborted fetuses with a severe form of the Majewski Syndrome (SRPS, Type Majewski), which exhibits a phenotype similar to kat2j mice comprising skeletal dysplasia, underdeveloped organs, and polycystic kidneys.[75] However, two cases of the Mohr-Claussen Syndrome (MCS) with milder phenotypes (still alive, oral and facial abnormalities) have been connected to reduced Nek1 protein levels mediated through a heterozygous mutation that prevents correct transcript splicing.[76]

PKD, SRPS, and MCS do not only share a Nek1 deficiency but also dysfunctional primary cilia, which is why these conditions are assigned to the ciliopathies.[77–79] The primary cilium is a thin, microtubule-based organelle that protrudes from the surface of most mammalian cells.[80] As a chemo- and mechanosensitive cellular compartment, it detects external stimuli and accordingly coordinates tissue development and homeostasis, e.g., proliferation, migration, differentiation, through pathways including Hedgehog, Notch, Wnt, Hippo, or PDGF.[81] In proliferating cells, the cilium forms in a cell cycle-dependent manner meaning that it assembles after mitosis in G1, remains during S/G2, and finally disassembles before mitosis.[80,81] This process, called ciliogenesis, is strongly impaired in cells from kat2j mice, SRPS, and MCS patients which display either shortened cilia or reduced numbers of this organelle.[75,76,82,83]

A causal link between Nek1 and ciliary integrity has been initially made by the Kobarg lab that identified factors with established functions in ciliogenesis and with associations to PKD such as Kif3A and tuberin as interactors of Nek1.[84–86] Further studies revealed that Nek1 locates to cilia in WT cells and is crucial for their elongation as shown by disrupted cilia assembly in Nek1-deficient cells.[82,87] In this context, Cep104 has been shown to promote the extension of ciliary microtubule in a Nek1-dependent manner by recruiting tuberin.[88] Moreover, Nek1 turned out to protect proper ciliary signaling through the regulation of a negative feedback loop that controls the abundance of PC-2, a ciliary transmembrane calcium channel.[89] A physiologic level of PC-2 is maintained by Taz which requires to be phosphorylated by Nek1 to form a complex with the E3 ligase. This complex subsequently catalyzes the ubiquitination and, thus, degradation of PC-2. In Nek1- deficient cells, PC-2 levels are drastically increased and this is considered to provoke not only severe cystogenesis in kat2j mice and SRPS patients but also defects in neuronal development. [90,91]

Nek1 also contributes to gametogenesis through its involvement during meiosis in which paired parental chromosomes are recombined and shuffled to generate diversified genetic material.[92] Spermatocytes and oocytes from kat2j mice have been observed to develop elongated or multipolar spindles and, thus, fail to properly align chromosomes before their segregation.[93,94] This process depends on the interaction of Nek1 with Wapl which regulates Smc3, a factor crucial for sister chromatid cohesion during prophase.[93] Although the exact processes by which Nek1 orchestrates meiotic processes remain to be elucidated, these studies provide solid evidence for the reason behind the impaired fertility observed in, especially male, kat2j mice.

1.3.2.2 The DNA damage response depends on Nek1

Apart from the developmental disorders mentioned above, mutated *nek1* is linked to the pathogenesis of an incurable, lethal neurodegenerative disease called amyotrophic lateral sclerosis (ALS). ALS selectively affects the functionality and viability of motor neurons and is usually diagnosed between the ages of 50 and 60, when symptoms such as respiratory distress, slurred speech, and muscular atrophy clinically manifest.[95] Although the exact cause of the disease remains elusive, early research has already suggested a mechanism related to dysfunctions in the DDR since ALS-derived motor neurons accumulate a large amount of DNA damage and suffer from chromosomal aberrations consequently leading to their degeneration.[96,97] The notion that genomic instability is a hallmark of ALS has been further supported by genetic studies of patients with a familial history of ALS, who exhibit mutations in approx. 30 genes mostly related to autophagy, the antioxidative system, and the DDR.[98,99] As a result of the "ice-bucket challenge", a charity event in 2014 that raised approx. $220 million to support ALS research, two independent mutations of *nek1*, resulting in a loss-of-function (p.Arg812Ter) and a missense (p.Arg261His) variant, have been identified as risk factors and are associated with 3.1% of all ALS cases.[101-104] This connection between dysfunctional Nek1 variants and the development of ALS is most likely attributable to the broad functions of Nek1 in the DDR, namely cell cycle control, DNA repair, and apoptosis regulation, which are required to maintain cellular genomic stability and tissue homeostasis.

First of all, Nek1-deficient cells fail to properly induce cell cycle checkpoints in response to IR and proliferate even in the presence of high amounts of DNA damage. Nek1 has been found in this context to be both, increasingly abundant and active in WT cells following genotoxic stress resulting, among other things, in a robust cell cycle arrest at the G1/S and G2/M transitions.[104–107] Although this checkpoint induction has been linked to the phosphorylation of Chk1 and Chk2, it remains controversial whether Nek1 activates these checkpoint kinases directly or indirectly through its interaction with ATR.[108,109]

In addition to their uncontrolled proliferation, cells without functional Nek1 are unable to resolve γH2AX foci and thus suffer from chromosomal aberrations and nuclei abnormalities caused by persisting high levels of DNA damage.[104–106,110] This Nek1-dependent phenotype was confirmed by the Löbrich lab, which eventually reported that Nek1 plays a central role in the DNA repair pathway HR by activating Rad54.[111] In more detail, Rad54 is an ATP-dependent motor protein that assists the nucleoprotein filament with strand invasion and dissociates Rad51 from the DNA after successful homology search (see section 1.2.2). Rad51, however, also functions independently of Rad54 during S phase, where it binds ssDNA to stabilize stalled replication forks. *Spies et al*. were therefore interested to elucidate how Rad54 is regulated to interact with Rad51 during HR but not during replication fork stalling.[111] The published data show that Nek1 activates Rad54 by phosphorylating its ATPase domain

(Ser572). However, the occurrence of phosphorylated Rad54 has been strictly associated with the G2 phase of the cell cycle, when the HR pathway requires Rad54 for its progression. Further experiments, especially with cells that produced a constantly active Rad54 variant, suggested that this restrictive regulation of Rad54 is a necessity to ensure replication fork stability during S phase by preventing the premature removal of Rad51. In summary, this study demonstrates that Nek1 is required to separate replication during S phase from DNA repair via HR in G2 phase by regulating Rad54's activity in a cell cycle-dependent manner.[111]

Finally, Nek1 regulates apoptosis induction by interacting with the key mitochondrial protein Vdac1.[112,113] Vdac1 is a pore complex that, under normal conditions, is stabilized by Nek1-dependent phosphorylation of its Ser193 and blocks the release of CytC from mitochondria into the cytoplasm.[114] Nek1-deficient cells have been shown to lose this phosphorylation on Vdac1 and to die even under sublethal doses of genotoxic stress due to increased permeability of Vdac1 and the subsequent CytC-dependent activation of caspases initiating apoptosis.[115,116]

1.4 Thesis composition

The following thesis presents the data of two projects each highlighting a different aspect of Nek1 in the DNA damage response.

- **Project 1 (Chapter 2)** focuses on the work completed in the Löbrich lab and examines the dependence of the HR pathway on Nek1 at different developmental stages.
- **Project 2 (Chapter 3)** comprises data collected in the Rödel lab and evaluates the potential of Nek1 as a therapeutic target for novel cancer treatments in the context of radiotherapy.

Both chapters are sectioned into the study's scope, used material and methods, obtained results, and a discussion. The thesis concludes with some remarks on research perspectives.

2 Project 1: Dependence of HR on Nek1 during development

2.1 Scope of the study

In 2015, the joint project *NeuroRad* was founded under the leadership of Prof. Dr. Löbrich to investigate the effects and consequences of medically relevant radiation doses on neuronal development together with other research groups from the TU Darmstadt, the GSI, and the FAU Erlangen. Within this consortium, the Löbrich lab aimed to characterize the DNA repair behavior of proliferating brain cells and especially focused on the question of whether the regulation of the HR pathway by Nek1 and Rad54 described *in vitro* by Spies *et al*. is also relevant *in vivo* (see section 1.3.2.2).[111] For this, mouse strains with altered HR pathways were established by Florian Frohns including Rad54 Knock-Out (KO) mice from the Kanaar lab and kat2j mice (hereinafter called Nek1KO) from the Jackson Laboratory.[69,117] As part of her PhD studies, Holly Thomas subjected these HR-deficient mice as well as HR-proficient wildtype (WT) mice to irradiation experiments and analyzed the effects of a Rad54 deficiency or a Nek1 deficiency on DSB repair in proliferating brain cells from both, embryonic and postnatal mice. She established an immunohistochemistry method for paraffined brain samples to identify cells in the late S phase and G2 phase, to which DNA repair by HR is restricted, and added a staining against Rad51 for the quantification of DSBs undergoing HR-mediated repair. Based on this approach, she found that proliferating brain cells of WT mice efficiently resolved radiation-induced Rad51 foci within 8 h after irradiation with 1 Gy independently of their developmental stage, whereas cells of Rad54KO mice displayed a severe DSB repair defect and were unable to decrease the amount of radiation-induced Rad51 foci. Strikingly, Nek1KO mice exhibited repair behaviors similar to both, WT and Rad54KO mice in dependency of their age. In 21-day-old postnatal Nek1KO mice, the resolution of Rad51 foci was significantly impeded similarly to Rad54KO mice. Brain cells of 14.5-day-old embryos as well as 4-day-old postnatal mice, however, removed Rad51 foci as efficiently as the respective wildtype cells (personally reported by Holly Thomas). In summary, Holly Thomas' studies confirmed for the first time that Rad54 and Nek1 are essential factors of the HR pathway *in vivo*. Her results furthermore indicated that Rad54 plays a fundamental role in the HR-mediated repair throughout development whereas Nek1 becomes important with developmental progression and is not essential in embryonic or early-postnatal organisms.

In light of these data, the following work aimed to characterize the differential regulation of Rad54 during development using functional immunofluorescence-based assays such as the quantification of Rad51 and γH2AX foci following irradiation. For this purpose, fibroblast lines from the previously mentioned mouse strains should first be established to validate the collected *in vivo* data. Whether Rad54 activity is also controlled in embryonic cells via the Ser572 site in its ATPase domain should be determined in experiments conducted with fibroblasts that produce unregulated Rad54 variants. Finally, the extent to which Nek1 and

other Nek kinases may be involved in embryonic HR was to be examined by subjecting embryonic fibroblasts to a screening procedure involving Nek-specific siRNAs.

2.2 Materials

2.2.1 Devices

Device (**Type**)	**Supplier**
Cell counting chamber (Neubauer improved)	Marienfeld Superior
Centrifuge (5451R)	Eppendorf
Centrifuge (5804R)	Eppendorf
Centrifuge (Biofuge pico)	Heraeus
Dual-mode Imaging System (Fusion FX)	Vilber Lourmat
Electrophoresis power supply (PowerPac 300)	Bio-Rad
Horizontal electrophoresis set (Horizon 58; 11-14)	Life technologies
Incubator (HERA cell 240i)	Thermo Fisher Scientific
Laminar flow hood (HERA safe)	Thermo Fisher Scientific
Microscope (Axioimager M1 microscope with ApoTome.2)	Zeiss
Microscope (Axiovert 200M with AxioCamMRm)	Zeiss
Microscope (Eclipse TS100)	Nikon
Microscope (Imager.Z2 with AxioCamMRm)	Zeiss
PCR cycler (Thermocycler)	Peqlab
pH meter (pMX2000)	WTW
Photometer (P-Class)	Implen
Pipetus	Hirschmann-Laborgeräte
Real-Time PCR System (StepOnePlus™)	Applied Biosystems
Scales (TE 1502S, TE 153S-DS)	Sartorius
Shaker (3011)	GFL
Thermomix (Comfort)	Eppendorf
Vertical Electrophoresis cell and accessories (Mini-PROTEAN ® Tetra)	Bio-Rad
Vortex (Genie 2)	Scientific Industries
Wet transfer system (Mini Trans-Blot® Cell)	Bio-Rad
X-Ray tube (Titan E Isovolt 160)	GE Technologies

2.2.2 Consumables

Consumable (**Type**)	**Supplier**
15/50 ml falcon tubes	Greiner Bio-One
35 mm/ 60 mm cell culture dishes	TPP
6-well cell culture plates	TPP
96-Well qPCR Plate (MicroAmp™ Optical)	Applied Biosystems
Blotting paper (703)	VWR
Cell culture flasks (T25/T75)	TPP
Cell scraper	Carl Roth

Cell strainer (40 µm pore size)	VWR
Cover Slips	Roth
Disposable Hematocytometer (C-Chip)	NanoEnTek
Disposable Polystyrene Serological Pipettes	Sarstedt
Glass beakers	Schott
Insulin syringes	B. Braun
Kim wipes	NeoLab
Microscope slides (Superfrost)	Carl Roth
Nitrocellulose Membrane (Amersham™ Protran™ Premium, 0.2 µm)	GE Healthcare
Parafilm	Bemis
Pasteur pipettes	Carl Roth
PCR tubes (0.2 ml)	Greiner
Pipette tips	Sarstedt
Pipette tips (filtered)	Carl Roth
Polystyrene Round-Bottom tubes	Becton Dickinson
Reaction tubes (1.5 ml, 2 ml)	Carl Roth
Sealing film (EASYseal™)	Greiner

2.2.3 Chemicals and premade buffers

Chemical	**Supplier**
10% Formalin (4% Formaldehyde)	Carl Roth
5-Ethynyl-2'-deoxyuridine (EdU, 10 mM)	Invitrogen
Agar-Agar, Agarose	Carl Roth
Ammonium persulfate (APS)	Carl Roth
Bovine serum albumin (BSA)	AppliChem
Bromophenol blue	Carl Roth
Complete™ Protease Inhibitor Cocktail (25x)	Roche
CutSmart buffer	New England Biolabs
DAPI	Sigma-Aldrich
Deoxycholic acid (DOC), sodium salt	Carl Roth
Deoxynucleotides (dNTP, 10 mM)	Thermo Fisher Scientific
Deoxynucleotides (dNTP, 10 mM)	New England Biolabs
Dimethyl sulfoxide (DMSO)	Sigma-Aldrich
Disodium hydrogen phosphate dihydrate (Na_2HPO_4 x 2 H_2O)	Carl Roth
Dithiothreitol (DTT)	Carl Roth
Ethanol	Carl Roth
FastStart Universal SYBR Green Master (Rox)	Merck
Glucose (Monohydrate)	Carl Roth
Glycerol, Glycine	Carl Roth
Hydrochloric acid (HCl)	Roth

Immersion Oil	Zeiss
Isopropanol	Carl Roth
Lysogeny broth (LB) medium, powder	Carl Roth
Lipofectamine RNAiMAX	Thermo Fisher Scientific
Lipofectamine 2000	Thermo Fisher Scientific
Magnesium chloride hexahydrate ($MgCl_2 \times 6\ H_2O$)	Carl Roth
Magnesium sulafte heptahydrate ($MgSO_4 \times 7\ H_2O$)	Carl Roth
Methanol	Carl Roth
Mounting medium (Vectashield®)	Axxora Alexis
Nuclease-free water	Thermo Fisher Scientific
PonceauS	Sigma-Aldrich
Potassium chloride (KCL)	Carl Roth
Potassium dihydrogen phosphate (KH_2PO_4)	Carl Roth
Protein Assay Dye Reagent Concentrate	Bio-Rad
Q5® reaction buffer	New England Biolabs
Roti Block (10x)	Carl Roth
Rotiphoresis gel 30	Carl Roth
Roti-Safe GelStain	Carl Roth
Skim milk powder	Carl Roth
Sodium chloride (NaCl)	Carl Roth
Sodium fluoride (NaF)	Carl Roth
Sodium hydroxide (NaOH)	Carl Roth
Sodium lauryl sulfate (SDS) pellets	Carl Roth
Sodium orthovanadate (Na_3VO_4)	Sigma-Aldrich
T4 DNA Ligase buffer	New England Biolabs
Taq DNA polymerase reaction buffer	Thermo Fisher Scientific
Tetramethylethylendiamine (TEMED)	Carl Roth
Trichloroacetic acid (TCA)	Carl Roth
Trichloroacetic acid (TCA)	Carl Roth
Tris(hydroxymethyl)aminomethane (TRIS)	Carl Roth
Triton X100	Carl Roth
TriTrack DNA Loading Dye (6X)	Thermo Fisher Scientific
Tween® 20	Carl Roth
WesternBright™ Quantum Blotting substrate	Advansta

2.2.4 Basic media, antibiotics, and supplements

Medium/Supplement	**Supplier**
Dulbecco's Modified Eagle's Medium (DMEM)	ThermoFisher Scientific
Optimized Minimal Essential Medium I (OptiMEMI)	ThermoFisher Scientific
Fetal bovine serum (FBS)	Biochrom

Non-essential amino acids (NEAA)	Biochrom
L-Glutamine (200 mM)	Sigma-Aldrich
Cell-Culture Guard	AppliChem
Accutase	Sigma-Aldrich
Ampicillin	Carl Roth
Kanamycin	Carl Roth

2.2.5 Buffers, media, and solutions

2.2.5.1 General Buffers

Phosphate-buffered saline (PBS), pH 7.4	Na_2HPO_4 x 2 H_2O	10 mM
	KH_2PO_4	1.8 mM
	NaCl	137 mM
	KCl	2.7 mM
	Milli-Q water	
TRIS-buffered saline (TBS), pH 7.6	TRIS base	20 mM
	NaCl	137 mM
	Milli-Q water	
TRIS buffer (TRIS), pH 6.8 or 8.0 or pH 8.8	TRIS base	1 M or 1.5 M
	Milli-Q water	
TRIS-Borate-EDTA buffer (TBE), pH 8.4	TRIS base	0.1 M
	Boric acid	0.9 M
	EDTA	20 mM
	Milli-Q water	

2.2.5.2 Bacterial cultivation

Lysogeny Broth (LB) medium	LB medium	2.5% (w/v)
	Ampicillin (if needed)	100 µg/ml
	Kanamycin (if needed)	50 µg/ml
	Milli-Q water	
LB plates	LB medium	2.5% (w/v)
	Agar-Agar	1.5% (w/v)
	Ampicillin (if needed)	100 µg/ml
	Kanamycin (if needed)	50 µg/ml
	Milli-Q water	
Super Optimal Broth with Catabolite Repression (S.O.C.)	LB medium	2.5% (w/v)
	KCl	2.5 mM
	$MgCl_2$ x 6 H_2O	10 mM
	$MgSO_4$ x 7 H_2O	10 mM
	Glucose	20 mM
	Milli-Q water	

2.2.5.3 Cell culture

Complete medium	FBS	10% (v/v)
	200 mM L-Glutamine	2 mM
	NEAA	1% (v/v)
	Cell Culture Guard	1% (v/v)
	DMEM	
Transfection medium	FBS	10% (v/v)
	200 mM L-Glutamine	2 mM
	NEAA	1% (v/v)
	DMEM	
PronaseE	1 M TRIS, pH 8.0	10 mM
	Pronase E	1.25 µg/µl
	EDTA	1 mM
	Milli-Q water	
CollagenaseD	CollagenaseD	2.5 µg/µl
	Complete Medium	

2.2.5.4 Cell lysis

Radioimmunoprecipitation Assay (RIPA) buffer	1.5 M TRIS, pH 8.0	50 mM
	NaCl	150 mM
	SDS	0.1% (w/v)
	DOC	0.5% (w/v)
	Triton-X100	1% (v/v)
	25x complete™ Protease Inhibitor Cocktail	4% (v/v)
	Na_3VO_4	1 mM
	NaF	2 mM
	Milli-Q water	

2.2.5.5 DNA analysis

1 or 2% Agarose gel	Agarose	1 or 2% (w/v)
	Roti-Safe gel-stain	0.005% (v/v)
	TBE buffer	

2.2.5.6 SDS-PAGE

5% SDS stacking gel	1 M TRIS, pH 6.8	125 mM
	30 % Acrylamide	5% (v/v)
	SDS	0.1 % (w/v)
	APS	0.15 % (w/v)
	TEMED	0.1 % (v/v)
	Milli-Q water	
8% SDS separation gel	1 M TRIS, pH 8.8	370 mM
	30 % Acrylamide	8% (v/v)

	SDS	0.1 % (w/v)
	APS	0.15 % (w/v)
	TEMED	0.11 % (v/v)
	Milli-Q water	
SDS running buffer, pH 8.8	TRIS base	25 mM
	SDS	3.5 mM
	Glycin	190 mM
	Milli-Q water	
6% Reducing loading buffer	1 M TRIS, pH 6.8	350 mM
	SDS	10.28% (w/v)
	Glycerol	50% (v/v)
	DTT	600 mM
	Bromophenol blue	0.05% (w/v)
	Milli-Q water	

2.2.5.7 Immunoblotting

Transfer buffer pH 8.3	TRIS base	25 mM
	Glycine	190 mM
	Methanol	20% (v/v)
	Milli-Q water	
Membrane staining solution	PonceauS	0.2% (w/v)
	TCA	3% (v/v)
	Milli-Q water	
TBS-Tween (TBS-T)	Tween20	0.1% (v/v)
	TBS	
Primary antibody dilution buffer	BSA	5% (w/v)
	TBS-T	
Blocking buffer	Skim milk powder	5% (w/v)
	TBS-T	

2.2.5.8 Immunofluorescence

PBS-Tween (TBS-T)	Tween20	0.1% (v/v)
	PBS	
Permeabilization buffer	Triton X-100	0.3% (v/v)
	PBS	
Blocking and antibody dilution buffer	10x Rotiblock	10% (v/v)
	Milli-Q water	
DAPI solution	DAPI	0.4 µg/ml
	Milli-Q water	

2.2.6 Kits

Kit	Supplier
Click-iT EdU Imaging Kit	Baseclick
QIAquick Gel Extraction Kit	Qiagen
QIAquick PCR Purification Kit	Qiagen
Genopure Plasmid Maxi Kit	Roche
RevertAid First Strand cDNA Synthesis Kit	Thermo Fisher Scientific
MasterPure™ Complete DNA and RNA Purification Kit	Lucigen
Z-R Plasmid Miniprep Classic kit	Zymo Research

2.2.7 Oligonucleotides

siRNA	Sense sequence (5'- 3')	Supplier
AllStars Control (Ctrl)	-	Qiagen
Rad54l	ccaccugguuauaacucuatt	Thermo Fisher Scientific
Nek1 (Smart Pool)	auagcuaaacgaaucgaaa ggugauuuguuuaaacgaa gcucgaacuugcauaggca gggauagaccaucagucaa	Dharmacon
Nek2	caucgucaguuacuaugautt	Thermo Fisher Scientific
Nek3	gauuggugucagaacuaatt	Thermo Fisher Scientific
Nek4	gaagcacgcuuuuaaugcatt	Thermo Fisher Scientific
Nek5	caugaagacuauacagacatt	Thermo Fisher Scientific
Nek6	ccaccgaccugacauuguatt	Thermo Fisher Scientific
Nek7	ggauaaugagcugaacauatt	Thermo Fisher Scientific
Nek8	ccuucgcacccaucucugatt	Thermo Fisher Scientific
Nek9	ccauucuuauuguugagaatt	Thermo Fisher Scientific
Nek10	ccaauguuguacguuauuatt	Thermo Fisher Scientific
Nek11	ggaccaagaugaagcgcautt	Thermo Fisher Scientific

All primers were purchased from Eurofins Genomics GmbH (Ebersberg, Germany). Primers for the genotyping and sequencing of cells as well as for the amplification of Gapdh via qPCR were designed by Emilie Renaud as part of the BMBF-funded NeuroRad project.

Primer	Forward sequence (5'- 3')	Reverse sequence (5'- 3')
Genotyping		
Nek1KO-PreSeq	cttacccagctgagccatgt	gcgtgattctgccttgagtt
Rad54KO	aggaagcatttattcgaagtattt and tttgcttcctcttgcaaacca	gttcaaagccagtcagcctag
mCherry	caggacggcgagttcatcta	gtcttgacctcagcgtcgta
Myogenin	ttacgtccatcgtggacagc	tgggctgggtgttagcctta
EGFP/LoxP	cgtgaagattgagcaggtgg	gcagatgaacttcagggtcag

Cre	gaacctgatggacatgttcagg	agtgcgttcgaacgctagagcctgt
LoxP	tctgtgtgagtgagcaggga	ctggcgctgacataggtctc
KI PreSeq	tgacaagtgtgtggcagag	gcagatgaacttcagggtcag
Sequencing		
Nek1KO Seq	gcacatagtgaggtaggtagg	-
KISeq	tgattacattctggccgtgactcg	-
qPCR		
Gapdh	cagcaaggacactgagcaaga	tatgggggtctgggatggaaa
Mphosph10	agtcaggatggcccctgtaa	tcgttctacgtcatcccaagc
Nek1	ttggaccacagcctctccca	cgggaatttgatgggcctgtt
Nek2	aagctgggggactttggact	gggaggcattagtgcacacag
Nek3	agagcagccagaggaaatcca	cagacccacctctgtcatcctc
Nek4	cactaccagccacgctcttct	cttgtttgccagtgtggcctt
Nek5	ggctaggatggagcatcccaat	acacaggatctggtcttcgct
Nek6	gcgggtgacctctcacagat	ttggcgggcttgatgtctcg
Nek7	cacaaggaatgcaagggccg	gctaccggcactccatccaa
Nek8	catcaagcatgtggcctgcg	ttctacaatggtgggctggct
Nek9	gaatatggacggctgggtttgg	aggtcccatcacagccacatt
Nek10	tgcaagtggagcccacaaga	cggcagtgagtcttttggagag
Nek11	tccttcattgagaccgtcggc	ggtgaagctttttctgcacggc
Site-directed mutagenesis		
siRNA resistance Nek3	aagataacgaaaaccctgattggctaa-gcgaactaaagaagcacgtaggatacg	cgtatcctacgtgcttctttagtt-cgcttagccaatcagggttttcgttatctt
siRNA resistance Nek5	agtttcaggagcacagatgtaaggagg-aacacgaggattacacagacagagcctttg	caaaggctctgtctgtgtaatcctcgt-gttcctccttacatctgtgctcctgaaact
K33R-substitution Nek3	gcaatcagacatttgcca-tgagggaaatcagactgctc	gagcagtctgatttccctca-tggcaaatgtctgattgc
K33R-substitution Nek5	cagaaagcagtcactgtgt-cataagagaaatcagtttgacaaag	ctttgtcaaactgatttct-cttatgacacagtgactgctttctg

2.2.8 Plasmids

Plasmid	Insert	Supplier
pCMV-SPORT6	Murine Nek3 wildtype cDNA	Dharmacon #MMM1013-202762621
pCMV-SPORT6	Murine Nek5 wildtype cDNA	Dharmacon #MMM1013-202804996
pEGFP-C1	Empty	Clontech
pEGFP-C1	Murine Nek3 wildtype cDNA	Self-made
pEGFP-C1	Murine Nek3 wildtype cDNA	Self-made
pEGFP-C1	Murine Nek3-K33R	Self-made
pEGFP-C1	Murine Nek5-K33R	Self-made

2.2.9 Antibodies

Primary antibodies	Ordering no.	Supplier	Dilution
Western Blot			
Mouse anti-GAPDH, polyclonal IgG	sc-25778	Santa Cruz Biotechnology	1:200000
Mouse anti-Nek1, Monoclonal IgG	sc-398813	Santa Cruz Biotechnology	1:500
Mouse anti-Nek3, Monoclonal IgG	sc-390872	Santa Cruz Biotechnology	1:100
Rabbit anti-Nek3, Polyclonal IgG	sab1302503 Pa5-110021	Sigma-Aldrich Invitrogen	1:1000 1:1000
Mouse anti-Nek5, monoclonal IgG	sc-515457	Santa Cruz Biotechnology	1:1000
Rabbit anti-Nek3, Polyclonal IgG	sab1301976 Pa5-101860	Sigma-Aldrich Invitrogen	1:1000 1:5000
Mouse anti-Rad54, monoclonal IgG	sc-374598	Santa Cruz Biotechnology	1:200
Immunofluorescence			
Chicken anti-GFP, polyclonal IgG	ab13970	Abcam	1:400, 1:1000
Goat anti-Rad54, polyclonal IgG	sc-5849	Santa Cruz Biotechnology	1:400
Mouse anti-phospho-H2AX, monoclonal IgG	05-636	Merck Millipore	1:1000
Rabbit anti-mCherry, polyclonal IgG	ab167453	Abcam	1:400
Rabbit anti-phospho-H3, polyclonal IgG	06-570	Merck Millipore	1:1000
Rabbit anti-Rad51, Polyclonal IgG	ab63801	Abcam	1:10000
Secondary antibodies	**Ordering no.**	**Supplier**	**Dilution**
Western Blot			
Donkey anti-mouse-HRP, Polyclonal IgG	715-035-150	Dianova	1:1000
Donkey anti-rabbit-HRP, Polyclonal IgG	711-035-152	Dianova	1:1000
Immunofluorescence			
Donkey anti-chicken Alexa Fluor488, polyclonal IgG	703-545-155	Dianova	1:1000
Donkey anti-mouse-Alexa Fluor 488, polyclonal IgG	A 21202	Invitrogen	1:1000
Donkey anti-rabbit-Alexa Fluor488, polyclonal IgG	A21206	Thermo Fisher Scientific	1:1000

Donkey anti-goat-Alexa Fluor647, polyclonal IgG	A21447	Molecular Probes	1:200
Donkey anti-mouse-DyLight550, polyclonal IgG	ab96876	Abcam	1:1000
Donkey anti-rabbit-DyLight550, polyclonal IgG	SA510039	Thermo Fisher Scientific	1:1000

2.2.10 Enzymes

Enzyme	Supplier
Q5® High-fidelity DNA polymerase	New England Biolabs
T4 DNA Ligase	New England Biolabs
Taq DNA Polymerase	Thermo Fisher Scientific
DpnI	New England Biolabs
NotI-High Fidelity (HF)	New England Biolabs
XbaI	New England Biolabs
XhoI	New England Biolabs
XmaI	New England Biolabs
PronaseE	AppliChem
CollagenaseD	Sigma-Aldrich

2.2.11 DNA/Protein ladders

Ladder	Supplier
GeneRuler 100 bp or 1kb DNA Ladder	Thermo Fisher Scientific
ProSieve QuadColor Protein Marker	Biozym

2.2.12 Bacterial strains

Strain	Supplier
E. coli DH5α Mix & Go Competent Cells	Zymo Research
E. coli DH10b Competent Cells	Thermo Fisher Scientific

2.2.13 Animals

Murine embryonic and postnatal fibroblast cell lines (MEF, MPF) were derived from the following mice strains:

Lab-intern name	Official name	Modification	Origin
Nek1 KO	C57BL/6 Nek1^{kat-2J}	Frameshift mutation in the Nek1 gene due to a spontaneous insertion of one guanine at position 966	The Jackson Laboratory [72]
Rad54 KO	C57BL/6 mRad54^{307neo}	Targeted mutation that disrupts the Rad54 gene through the insertion of a neomycin resistance gene	Prof. Dr. Kanaar, Erasmus Medical Center, The Netherlands [117]

Rad54S/A or S/E KI	-	“Inactive” Knock-In expressing a mCherry-tagged wildtype Rad54	Generated by F. Frohns and E. Renaud in cooperation with Cyagene
Rad54S/A or S/E KIact	-	“Active” Knock-In expressing a GFP-tagged Rad54 variant in which the serine residue 572 is either substituted to alanine (A) or glutamate (E)	Self-Bred with Rad54 S/E or S/A Knock-In (KI) as progenitors

KO, Knock-Out; KI, Knock-In; KIact., activated Knock-In

2.2.14 Software and internet resources

Software/Resource	Developer	Application
ChemiCapt	Vilber Lourmat	Agarose gel image aquisition
Excel 2019	Microsoft	Calculation and graph design
FusionCaptAdvance FX7	Vilber Lourmat	Western Blot image acquisition
ImageJ2 Fiji	Open Source	Fluorescence image acquisition
Zen 2.6 blue edition	Carl Zeiss	Fluorescence image aquisition
Metafer 4	Metasystems	Slide scanning
NCBI primer designing tool	National Institutes of Health	Primer design
Serial Cloner v2.6.1	SerialBasics	Primer design and cloning
StepOnePlus™ Software v2.3	Applied Biosystems	qPCR data analysis

2.3 Methods

2.3.1 Cell biology

2.3.1.1 Fibroblast isolation

Fibroblast isolation was initiated by the pairing of mice described in 2.3.12 according to the breeding schemes listed in table 2. For the generation of murine embryonic fibroblast (MEF) lines, female mice were checked daily after mating for a vaginal plug which confirms that fertilization has occurred.[118] Embryos were removed from pregnant mice 13.5 days after fertilization according to a protocol by Durkin *et al*. applied with small changes.[119] The isolated embryos were decapitated, shredded, and subsequently digested in 3 ml of accutase solution for 2 h at 37°C. 10 ml of complete medium were added to stop the digestion process and the resulting suspension was separated from undigested tissue using a cell strainer with a pore size of 45 µm. After a 5 min centrifugation at 200 x g and 4°C, fibroblasts were taken up in 5 ml complete medium, transferred into a T25 culture flask, and incubated at standard conditions

(37°C, humidified atmosphere with 5% CO_2). Murine postnatal fibroblast (MPF) lines were prepared from the ears of 21-day-old mice similar to a protocol by Khan *et al.*[120] For this, mice were sacrificed by cervical-dislocation, and both ears were cut off and disinfected for 3 min in 70% ethanol. After airdrying, ears were rigorously shredded and digested in 1.5 ml of a PronaseE/CollagenaseD-enzyme mixture at 37°C under shaking for at least 2 h. Similar to the generation of MEF lines, the enzymatic process was stopped by the addition of 10 ml of complete medium to the suspension, followed by cell straining, centrifugation, transfer into a T25 culture flask, and incubation at standard conditions. 24 h after isolation, the medium of all MEF and MPF lines was changed and cultures were continuously incubated. Table 3 summarizes all fibroblasts cell lines that were used for experiments.

Tab. 2 Mice breeding schemes

Mouse strain	Breeding scheme	Genetic outcome
Nek1KO	het × het	Wildtype (WT), het, hom
Rad54KO	het × hom	het, hom
Rad54S/**AKIact**, **S**/**EKIact**	het × hom or hom × hom	het, hom

2.3.1.2 Fibroblast immortalization and culture

The work with primary fibroblasts of both, embryonic and postnatal origin is often problematic due to their limited replicative lifespan and the onset of senescence early after isolation also called the *Hayflick limit*.[121,122] This significantly impedes experimental work not only through a high demand for animals to generate adequate cell masses. The most frequently used strategy to bypass this difficulty is the genetic modification of cells to express factors, e.g., the SV40 large T antigen, which triggers the expression of intrinsic oncogenes and, thus, cellular proliferation.[123] However, immortalization can also occur spontaneously especially in primary cells of murine origin through cellular mechanisms that are not fully understood.[122] To avoid expensive and laborious procedures, the following experiments were accomplished using fibroblasts spontaneously immortalized according to a protocol by Xu *et al.*[124]. MEF and MPF cell lines from 2.1.1 were passaged when their confluency reached 90%. In detail, cells were washed with PBS and detached from the flask bottom using 1 ml of accutase solution for 5 min at 37°C. Fibroblasts were then resuspended in 3 ml of complete medium, splitted in a ratio of 1/2 or 1/3 in a new T25 flask containing 5 ml of complete medium, and incubated under standard conditions (37°C, humidified atmosphere with 5% CO_2). When a growth stop was observed in fibroblast lines after 6 to 12 passages, splitting was suspended and the culture medium was changed once a week. Within 4 to 12 weeks, fibroblasts spontaneously immortalized and started to proliferate gradually. At a confluency of 90%, fibroblasts were splitted again in a ratio of 1:2 to 1:3 and higher (1:5 to 1:10) with increasing passage number. Experiments were conducted when cell lines were exponentially proliferating (starting from

passages 15 to 25) and successfully genotyped for homozygosity of their respective genetic modification as described in section 2.3.2.1.

Tab. 3 Fibroblast cell lines established from mice described in section 2.2.12

Murine embryonic fibroblasts (MEF)	Murine postnatal fibroblasts (MPF)
Wildtype (WT)-1*, -2*	Wildtype (WT)-1*, -2
Nek1KO-1*, -2*	Nek1KO-1*, -2*
Rad54KO-1*, -2*	Rad54KO-1*, -2
Rad54S/AKIact-1*, -2	Rad54S/AKIact-1, -2
Rad54S/EKIact-1*, -2*	Rad54S/EKIact-1, -2

* Cell lines were isolated by Emilie Renaud and Florian Frohns as part of the BMBF-funded NeuroRad project.

2.3.1.3 Seeding

To increase cell mass, fibroblasts were splitted in a ratio of 1:3 from T25 into T75 flasks containing 15 ml of complete medium. Single-cell suspensions were prepared at a confluency of 90 % through the treatment of fibroblasts with 2 ml of accutase solution for 5 min at 37°C and subsequent resuspension in 5 ml of complete medium or, in case of siRNA and plasmid transfection, in 5 ml of transfection medium. The number of cells within the suspensions was determined using Neubauer hemocytometers and 10 µl of each suspension. Cells were then seeded for experiments as shown in table 4 and incubated at standard conditions (37°C, humidified atmosphere with 5% CO_2) until further use. For immunofluorescent experiments, cells were seeded into cell culture dishes equipped with sterilized glass coverslips.

Tab. 4 Cell numbers seeded into experiments

Cells	Experiment	Culture vessel	Amount of medium	Cell number seeded
Native	Protein, DNA or RNA isolation	6 well plate	2 ml	0.6 - 1.2 × 10^5
	Immunofluorescence	60 mm dish with 12 coverslips	5 ml	0.4 - 1.0 × 10^5
siRNA transfected	Protein or RNA isolation	6 well plate	2 ml	0.2 - 0.9 × 10^5
	Immunofluorescence	35 mm dish with 4 coverslips	2 ml	0.2 - 0.4 × 10^5

2.3.1.4 siRNA and plasmid transfection

Genes of interest were knocked down by transfection of fibroblasts with siRNAs listed in section 2.2.7 and Lipofectamine RNAiMAX directly after seeding. Per transfection, each siRNA was diluted in 500 µl of OptiMEMI medium to a final concentration of 100 nM. After an incubation of 5 min, 6.5 µl of Lipofectamine RNAiMAX were added. The solution was gently mixed by inversion, incubated for 5 min at room temperature (RT), and subsequently dropped onto cells. Fibroblasts were incubated with siRNA/RNAiMAX complexes for 72 h at standard

conditions (37°C, humidified atmosphere with 5% CO_2) before Protein/RNA isolation and immunofluorescent experiments.

For rescue assays, pEGFP constructs containing Nek3 and Nek5 gene variants described in section 2.2.8 (see section 2.3.2.3 for cloning) were delivered into fibroblasts 24 h after siRNA transfection using Lipofectamine 2000 as instructed by the manufacturer. Shortly, 10 µg of plasmid DNA were mixed with 6 µl of Lipofectamine 2000 in 250 µl of OptiMEMI medium and left at RT for 30 min. In the meantime, fibroblasts were provided with fresh transfection medium to reduce the cellular toxicity of a double-transfection through the removal of siRNA/RNAiMAX complexes. Fibroblasts were then transfected by dropwise addition of the formed Plasmid/Lipid complexes followed by incubation at standard conditions for 6 h. Afterwards, fibroblasts were provided with fresh transfection medium and kept at standard conditions for 48 h.

2.3.1.5 DNA damage induction

Fibroblasts were treated with 10 µM of the thymidine analog 5-Ethynyl-2'-Deoxyuridin (EdU). 1 h before irradiation to allow for the identification of S-Phase cells in later applications. DNA damages such as DNA double-strand breaks (DSBs) were induced in cells by irradiation with high-dose X-rays produced by a Titan E Isovolt 160 X-ray tube at a voltage of 90 kV and a current of 19 mA. Dishes with cells were placed onto a 1 mm aluminum plate before application of 2 Gy with a dose rate of 0.981/min. When cells were seeded on glass coverslips, the applied dose was divided by a factor of 3 to correct for the additional damage induced by secondary radiation effects from the glass.[125]

2.3.1.6 Fixation and immunofluorescence staining

For fixation at time points indicated in the figures, fibroblasts on coverslips were washed once with PBS and covered with 1.5 ml of 4% paraformaldehyde (PFA) for 15 min at RT. Cells were then washed three times for 10 min with PBS and permeabilized with 0.3% Triton for 5 min at RT. Unspecific antibody binding was prevented by incubation of cells in 2 ml of blocking buffer for 30 min at RT. Meanwhile, primary antibodies were diluted in antibody dilution buffer as listed in section 2.2.9. Coverslips with cells were then transferred into a humid chamber, covered with 50 µl of primary antibody solution. Following incubation at 4°C overnight, cells were washed three times for 10 min with PBS-T and incubated with secondary antibodies diluted in antibody dilution buffer for 1 h at RT in the dark. Cells were washed again three times with PBS-T before EdU was stained using the EdU Click-iT kit as instructed by the manufacturer. After a final wash with PBS, fibroblasts were treated with a DAPI solution for 5 min at RT to stain cellular DNA. Finally, coverslips were mounted onto glass slides and sealed with clear nail polish.

2.3.1.7 DNA damage repair analysis

The repair of X-ray-induced DNA damage was analyzed in a cell cycle phase-specific manner

focusing on the repair behavior of cells in the G1 or G2 phase. For this, cells on slides prepared after immunofluorescence staining were examined on an Axiovert 200M microscope. The software Metafer4 was used to scan the slides for cells at 10x magnification. During the scanning process, a histogram was generated that plotted the DAPI signals of single nuclei against their EdU signal (Fig. 4A). Based on the resulting distribution, G2 phase cells were distinguished from G1 phase cells based on their doubled DNA content and, thus, higher DAPI signal. Since fibroblast cultures often contained two populations consisting of either diploid G1/G2 cells or tetraploid G1/G2 cells, respectively, phospho-Histone3 (pH3) was stained additionally to distinguish between diploid G2 phase and tetraploid G1 phase cells. S phase cells were differentiated from the G1/G2 population through their EdU signal which builds up exclusively during replication and allows for the identification of cells that were irradiated in S-phase or entered S phase after irradiation (Fig. 4B). DNA damage repair was evaluated by counting γH2AX foci (DNA DSBs) or Rad51 foci (HR-specific repair) at different time points after irradiation in EdU-negative, phospho-Histone 3 (pH3)-positive diploid G2 cells at 1000x magnification. One experiment consisted of 50 cells analyzed per condition to ensure statistical significance. Immunofluorescent images were taken at an Imager.Z2 microscope with an AxioCamMRm or an Axioimager M1 microscope with ApoTome.2 at 1000x magnification and processed with ImageJ or ZEN Blue as described in the respective figure legends.

2.3.2 Molecular biology

2.3.2.1 Genotyping

DNA from fibroblasts was isolated with the MasterPure Complete DNA and RNA Purification kit according to the manufacturer's instructions. DNA concentration was determined by photometric measurements and PCR samples were set up with 500 ng of DNA and the primers listed in 2.2.7. Table 5 summarizes the strategies and respective PCR conditions used to specify the genotypes of fibroblasts. All primers and PCR programs used for genotyping were designed and optimized by Emilie Renaud as part of the BMBF-funded NeuroRad project. 5 µl of the resulting amplicon solutions were mixed with TriTrack DNA Loading Dye and loaded onto a 2 % agarose gel supplemented with Roti-Safe. DNA fragments and 4 µl of the respective GeneRuler DNA ladder were separated at 100 V for 1 h. DNA was finally visualized with the Fusion FX dual imaging system.

In the case of the Nek1KO- and KI-PreSeq PCRs, amplicons were purified with the QIAquick PCR Purification Kit according to the manufacturer's instructions and sent for sequencing with the respective sequencing primers (see section 2.2.7). All experiments were conducted with fibroblasts homozygous for their genetic modification.

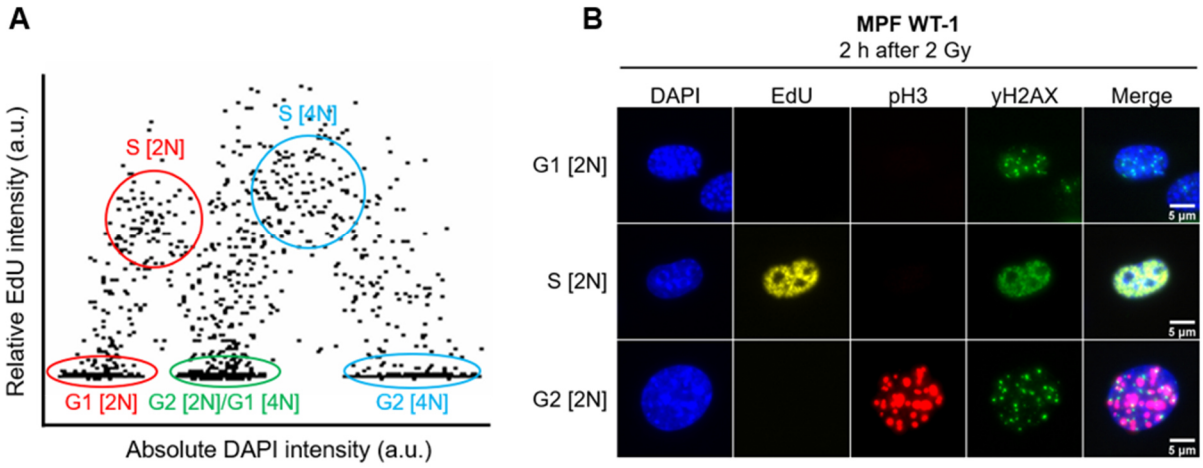

Fig. 4 DNA damage repair analysis. **A** Cell cycle phases were identified using the Metafer4 software (Metasystems). The intensities (a.u.) for EdU and DAPI were plotted into a histogram used to identify EdU-positive S phase cells. EdU-negative cells were distinguished by their DAPI intensity being either low (G1 phase cells) or high (G2 phase cells). pH3 served as a marker for G2 phase cells and was needed to discriminate between diploid G2 phase cells and tetraploid G1 phase cells. **B** Representative image of the γH2AX/EdU immunostaining in WT mouse postnatal fibroblasts (MPF). Cells were treated with 10 µM EdU for 1 h and then irradiated with 2 Gy, fixed 2 h thereafter and stained for γH2AX (green), phospho-Histone 3 (pH3, red) and EdU (yellow) using specific antibodies. DNA was stained using DAPI (blue).

2.3.2.2 Quantitative real-time PCR

Similar to DNA, RNA was isolated from fibroblasts according to the protocol of the MasterPure Complete DNA and RNA Purification Kit. 1 µg of RNA was then reverse-transcribed into cDNA as described in the manual of the RevertAid First Strand cDNA Synthesis kit.

Primers for qPCR were designed with the NCBI primer design tool except for the primer pair against Gapdh which was established by Emilie Renaud as part of the BMBF-funded NeuroRad project. Appropriate annealing temperatures that ensured the specificity of all primer pairs were determined in a PCR set up with 3 units of *Taq*-Polymerase, 0.3 µM of primers, and the following program: 94°C for 3 min, 35 cycles at 94 °C for 1 min, 58 °C or 60°C or 62°C for 1 min and 72°C for 1 min, 72°C for 10 min. After amplification, amplicons were separated at a 2% agarose gel as described in 2.3.2.1 and analyzed using the Fusion FX dual imaging system. qPCR was set up with serially diluted cDNA (1:10 to 1:10,000) prepared from MEF WT cells to determine the amplification efficiency of the primers or with cDNA (diluted 1:3) prepared from cells after irradiation or transfection with siRNA. The diluted cDNA was mixed with FastStart Universal SYBR Green Master Mix and 0.2 µM of the respective primers before amplification in a StepOnePlus™ light cycler under the following conditions: 95°C for 10 min, 40 cycles at 95 °C for 15 sec, and 58 °C for 60 sec. A melting curve was staged right after each amplification process to confirm the specificity of all primer pairs. qPCR data were collected from three independent experiments (technical duplicates). Fold changes in

expression levels were calculated based on the resulting cycle thresholds and the $2^{-\Delta\Delta Ct}$ method in which the *Gapdh* values served as normalization for cDNA content.

Tab. 5 Strategies for the genotyping of fibroblasts established by Emilie Renaud

Modification	PCR aim	Primers	Pol.*	Conditions
Nek1KO	Amplification of the mutation harboring region for sequencing at MycroSynth	Nek1KO-PreSeq	Q5	1 cycle at 98°C for 30 sec, 30 cycles at 98°C for 10 sec, 67°C for 30 sec and 72°C for 30 sec, 1 cycle at 72°C for 2 min
Rad54KO	Discrimination between WT, heterozygous and homozygous alleles	Rad54KO	Taq	1 cycle at 94°C for 3 min, 35 cycles at 94°C for 1 min, 55°C for 1 min and 72°C for 1 min, 1 cycle at 72°C for 10 min
Rad54KI	Control for Cre-mediated recombination: mCherry gene is amplified when recombination failed; Myogenin serves as an amplification control	mCherry + Myogenin	Q5	1 cycle at 98°C for 30 sec, 30 cycles at 98°C for 10 sec, 67°C for 30 sec and 72°C for 30 sec, 1 cycle at 72°C for 2 min
	Control for Cre-mediated recombination: long-fragment is amplified when recombination was successful	EGFP/LoxP	Q5	1 cycle at 98°C for 30 sec, 30 cycles at 98°C for 10 sec, 66°C for 30 sec and 72°C for 30 sec, 1 cycle at 72°C for 2 min
	Check for the abundance of the Cre gene; Myogenin serves as an amplification control	Cre + Myogenin	Q5	1 cycle at 98°C for 30 sec, 30 cycles at 98°C for 10 sec, 67°C for 30 sec and 72°C for 30 sec, 1 cycle at 72°C for 2 min
	Discrimination between heterozygous and homozygous Knock-In alleles	LoxP	Q5	1 cycle at 98°C for 30 sec, 30 cycles at 98°C for 10 sec, 69°C for 30 sec and 72°C for 30 sec, 1 cycle at 72°C for 2 min
	Amplification of the mutation harboring region for sequencing at MycroSynth	KI PreSeq	Q5	1 cycle at 98°C for 30 sec, 30 cycles at 98°C for 10 sec, 66°C for 30 sec and 72°C for 30 sec, 1 cycle at 72°C for 2 min

* Pol., Polymerase

2.3.2.3 Cloning of pEGFP-Nek3 and -Nek5 constructs

The specificity of siRNAs against Nek3 and Nek5 was confirmed by rescuing knockdown-mediated phenotypes through the overexpression of Nek3 or Nek5 genes from plasmid constructs. For this, pCMV-SPORT6 plasmids were purchased from Dharmacon which contained cDNA prepared from murine wildtype mRNA of either Nek3 or Nek5 flanked by XmaI and XbaI restriction sites. The Nek3 or Nek5 cDNA was cloned from pCMV-SPORT6 plasmids into pEGFP-C1 vectors, thereby facilitating the production of GFP-tagged Nek3 or Nek5. XbaI

is a methylation-sensitive restriction enzyme and its restriction site is often blocked by methyl groups in plasmids that were isolated from commonly used cloning strains such as *E. coli* DH5α. Consequently, pCMV-SPORT6 plasmids, as well as the pEGFP-C1 vector, were amplified in *E. coli* DH10b which lack certain operons necessary for the expression of epigenetic modifiers such as the adenine-N6 methyltransferase (Dam).[126]

E. coli DH10b cells were mixed with 200 ng of plasmid DNA and transformed using the heat shock method as follows: 30 min on ice, 45 sec at 42°C, and 2 min on ice. Bacterial cells were then taken up in 450 µl of SOC medium and incubated for 1 h at 37°C under rigorous shaking followed by plating onto pre-warmed LB plates supplemented with either ampicillin (LB/Amp; pCMV-SPORT6) or kanamycin (LB/Kan; pEGFP). After incubation overnight at 37°C, colonies were picked, transferred into 10 ml of LB/Amp or LB/Kan medium, and cultured overnight at 37°C under rigorous shaking. Plasmids were isolated using the Z-R Plasmid Miniprep Classic kit as instructed by the manufacturer and subjected to digestion with XmaI and XbaI.

1 µg of plasmids isolated from *E. coli* DH10b was double-digested with 10 units of XmaI and 10 units of XbaI in CutSmart buffer overnight at 37°C. The digested DNA was separated in a 1% agarose gel. Following visualization, fragments of interest were isolated from the agarose gel using the QIAquick Gel Extraction Kit according to the manufacturer's instructions. For ligation, 1 pmol of the linearized pEGFP plasmid was incubated with 3 pmol of the Nek3 or Nek5 cDNA fragment and T4 DNA Ligase in ligase buffer for 2h at 25°C followed by heat inactivation of the ligase at 65°C for 20 min. *E. coli* DH5α cells were subsequently transformed with 5 µl of the ligation products using the heat shock method as described above, plated onto pre-warmed LB/Kan plates, and incubated overnight at 37°C. Colonies were picked, transferred into 5 ml of LB/Kan medium, and cultured for 8 h at 37°C under rigorous shaking. 1 ml of these precultures was added to 300 ml of LB/Kan medium and incubated overnight at 37°C. pEGFP constructs were then purified from liquid cultures using the Genopure Plasmid Maxi kit as instructed by the manufacturer. Correct ligation was confirmed with a double-digest of the purified pEGFP constructs using XhoI and NotI-HF restriction enzymes and sequencing with standard primers (EGFPC-for, SV40-pArev) at the Mycrosynth AG. Since the pEGFP-Nek3wt and -Nek5wt plasmids were used in combination with siRNAs depleting Nek3 or Nek5, site-directed mutagenesis (SDM) was applied to confer a siRNA resistance through the substitution of several nucleotides at the siRNA binding sites. For SDM similar to a protocol by Edelheit *et al*., two samples per pEGFP plasmid were set up consisting of 500 ng DNA and 40 pmol of either the forward or reverse primer, thereby preventing primer dimer formation as well as undesired primer amplification.[127] Both samples were mixed with Q5 polymerase and amplified in a thermal cycler under the following conditions: 94°C for 2 min, 30 cycles at 94 °C for 40 sec, 55 °C for 40 sec, and 72°C for 7.5 min followed by a final step at 72°C for 7.5 min. The samples were then combined, thoroughly mixed, cooked at 95°C for 5 min, and cooled

down at RT to 37°C. Samples were digested with 30 units of the restriction enzyme DpnI to destroy methylated parental plasmids that served as starting material for SDM but were not substituted. The resulting plasmids modified by SDM were amplified in *E. coli* DH5α and isolated from liquid cultures as described before. The successful substitution of nucleotides by the described SDM procedure was confirmed by sequencing with standard primers (EGFPC-for, SV40-pArev) at the Mycrosynth AG. pEGFP plasmids harboring sequences for kinase defective variants (K33R) of Nek3 or Nek5 were generated accordingly combining the siRNA resistant wildtype constructs with the respective SDM primers.

2.3.3 Biochemistry

2.3.3.1 SDS-PAGE and Immunoblotting

Total protein was extracted from fibroblasts using radioimmunoprecipitation assay (RIPA) buffer at the time points indicated in the respective figures. In detail, cells were washed shortly with PBS and scraped from well bottoms in ice-cold RIPA buffer. The resulting suspension was transferred into a reaction tube and incubated on ice for 30 min to ensure the complete lysis of cells. The protein-containing fraction was separated from cellular debris by centrifugation for 15 min at 4°C and 16,100 x g and transferred to new reaction tubes before storage at -80°C. After determination of the concentration using the Protein Assay Dye Reagent Concentrate according to the manufacturer's instructions, protein extracts were subjected to sodium dodecyl sulfate-polyacrylamide gel electrophoresis (SDS-PAGE) and immunoblotting for analysis. First of all, 35 µg of protein were supplemented with 6x reducing loading buffer and denatured by heating for 10 min at 95°C. Protein samples, as well as a prestained protein ladder, were subsequently loaded onto an SDS gel (5% stacking, 8% separation) and separated at 90 mA for at least 1.5 h. After electrophoresis, the SDS gel was placed onto a nitrocellulose membrane surrounded by blotting paper and sponges to prevent air bubble formation. The gel/membrane sandwich was placed into a blotting tank filled with cold transfer buffer, and proteins were blotted onto the membrane with a current of 310 mA for 3 h. Before cutting at desired protein sizes, the membrane was stained with Ponceau S solution for 1 min and washed with MilliQ water. Unspecific antibody binding was prevented by blocking the membrane with blocking solution for 1 h at RT before incubation overnight at 4°C with primary antibodies diluted in primary antibody dilution buffer. Following washing with TBS-T three times for 10 min, the membrane was incubated for 1 h at RT with secondary antibodies diluted in blocking buffer and washed again with TBS-T three times for 10 min followed by a final wash with TBS for 10 min. Protein bands were visualized with the Fusion FX imager after incubation of the membrane with the WesternBright Quantum blotting substrate for 15 min at RT.

2.3.4 Statistics

Experimental data were gathered from three experiments and shown in figures as mean values +/- standard deviations. Statistics were calculated in Microsoft Excel using the student's T-test for independent samples and considered significant when reaching a p-value of at least 0.05.

2.4 Results

2.4.1 Nek1 deficiency affects HR-mediated repair in MPF but not MEF

As previously described, Nek1 is an essential factor for the successful HR-mediated repair of DSBs in cellular models of advanced developmental stages such as HeLa cells or tissue of 21-day-old mice. However, Nek1 seems to be dispensable for HR-mediated repair in cells of younger origin as shown in *in vivo* studies conducted with embryonic or 4-day-old mice. To evaluate this condition and provide a basis for proceeding studies on the underlying mechanism, murine embryonic and postnatal fibroblast lines (MEF or MPF, respectively) were established from WT, Nek1KO, and Rad54KO mice (see section 2.2.12). Following validation of their homozygosity by genotyping (see section 2.3.2.1, data not shown) and immunoblotting (Fig. 5A and 5B), fibroblasts were subjected to preliminary experiments comparing their repair capacities after DNA damage induction using γH2AX and Rad51 foci assays. For this, MPF and MEF lines were irradiated with 2 Gy, fixed 2 h or 6 h thereafter, and stained for cell cycle markers in combination with γH2AX as a general DSB marker or with Rad51 labeling DSBs undergoing HR-mediated repair. The resulting γH2AX and Rad51 foci were quantified in EdU-negative G2 phase fibroblasts as described in section 2.3.1.7 and corrected for endogenously arising foci in the unirradiated control samples thereby focusing the studies on the repair of radiation-induced DSBs. As a result, MPF lines accumulated a similar number of γH2AX foci independently of their genotype 2 h after irradiation (Fig. 5C). Within the following 4 h, WT MPF efficiently repaired these induced DSBs as shown by a significant reduction in their γH2AX foci level by around 75 %. In contrast, Nek1KO MPF and Rad54KO MPF exhibited a significant defect in DSB repair, since around 55% and 75% of γH2AX foci observed 2 h after irradiation were still present at the late time point, respectively. A similar pattern of results was obtained with the Rad51 foci assay (Fig. 5E). Accordingly, the number of DSBs associated with Rad51 was comparable between all genotypes at the early time point. Over time, WT MPF were able to reduce these HR events by around 75%, while Nek1KO MPF and Rad54KO MPF failed to resolve the majority of Rad51 foci. Comparing both assays, it was observed that the levels of remaining Rad51 foci in Nek1KO MPF and Rad54KO MPF at the late time point corresponded to their respective amounts of unresolved γH2AX foci. The data thus provided evidence that the deficiency in Nek1 impairs DSB repair in MPF like a Rad54 deficiency through a defect in the HR pathway.

In the case of MEF lines, WT MEF and Rad54KO MEF resembled the repair behaviors of their

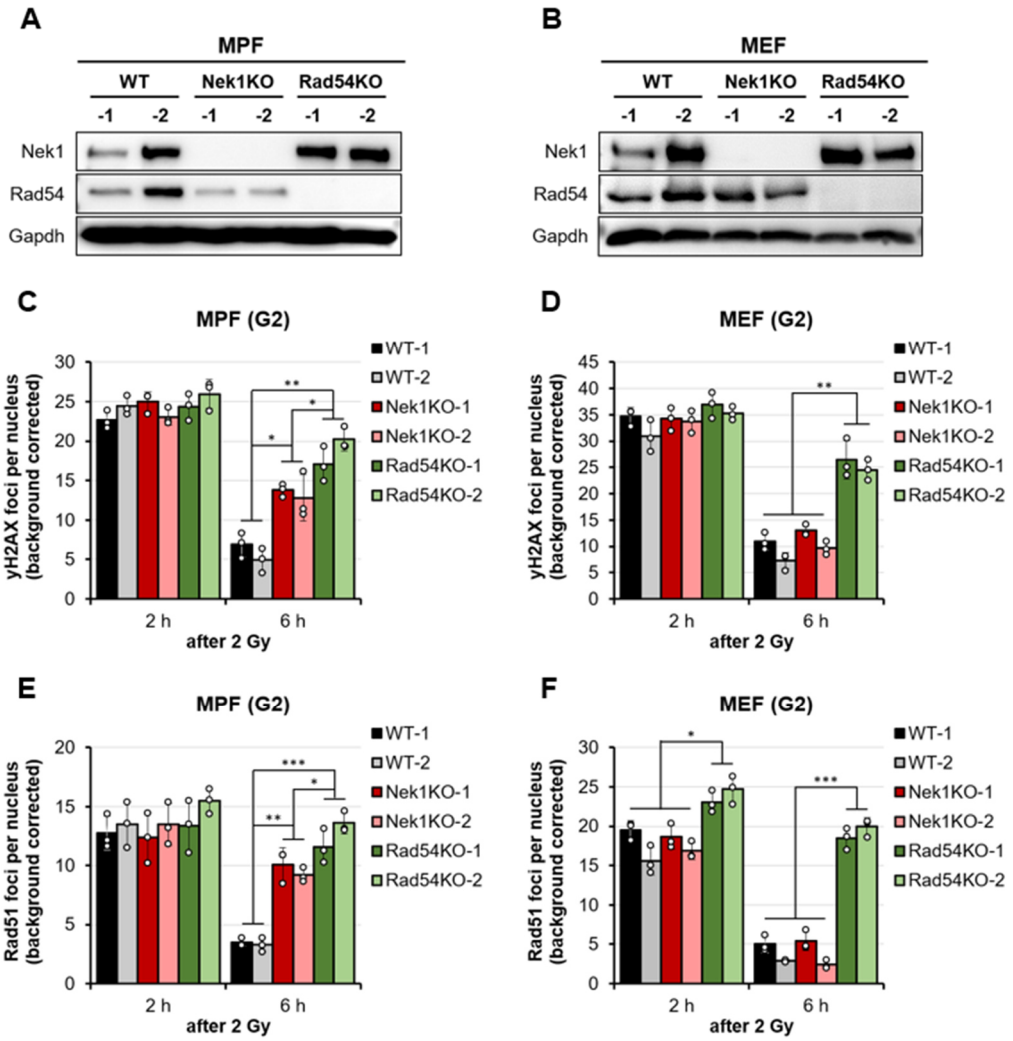

Fig. 5 Repair of radiation-induced DSBs in murine postnatal and embryonic fibroblasts. A, **B** Representative Western Blots showing the protein levels of Nek1 and Rad54 in two lines of untreated WT, Rad54KO and Nek1KO MPF (**A**) and MEFs (**B**). Gapdh served as loading control. **C**, **D** γH2AX foci assay in MPF (**C**) and MEF (**D**) lines. Fibroblasts were treated with 10 µM EdU for 1 h and then irradiated with 2 Gy, fixed 2 h or 6 h thereafter and stained for γH2AX, phospho-Histone 3 (pH3) and EdU. **E**, **F** Rad51 foci assay in MPF (**E**) and MEF (**F**) lines. Fibroblasts were treated as described for the γH2AX assay but stained for Rad51. Data are shown as mean values ± SDM (n=3). White circles indicate results from individual experiments derived from 50 EdU-negative, pH3-positive G2 phase cells. Spontaneous foci (background) were subtracted. *$p < 0.05$; **$p < 0.01$; ***$p < 0.001$; (Student's T-test). MPF, murine postnatal fibroblast; MEF, murine embryonic fibroblast

postnatal counterparts with around 75% of γH2AX or Rad51 foci being repaired in WT MEF and around 70% of γH2AX foci and 80% of Rad51 foci left unresolved in Rad54-deficient cells (Fig. 5D and 5F). Strikingly, Nek1KO MEF displayed a strong efficiency in the clearance of both, γH2AX and Rad51 foci to a level comparable with the level in WT MEF, thereby contradicting the repair defect measured in Nek1-deficient postnatal fibroblasts. In summary, these results reflected the situation observed *in vivo* and confirmed the applicability of the established fibroblast lines for further studies.

Given the opposing repair behaviors seen in Nek1-deficient MPF and MEF, γH2AX foci assays

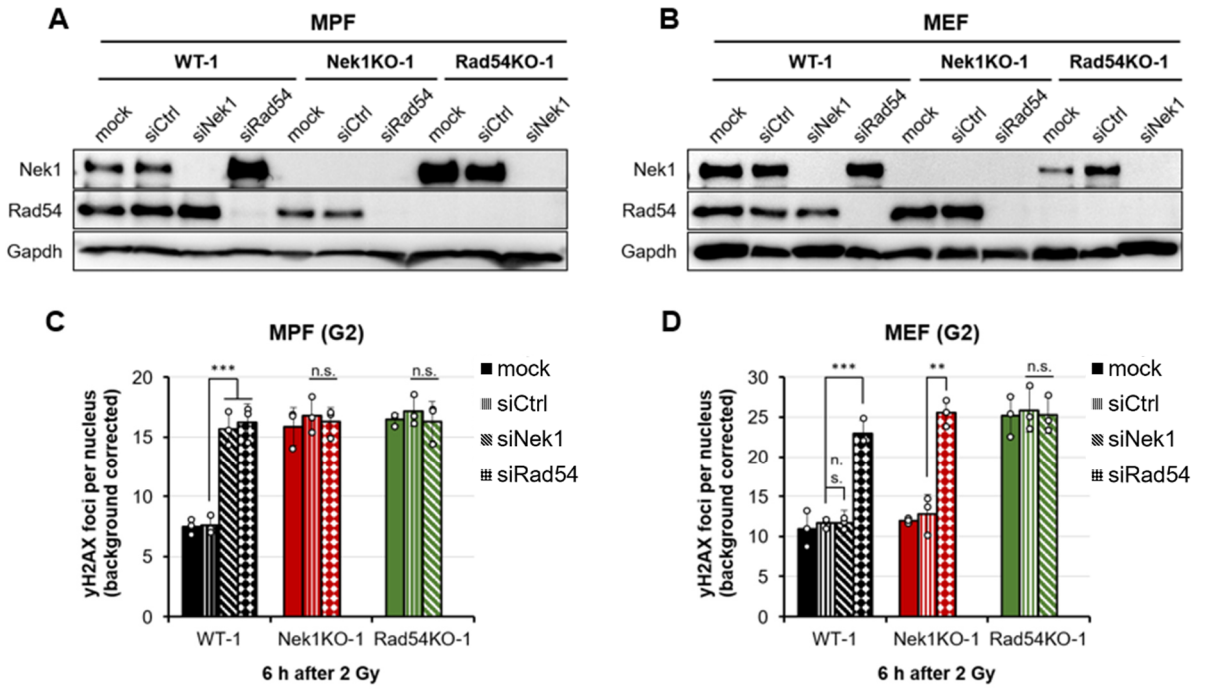

Fig. 6 Repair of radiation-induced DSBs in murine postnatal and embryonic fibroblasts transiently depleted for Nek1 and Rad54. A, **B** Representative Western Blots showing the protein levels of Nek1 and Rad54 in WT, Rad54KO and Nek1KO MPF (**A**) and MEFs (**B**) following transfection with 100 nM unspecific control, Nek1- or Rad54-specific siRNA for 72 h at standard conditions. Gapdh served as loading control. **C**, **D** γH2AX foci assay in MPF (**C**) and MEF (**D**) lines. 72 h after siRNA transfection, fibroblasts were treated with 10 µM EdU for 1 h and then irradiated with 2 Gy, fixed 6 h thereafter and stained for γH2AX, phospho-Histone 3 (pH3) and EdU. Data are shown as mean values ± SDM (n=3). White circles indicate results from individual experiments derived from 50 EdU-negative, pH3-positive G2 phase cells. Spontaneous foci (background) were subtracted. $^{**}p < 0.01$; $^{***}p < 0.001$; n.s.: non-significant (Student's T-test). MPF, murine postnatal fibroblast; MEF, murine embryonic fibroblast

elaborate on the connection between Nek1 and the HR repair pathway. Accordingly, fibroblasts were transfected with control, Nek1- or Rad54-specific siRNAs and incubated for 72 h at standard conditions to robustly knockdown *nek1* and *rad54* (Fig. 6A and 6B). After irradiation with 2 Gy, the γH2AX foci assay was conducted as previously described focusing on EdU-negative G2-phase cells at the late timepoint of HR-mediated repair 6 h after irradiation. WT MPF depleted for either Rad54 or Nek1 exhibited a strong DSB repair defect leaving twice as many γH2AX foci unresolved than in fibroblasts transfected with unspecific siRNA (Fig. 6C). These knockdown-induced repair defects in WT fibroblasts corresponded to the defects visualized in the respective KO fibroblast lines. However, the depletion of Rad54 in Nek1KO MPF, and vice versa, was not associated with an enrichment of unrepaired DSBs beyond the level already detectable in the respective siCtrl-transfected KO cells. This epistatic relationship of Nek1 and Rad54 consolidated the previous finding that Nek1 belongs to the HR repair pathway. In contrast, the capacity of WT MEF to repair DSBs was significantly affected by the depletion of Rad54 but not by the depletion of Nek1 (Fig. 6D). Furthermore, the amount of

γH2AX foci in MEF deficient for both, Rad54 and Nek1 did not rise above the level observed in Rad54KO MEF, thereby excluding a synergistic relationship between these factors at embryonic stages. Collectively, these data indicated that the regulation of Rad54 changes during development and prompted the question of whether Rad54 could function independently of phosphorylation and may thus be constantly active in embryonic cells.

2.4.2 Regulating Rad54 is crucial for both, MPF and MEF

Although the data presented in the prior section confirmed that Nek1 is part of the HR pathway in MPF, it needed to be clarified whether it regulates HR like already described for HeLa cells by activating Rad54 through phosphorylation of the serine residue at position 572 (Ser572). To address this question, two novel mouse strains were generated by Florian Frohns and Emilie Renaud in cooperation with the company Cyagene as part of the BMBF-funded NeuroRad project. These mice were supplied with a conditional Knock-In (KI) system in exon 12 of the Rad54 gene where the Ser572 is located. The KI system consisted of two segments, a floxed WT Rad54 gene sequence connected to the mCherry gene and an unfloxed Rad54 exon variant coupled to the EGFP gene (Fig. 7A) which harbors a mutation that results in the substitution of the Ser572 residue to either alanine (Rad54S/A) or glutamate (Rad54S/E). When pairing these mice with Cre mice, the WT Rad54 gene cassette is removed from the genome through Cre-mediated recombination of the LoxP sites (Fig. 7A) and the mutant Rad54 gene is expressed (activated, act) in the descendant mice. As a result, a GFP- tagged Rad54 protein is produced that, according to previous studies in HeLa cells, is phosphodefective, not activatable, in the Rad54S/AKIact strain or phosphomimetic, permanently active, in the Rad54S/EKIact strain.[111] Since endogenously produced recombinases can contribute to the formation of DSBs, these mice were backcrossed with WT mice to remove the Cre gene from the genome.[128]

For the following studies, postnatal fibroblast lines were established from both Rad54KIact strains, spontaneously immortalized, and genotyped to verify the successful removal of the WT Rad54 locus and the Cre gene as well as to determine homozygosity of the KI alleles using several PCR assays established by Emilie Renaud (see section 2.3.2.1, data not shown). The functional expression of both Rad54 gene variants was controlled with immunofluorescent assays. For this, Rad54KIact fibroblasts were irradiated with 2 Gy, fixed 3 h thereafter, and stained for Rad54, GFP, and either mCherry or the DSB marker γH2AX. Rad54S/AKIact and Rad54S/EKIact fibroblast lines exhibited Rad54 foci which colocalized with GFP but not mCherry confirming both, the production of the Rad54 variants and the removal of the WT Rad54 gene cassette (Fig. 7B). Moreover, both proteins colocalized with γH2AX foci indicating that the introduced mutations did not interfere with the recruitment of Rad54 to sites of DNA damage (Fig. 7C). Finally, γH2AX foci assays were conducted and evaluated similarly to the

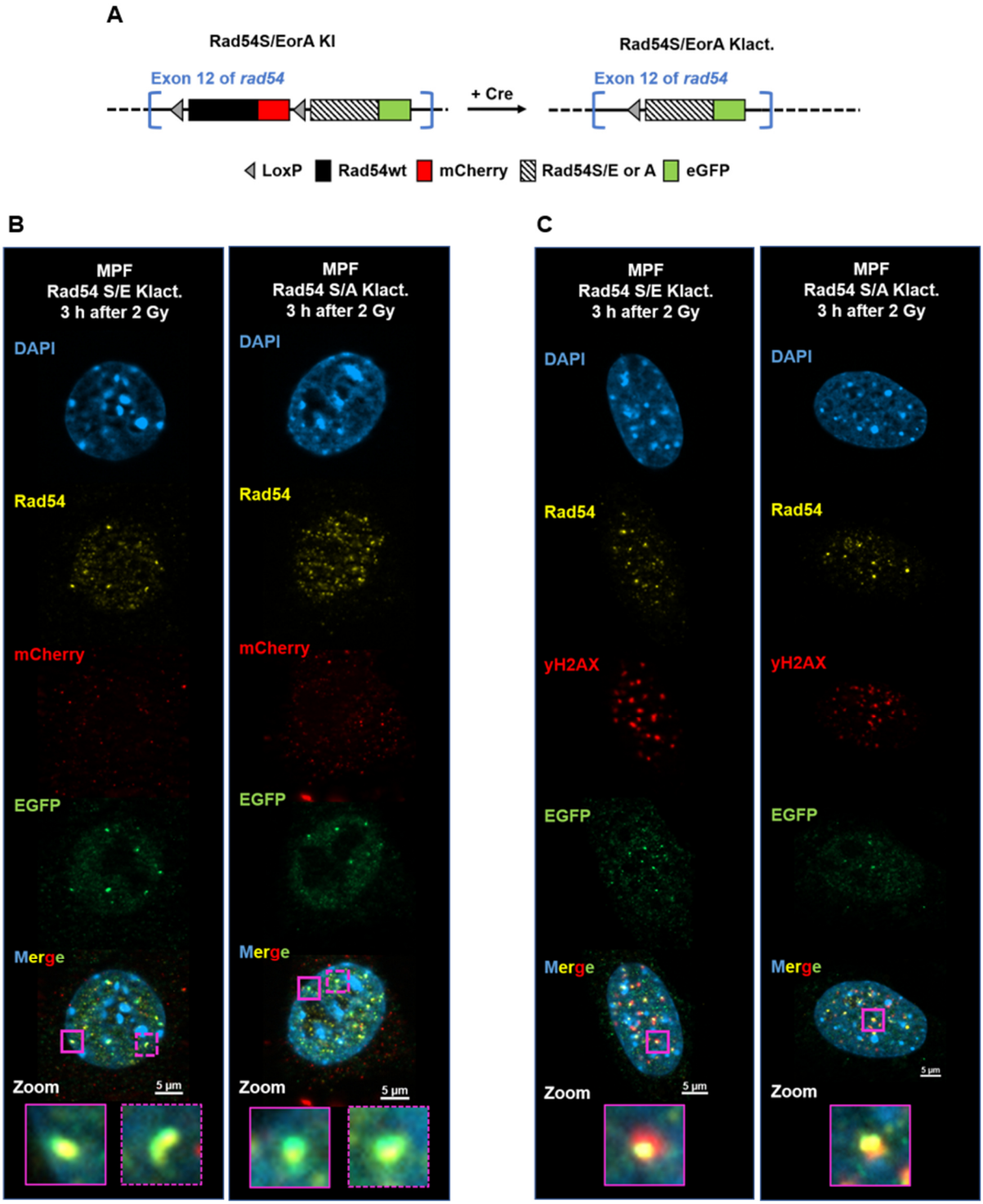

Fig. 7 Introduction of the Rad54Klact mice and fibroblast lines. A Schematic presentation of the genetic modifications in Rad54 mutant mice. Founder mice (Rad54S/EorA KI, left) harbor a conditional Knock-In (KI) system consisting of a wildtype Rad54-mCherry cassette and a mutant Rad54-GFP cassette. Recombination of the LoxP site flanking the wildtype Rad54 cassette was induced by mating with mice expressing Cre recombinase. As a result of Cre-mediated recombination, the descendant mice (Rad54S/E or A Klact, right) lose the wildtype Rad54 cassette and express the mutated one harboring the S572E or S572A substitutions. These mice were finally backcrossed with WT mice to remove the Cre gene from the genome and, thus, to avoid potential Cre-related DSB induction. **B**, **C** Representative images of colocalization studies done with Rad54Klact postnatal fibroblasts. Fibroblasts were irradiated with 2 Gy, fixed 3 h thereafter and stained for DNA (DAPI, blue) Rad54 (yellow), mCherry (red), EGFP (green) in (**B**) or for DNA (DAPI, blue), Rad54 (yellow), γH2AX (red),

EGFP (green) in (**C**). Examples of Rad54-GFP and Rad54-GFP-γH2AX colocalizations are depicted in a magnified version (Zoom). Images were taken at a 1000x magnification using an Axioimager M1 microscope equipped with an ApoTome.2. MPF, murine postnatal fibroblast

experiments done with KO fibroblasts (see section 2.4.1) to examine the effects of the modified Rad54 proteins on HR-mediated repair. Interestingly, unirradiated Rad54S/EKIact fibroblasts accumulated twice as many endogenous γH2AX foci compared to WT, Rad54KO, and Rad54S/AKIact fibroblasts (Fig. 8A) indicating that the production of a constantly active Rad54 variant negatively affects the ability of these cells to cope with endogenously arising replication stress. After irradiation with 2 Gy, all Rad54KIact fibroblast lines induced around 10 γH2AX foci more compared to WT or Rad54KO fibroblast lines (Fig. 8B). Consequently, the number of γH2AX foci left at the late timepoint was normalized to the respective number of induced foci to facilitate the comparison between the repair behaviors observed in WT, Rad54KO, and Rad54KIact fibroblast lines (Fig. 8C). Rad54S/EKIact fibroblasts efficiently repaired radiation-induced DNA damage and approached a level of remaining DSBs similar to WT fibroblasts. Rad54S/AKIact fibroblasts rather behaved like Rad54KO fibroblasts and, thus, exhibited a strong repair defect with around 80% of radiation-induced DSBs left unrepaired. Together, these data underlined the importance of the Ser572 residue for the spatiotemporally correct activation of Rad54.

To verify the Ser572 residue as the site for Nek1-mediated phosphorylation, γH2AX foci were counted in irradiated Rad54KIact MPF transiently depleted for Nek1 (Fig. 8D). The repair efficiency of Rad54S/EKIact fibroblasts did not depend on the availability of Nek1 as shown by a constant amount of 15 foci left unresolved in all conditions 6 h after irradiation (Fig. 8E). This indicates that producing a permanently active form of Rad54 rescues the DSB repair defect observed in Nek1-depleted WT MPF (see Fig. 8C). Depleting Nek1 in Rad54S/AKIact fibroblasts did not aggravate the already existing repair defect showing that the absence of the Ser572 residue suffices to resemble the effect of a Nek1 deficiency in WT fibroblasts. In conclusion, these results ultimately confirmed that murine Nek1 regulates HR in postnatal fibroblasts similarly to human Nek1 in HeLa cells by activating Rad54 through phosphorylation of its Ser572 and that this process is essential to maintain the functionality of HR in postnatal cells.

As shown in section 2.4.1, HR-mediated repair in MEF was not affected by the depletion of Nek1 thereby clearly contradicting the situation observed in postnatal fibroblasts. To examine whether Rad54 needs to be activated by phosphorylation also in embryonic stages, γH2AX foci assays were repeated with MEF isolated from both Rad54KIact mouse strains as described for the respective MPF lines. Accordingly, MEF producing the constantly active Rad54S/E protein accumulated a high amount of spontaneous DSBs (Fig. 8F) but were able to cope with radiation-induced DSBs very efficiently (Fig. 8G). MEF producing the phosphode-

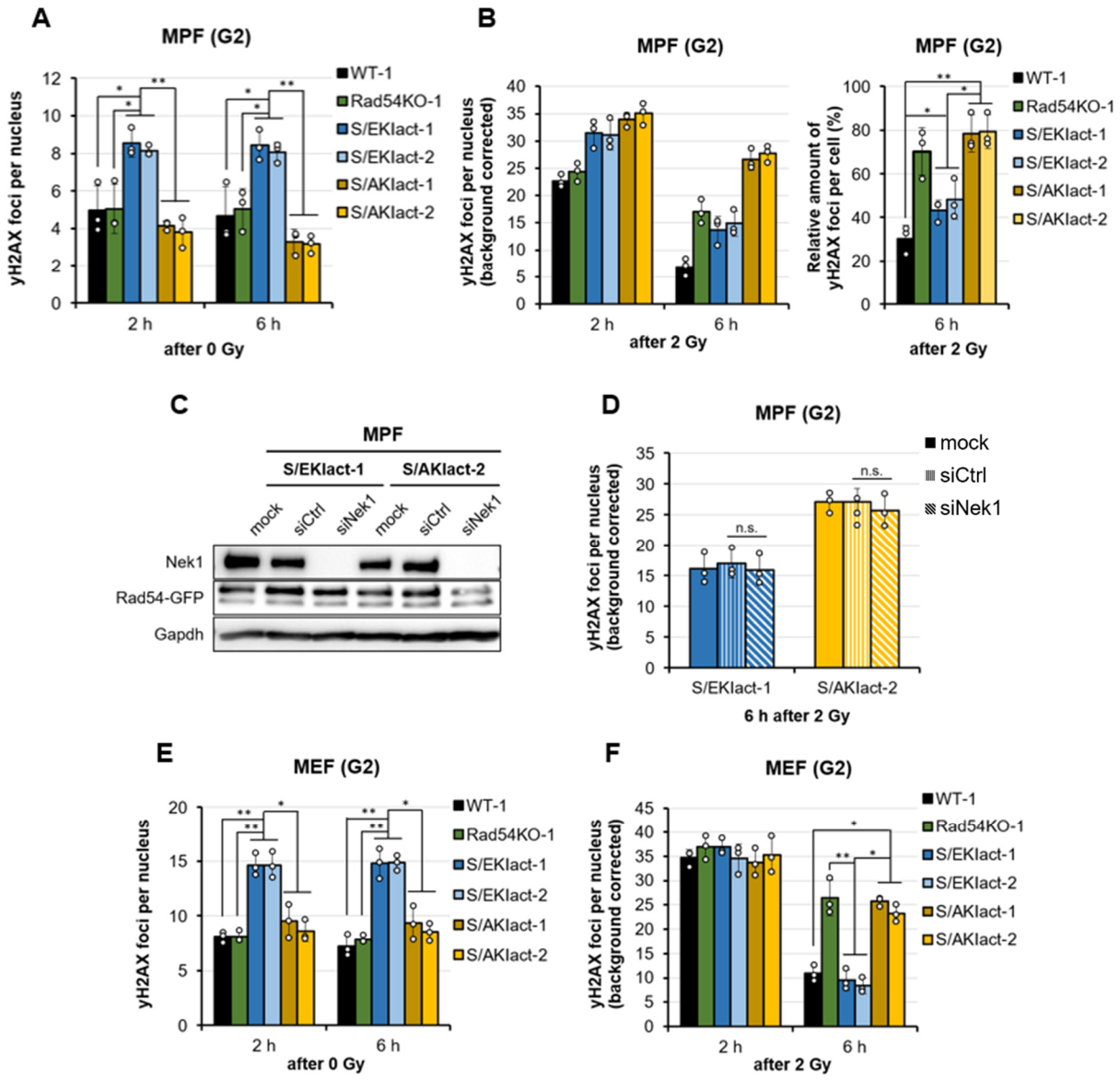

Fig. 8 Repair of radiation-induced DSBs in murine postnatal and embryonic KI fibroblasts. A γH2AX foci assay in unirradiated WT, Rad54KO and Rad54KIact MPF lines. Fibroblasts were treated with 10 µM EdU for 1 h, fixed 2 h or 6 h thereafter and stained for γH2AX, phospho-Histone 3 (pH3) and EdU. **B** γH2AX foci assay in irradiated WT, Rad54KO and Rad54KIact MPF lines (**left**). Fibroblasts were treated with 10 µM EdU for 1 h, fixed 2 h or 6 h after irradiation with 2 Gy (see **A** for staining). Data from WT-1 and Rad54KO-1 MPF were pasted from **figure 5C** (see **right** panel for legend). Relative amount of residual γH2AX foci in MPF lines (**right**). γH2AX foci remaining 6 h post irradiation were normalized to the respective foci numbers 2 h after irradiation. **C** Representative Western Blot showing the protein levels of Nek1 and Rad54 in WT and Rad54KIact MPF following transfection with 100 nM unspecific control or Nek1-specific siRNA for 72 h at standard conditions. Gapdh served as loading control. **D** γH2AX foci assay in Rad54KIact MPF lines. 72 h after siRNA transfection, fibroblasts were treated with 10 µM EdU for 1 h and then irradiated with 2 Gy, fixed 6 h thereafter and stained for γH2AX, phospho-Histone 3 (pH3) and EdU. **E**, **F** γH2AX foci assay in unirradiated (**E**) and irradiated (**F**) WT, Rad54KO and Rad54KIact MEF lines (see **A**, **B** for treatment). Data from WT-1 and Rad54KO-1 MEFs shown in (**F**) were pasted from **figure 5D**. Data are shown as mean values ± SDM (n=3). White circles indicate results from individual experiments derived from 50 EdU-negative, pH3-positive G2 phase cells. Spontaneous foci (background) were subtracted. *$p < 0.05$; **$p < 0.01$; n.s.: non-significant (Student's T-test). MPF, murine postnatal fibroblast; MEF, murine embryonic fibroblast

fective Rad54S/A variant, however, developed a strong repair defect following irradiation which resembled the defect mediated by the Knock-Out of Rad54 (Fig. 8G). These results demonstrate that Rad54 needs to be activated in embryonic cells and, more importantly, that this activation is subject to regulation to prevent negative effects on the handling of endogenously arising replication stress during S phase. Under consideration of this and the previously shown data, the functionality of HR-mediated repair in MEF was assumed to be secured by a second kinase that compensates for the loss of Nek1 in HR.

2.4.3 Nek3 and Nek5 regulate HR in MEF

The observation that Rad54's activity is regulated also in MEF sparked substantial interest in the identification of the kinase that assists Nek1 in HR at embryonic stages. The Nek kinase family contains 10 other members which accordingly share high homology in their kinase domains and could therefore possibly accept Rad54 as a substrate (see section 1.3). Considering that embryonic and postnatal fibroblasts mainly differ in their level of differentiation, it was speculated that another Nek gene may be highly expressed in MEF and, during the process of differentiation, is downregulated in MPF. Consequently, the expression levels of all Nek genes were analyzed in both, WT MEF and WT MPF using an SYBR green-based qPCR assay. For this, total RNA was isolated from unirradiated fibroblasts, reversely transcribed into cDNA, combined with Nek-specific primers (see section 2.2.7), and finally subjected to qPCR. Fold changes (FC) in Nek gene expression were assessed with the $2^{-\Delta\Delta Ct}$ method normalizing the resulting expression levels of the Nek genes in WT MEF to their respective levels in WT MPF. Nek1, 2, 6, 7, 8, 9, 10, and 11 genes were similarly expressed in both, embryonic and postnatal fibroblasts (Fig. 9A). The expression of *nek4* and *nek10* was significantly downregulated in MEF compared to MPF whereas *nek3* and *nek5* were expressed 3-fold and 5.5-fold higher in MEF, respectively, implying an important role for these kinases at embryonic stages.

Since these results alone did not allow reliable statements about the involvement of Nek kinases in the HR pathway, a functional siRNA screen was included in this study to evaluate the consequences of depleted Nek kinases on HR-mediated repair. For this, WT and Nek1KO MEF were transfected with unspecific control or Nek-specific siRNAs as described before and subjected to the γH2AX foci assay. The successful knockdown of Nek genes was validated using the aforementioned qPCR assay in which the siCtrl-samples served as a basis for normalization (Fig. 9B). In contrast to the loss of Rad54, the depletion of Neks did not confer a DSB repair defect in WT MEF (Fig. 9C) or Nek1KO MEF (Fig. 9D). This result implies that the Nek family members may be not involved in the HR of embryonic cells. However, from a different view, it could also suggest that a combination of Nek kinases redundantly regulates HR-mediated repair at embryonic stages independently of Nek1. Knowing that Nek3 and Nek5 are not only phylogenetically closer related to Nek1 than the other Nek family members (see

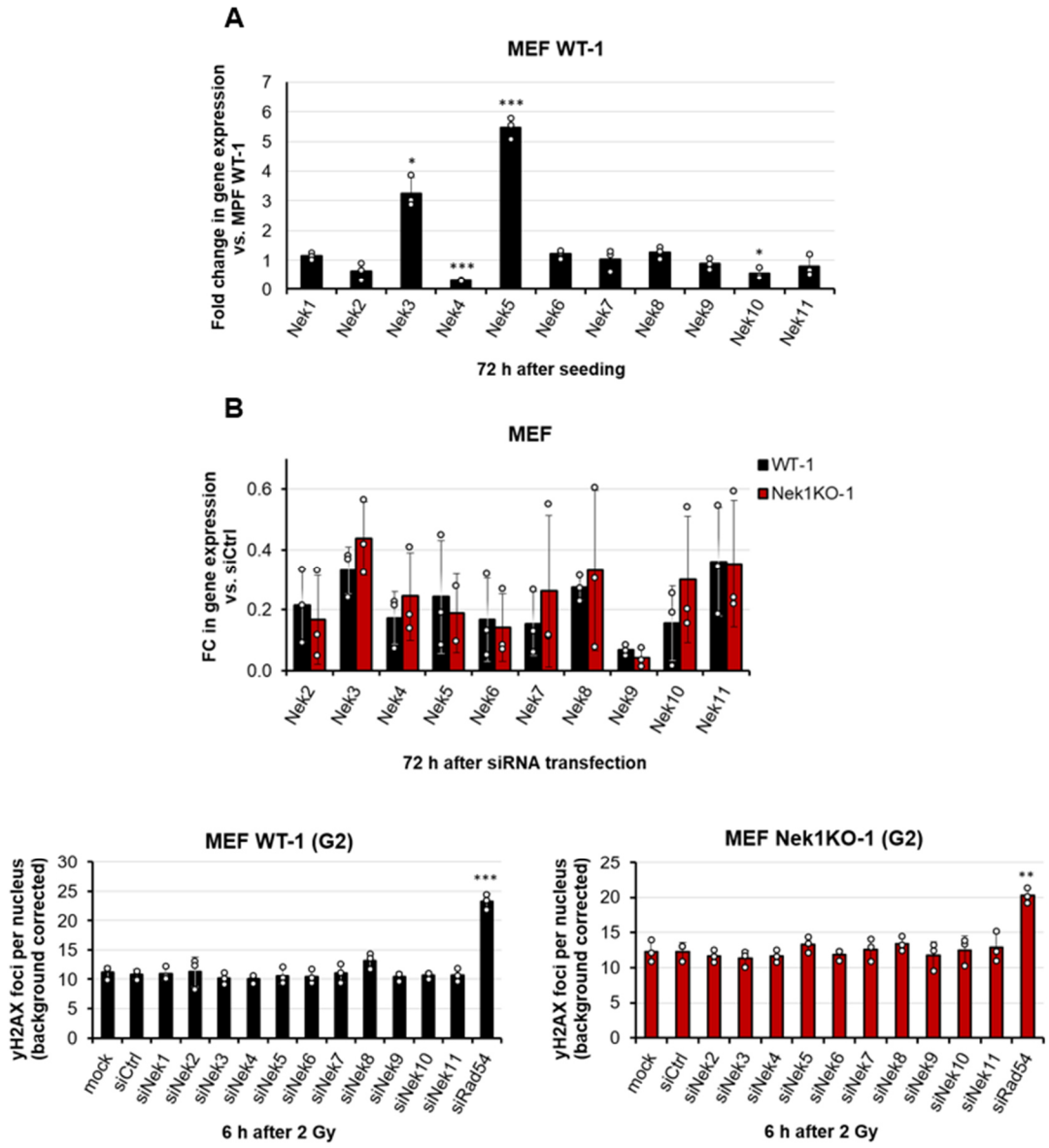

Fig. 9 Expression levels of Nek genes in murine WT fibroblasts and repair of radiation-induced DNA damage following Nek depletion in murine embryonic WT and Nek1KO fibroblasts. **A** Differential gene expression analysis in untreated WT MEF. RNA was isolated from untreated fibroblasts 72 h post seeding, converted into cDNA, and finally analyzed using qPCR and specific primers. Fold changes in expression were calculated with the $2^{-\Delta\Delta Ct}$ method using *Gapdh* as a reference gene and normalizing the expression levels of *neks* in WT MEF to their respective level in WT MPF. **B** Gene expression analysis in WT and Nek1KO MEF following siRNA transfection. Fibroblasts were treated with 100 nM unspecific control or Nek-specific siRNA for 72 h at standard conditions. Fold changes in expression were again calculated with the $2^{-\Delta\Delta Ct}$ method using *Gapdh* as a reference gene and normalizing the expression levels of *Neks* in fibroblasts treated with Nek-specific siRNAs to their respective level in fibroblasts treated with siCtrl. **C**, **D** γH2AX foci assay in WT (**C**) and Nek1KO (**D**) MEF. 72 h after siRNA transfection, fibroblasts were treated with 10 µM EdU for 1 h and then irradiated with 2 Gy, fixed 6 h thereafter, and stained for γH2AX, phospho-Histone 3 (pH3), and EdU. Data are shown as mean values ± SDM (n=3). White circles indicate results from individual experiments which in the case of γH2AX foci assays in **C** and **D** were derived from 50 EdU-negative, pH3-positive G2 phase cells. Spontaneous foci (background) were subtracted. *p < 0.05, **p < 0.01; ***p < 0.001; versus WT MPF or siCtrl (Student's T-test). MPF, murine postnatal fibroblast; MEF, murine embryonic fibroblast

section 1.3.1) but are also significantly higher expressed in MEF compared to MPF, it was hypothesized that both kinases might be able to phosphorylate Rad54 and, thus, replace Nek1 in the HR pathway at embryonic stages. MEF lines were therefore depleted for both, Nek3 and Nek5 using the aforementioned siRNAs and processed to generate protein lysates for the validation of the double-knockdown via immunoblotting. Unfortunately, several supposedly Nek3- and Nek5-specific antibodies were purchased and tested (see section 2.2.9), but none of them was found to be suitable for knockdown validation. Due to this circumstance, qPCR analyses had to be applied to detect and confirm the depletion of Nek3 and Nek5 in fibroblasts (Fig. 10A and 14B). Subsequently, WT and Nek1KO MEF were irradiated with 2 Gy and subjected to the γH2AX foci assay as described before. Both cell lines were able to resolve γH2AX foci as efficiently as siCtrl-treated cells when depleted for either Nek3 or Nek5, yet exhibited around 10 more unresolved γH2AX foci than the respective control cells when transfected with both, siNek3 and siNek5 (Nek3+5, Fig. 10C). Nek3+5-depleted Rad54KO MEF, however, did not accumulate more DSBs than siCtrl-transfected fibroblasts (Fig. 10C), which was also observed for Nek3+5-depleted WT postnatal fibroblasts (Fig. 10D). Together, these results clarified several issues. First of all, since the codepletion of Nek3 and Nek5 impaired DSB repair in WT MEF like a Rad54 deficiency while not aggravating the already existing repair defect in Rad54KO MEF, both kinases function epistatically to Rad54. In this context, it is noteworthy that Nek3 and Nek5 can compensate for each other, considering the unaffected repair behavior of WT MEF lacking either Nek3 or Nek5. Secondly, Nek1 is not relevant for the functionality of HR-mediated repair at embryonic stages as shown by the similarly affected repair behaviors of WT and Nek1KO MEF in a Nek3+5-depleted background. Finally, given the absent effects on DSB repair in Nek3+5-depleted WT MPF, the affiliation of both kinases with the HR pathway is most likely restricted to embryonic cells.

To determine whether Nek3 and Nek5 regulate HR in embryonic cells similarly to Nek1 in postnatal cells in dependency of Rad54's Ser572 residue, Nek3+5-depleted Rad54KIact MEF were subjected to the γH2AX foci assay. Strikingly, Rad54S/EKIact fibroblasts repaired radiation-induced DSBs efficiently independently of their Nek3+5 status (Fig. 10E) indicating that they can evade the Nek3+5- mediated DSB repair defect observed in the WT fibroblasts through the production of a permanently active form of Rad54. In addition, the already existing repair defect in Rad54S/AKIact fibroblasts was unperturbed following the depletion of Nek3+5. Collectively, these results demonstrate that HR-mediated repair in embryonic cells depends on Nek3 and Nek5 for the activation of Rad54.

The hypothesis of Nek3 and Nek5 having a redundant function which is crucial for embryonic HR was further tested in rescue assays, in which Nek3+5-depleted WT and Nek1KO MEF were transfected with plasmids expressing siRNA-resistant, GFP-tagged wildtype or mutant variants of *nek3* and *nek5*. These variants were generated similarly to the already published

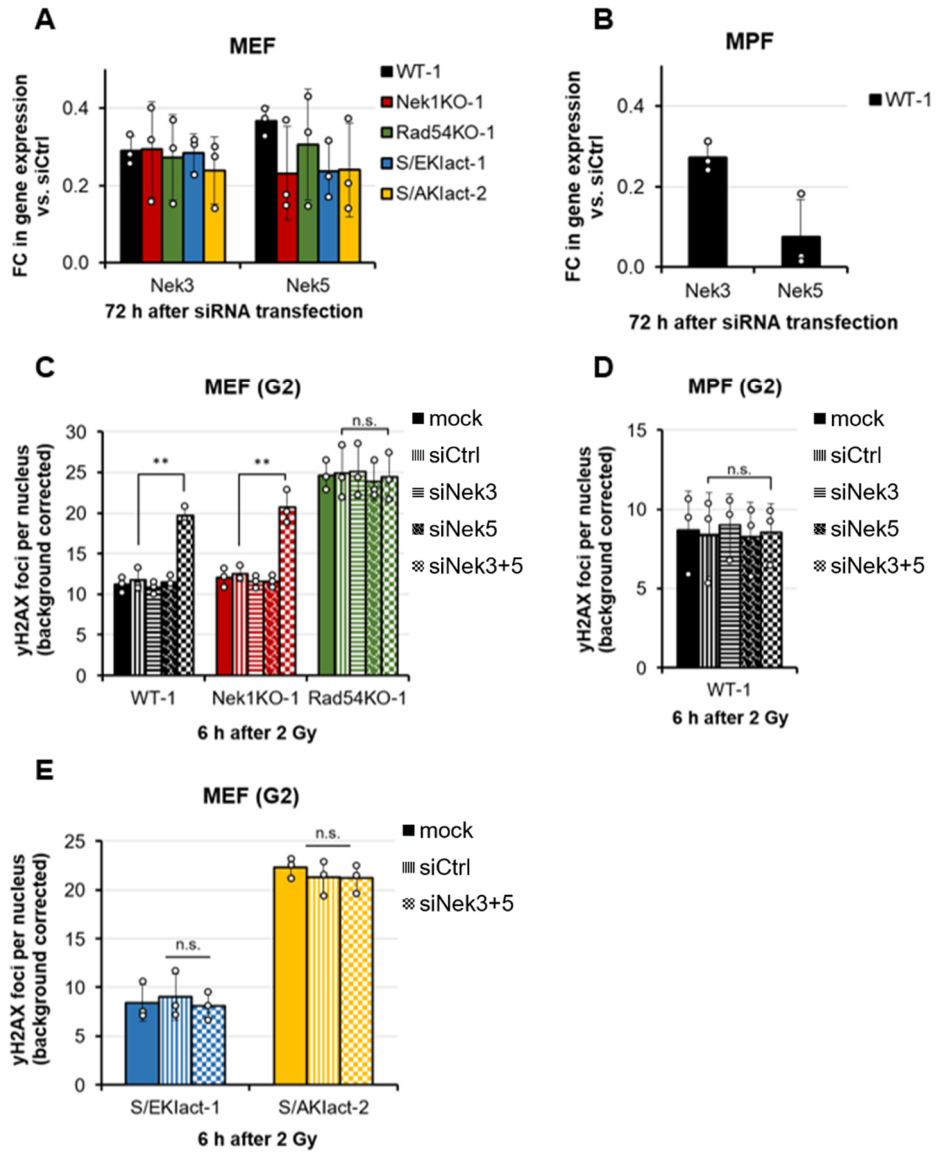

Fig. 10 Repair of radiation-induced DSBs in Nek3- and Nek5-depleted murine postnatal and embryonic fibroblasts. A, **B** Gene expression levels of Nek3 and Nek5 in WT, Rad54KO, Nek1KO MEFs and Rad54KIact (**A**) as well as WT MPF (**B**) following transfection with both, 100 nM Nek3- and Nek5-specific siRNAs for 72 h at standard conditions. Values are depicted as fold change to samples treated with siCtrl. **C**-**E** γH2AX foci assay in WT, Nek1KO, Rad54KO MEF (**C**), Rad54KIact MEF (**D**) and WT MPF (**E**). 72 h after siRNA transfection, fibroblasts were treated with 10 µM EdU for 1 h, irradiated with 2 Gy, fixed 6 h thereafter and stained for γH2AX, phospho-Histone 3 (pH3) and EdU. γH2AX foci were counted in 50 EdU-negative, pH3-positive G2 phase cells per experiment. Spontaneous foci (background) were subtracted. Data are shown as mean values ± SDM (n=3). White circles indicate results from individual experiments. $^{**}p < 0.01$; n.s.: non-significant (Student's T-test). MPF, murine postnatal fibroblast; MEF, murine embryonic fibroblast

kinase-dead form of Nek1 by substituting the highly conserved Lysin33 residue with Arginine (K33R).[111] After verification of the successful depletion of endogenous Nek3 and Nek5 via qPCR (Fig. 10A) and the production of GFP-Nek3 and -Nek5 by immunofluorescence (Fig. 11A and 11B), fibroblasts were irradiated and subjected to the γH2AX foci assay measuring the amount of DSBs in GFP-positive, pH3-positive, EdU-negative G2-phase cells at the late

timepoint of repair 6 h after irradiation. Nek3+5-depleted WT and Nek1KO MEF producing only GFP exhibited around 10 residual γH2AX foci more than Nek3+5 proficient cells (Fig. 11C). This repair defect was not detectable in fibroblasts that were depleted for endogen ous Nek3+5 but produced the siRNA-resistant wildtype forms of Nek3 or Nek5. Conversely, complementing the Nek3+5 depletion in MEF with the kinase-dead Nek3-K33R or Nek5-K33R variants resulted in a similar amount of unrepaired DSBs compared to GFP-producing Nek3+5-depleted fibroblasts. Taken together, these observations confirm the specific downregulation of Nek3+5 using the aforementioned siRNAs and consolidated the hypothesis that, instead of Nek1, Nek3 and Nek5 are necessary for the functional repair of DSBs via HR in embryonic fibroblasts.

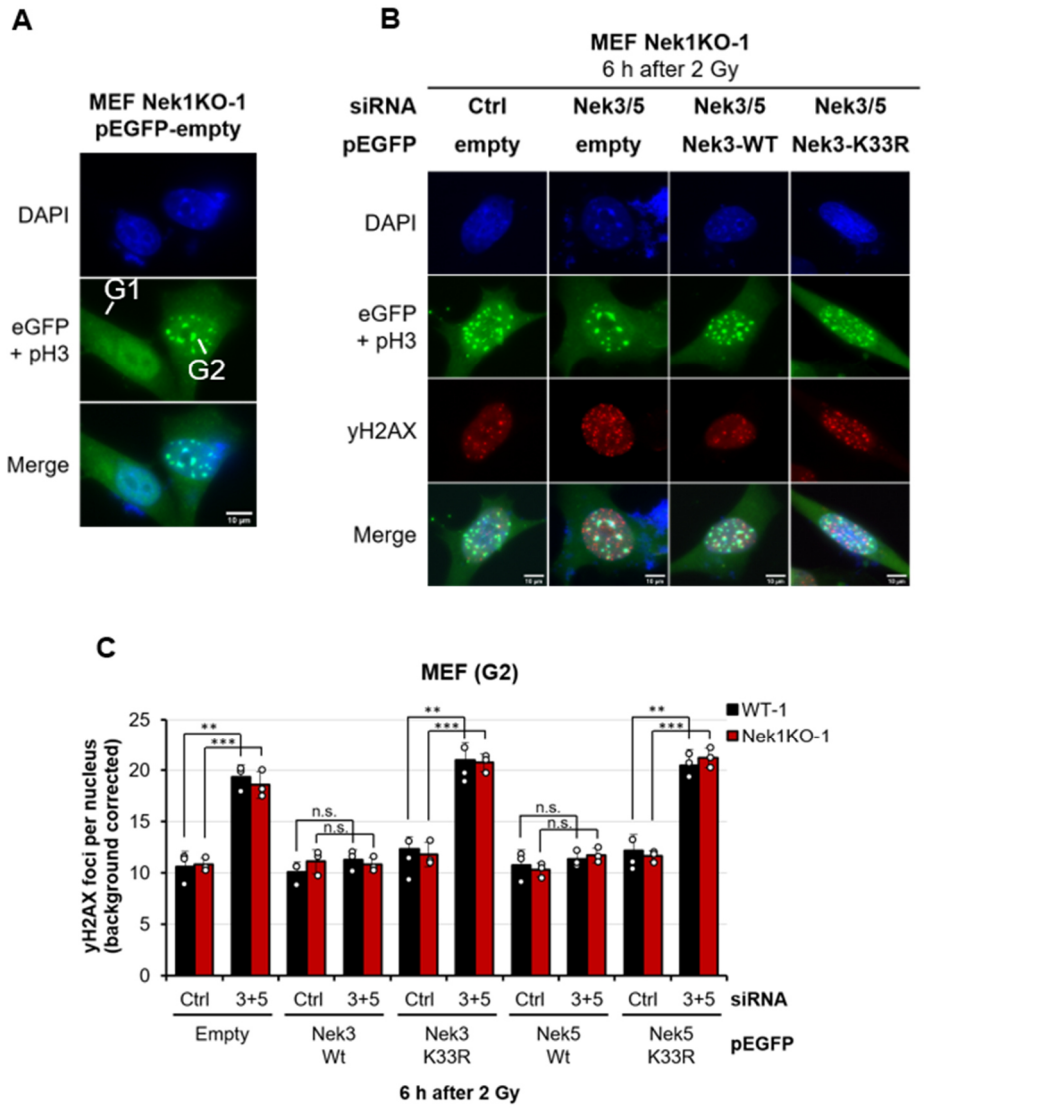

Fig. 11 Repair of radiation-induced DSBs in murine postnatal and embryonic fibroblasts expressing Nek3 or Nek5 variants. A Representative fluorescent images demonstrating how GFP-positive G1 cells were discriminated from GFP-positive G2 cells using a pH3-GFP double staining. Nek1KO MEFs were transfected with 10 µg of pEGFP and stained 48 h afterwards for DAPI, phospho-Histone 3 (pH3) and GFP. Since the GFP signal spreads across the whole cell and the pH3 signal is not only restricted to the nucleus (see also Fig. 4) but also very foci-like, both targets can be stained in the same channel without being confused. **B**, **C** Rescue assay in WT and Nek1KO MEFs. Fibroblasts were treated with 100 nM unspecific control or Nek3- and Nek5-specific siRNAs for 24 h at standard conditions followed by transfection with 10 µg of plasmids coding for only GFP, the wildtype form of Nek3+5 (Wt) or a kinase-dead variant of Nek3+5 (K33R). 48 h after plasmid transfection, fibroblasts were treated with 10 µM EdU for 1 h and then irradiated with 2 Gy, fixed 6 h thereafter and stained for γH2AX, pH3, GFP and EdU. Representative fluorescent images are presented in **B** and data are shown in **C** as mean values ± SDM (n=3). White circles indicate results from individual experiments derived from 50 EdU-negative, pH3/GFP-positive G2 phase cells. Spontaneous foci (background) were subtracted. $^{**}p < 0.01$; $^{***}p < 0.001$; n.s.: non-significant (Student's T-test). MEF, murine embryonic fibroblast

2.5 Discussion

Homologous recombination has been a prominent subject of research for at least 50 years and its basic mechanism is therefore well understood. In light of this study, however, there is still much to be learned about the dynamics of higher-level regulations that integrate this pathway into an evolving cellular signaling network while ensuring its spatiotemporally correct progression.

The data described in this thesis further strengthens Nek1's role in HR firstly described by Spies *et al*.[111] More importantly though, they demonstrate that Rad54's activity needs to be regulated throughout development and that the kinases required for this process change in response to an organism's developmental stage: Nek3 and Nek5 redundantly activate Rad54 in embryonic cells whereas Nek1 exclusively controls this procedure in adult cells.

Notably, the changing involvement of Nek1 in HR has been recognized in recent ALS-associated research. As outlined in the introduction, dysfunctional Nek1 variants are strongly correlated with the onset of ALS and, in some cases, even represent the monogenic cause of disease.[101] To elucidate whether Nek1's DDR-related functions play a pivotal role in this association, Higelin *et al*. characterized the DNA repair behavior of induced pluripotent stem cells (iPSCs) and differentiated motor neurons, which were derived from an ALS patient with drastically reduced Nek1 protein levels due to a heterozygous mutation in the respective gene.[103] By quantifying γH2AX-positive nuclei 1 h and 24 h after irradiation with 0.5 Gy, a significant repair defect was detected in young *nek1*-mutated motor neurons (21 days in culture) which became even stronger with increasing cell maturation (42 days in culture). Strikingly, the corresponding iPSC population exhibited a robust decline in γH2AX-positive nuclei within 23 h after irradiation suggesting that the induced DNA damage was efficiently repaired despite the mutation-related loss of functional Nek1.[103] Although the approach including cell model and methodology fundamentally differs and thus complicates data comparability, the general outcome of this study is consistent with the here presented work demonstrating that adult Nek1KO fibroblasts suffer from a repair defect after irradiation, whereas embryonic Nek1KO fibroblasts do not.

Based on the depicted data, it is fair to wonder whether Nek1's functionality transforms in the course of cellular differentiation. Evidence for this idea can be derived from research of the Kobarg lab, which studied the interactome of Nek1 twice. In the first study, a yeast-two-hybrid screen was conducted that eventually detected proteins with functions in ciliogenesis (Kif3A, tuberin, FEZ-1 and -2, etc.), the cell cycle (ATRX, 14-3-3), and/or DNA repair (ATRX, Mre11) as interactors of Nek1.[84] The second study focused more on Nek1's interactome in response to genotoxic stress.[69] The authors thus treated Flag-Nek1 producing human embryonic kidney cells (HEK) with cisplatin and subjected them to a LC-MS-based immunoprecipitation (IP) assay. As a result, many ciliary proteins, such as Filamin-A or Kif13A, and DDR factors, such

as ATR or FancA, were again associated with Nek1. However, although it can certainly be considered a key substrate of Nek1, Rad54 never emerged as interacting partner in any of these experiments. This was particularly surprising in case of the latter study since cisplatin induces crosslinks in the DNA that potentially disrupt the replication machinery during S phase and, thus, contribute to the formation of structurally specific DSBs, so-called one-ended DSBs. As these lesions are solely repairable via HR, the cisplatin treatment should have increased the number of Nek1-Rad54 interactions to a level detectable with IP. Interestingly, a review of the employed methods revealed that both Kobarg studies relied on the expression of a Nek1 cDNA from human fetal brain either for the modification of yeast cells or for Flag-Nek1 production.[69,84] This potentially explains why Rad54 could not be detected in these experiments as, according to the data presented in the last sections, Rad54 most likely is not a substrate of Nek1 in embryonic cells (further referred to as “embryonic” Nek1).

The same observation can be made for two other factors, namely Chk1 and Chk2, which were not identified as interactors by the Kobarg laboratory, despite being linked to Nek1. According to Chen *et al*., Nek1 phosphorylates Chk1 and Chk2 to regulate cell cycle progression in response to DNA damage induced by IR, UV, oxidative stress, or cisplatin.[105,109] Strikingly, this direct association was demonstrated in differentiated cell models including human renal tubular epithelial cells as well as murine postnatal fibroblasts. Liu *et al*. conducted quite similar studies, but used HEK cells and demonstrated that Nek1 is indeed involved in cell cycle regulation, but only indirectly by activating ATR.[108] In summary, the described data argues for a dynamic functionality of Nek1 during development which might present as follows:

a) In embryonic cells, Nek1 seems to associate mostly with factors that are involved in ciliogenesis and cell cycle regulation, such as Kif13A,14-3-3, and ATR. It may therefore be important to ensure proper tissue growth by regulating cell cycle progression in response to ciliary signaling.

b) In differentiated cells, however, Nek1 might interact with a different subset of factors mostly associated with the DDR, such as Rad54 or Chk1/2, to protect the established cellular system from genotoxic stressors including IR or oxidative stress.

To examine the accuracy of this assumption and, more importantly, to define Nek1’s dynamic roles during development more intensively, the aforementioned interactome studies should be repeated with a Nek1 cDNA from an adult cell model such as postnatal fibroblasts.

There is no information available at this point to explain how Nek1’s functional change could be regulated. A mechanism that might be interesting in this context is alternative splicing which allows a single gene to encode for multiple protein isoforms by variably processing the transcribed mRNA precursor (exon skipping, intron retention, etc.).[129] The resulting protein isoforms differ in structure and regulatory motif composition (interaction sites, localization

signals, etc.), and can ultimately have altered functionalities. Research shows that this process is coordinated in a spatiotemporal manner to organize e.g., neuronal development or cytoskeleton organization.[130,131] It seems therefore quite possible that Nek1's functional change during development is related to a differential expression of the respective gene, which can code for 11 transcript variants in humans (4 transcripts in mice). A comparison of the resulting Nek1 isoforms using the NCBI alignment tool revealed that they mostly differ in the sequence of their regulatory domain. Isoform-specific expression analyses, using e.g., RNA sequencing techniques, and proteomics should be employed to clarify which isoforms are produced in embryonic and adult cells and if/how they differ in terms of regulatory motifs such as interaction sites.

Focusing more on Nek3 and Nek5, there are far too less data available to strengthen their involvement in embryonic HR-mediated DSB repair described in this thesis.

Nek3 has never been connected to DSB repair or even DDR-related processes. A yeast two-hybrid screen performed by the Kobarg lab identified 27 potential Nek3 interactors, including ciliary proteins, such as Spag1 or Cluap1, but also PCNA, which is implicated in both, DNA replication and repair.[132] This study at least moves Nek3 closer to the DDR, however, the functional relevance of the Nek3-PCNA interaction is to be shown.

Although Nek5 is slightly better characterized in the context of the DDR, a clear link to DSB repair has never been made. Melo-Hanchuk *et al*. demonstrated that Nek5 is required for an adequate response of embryonic HEK cells towards etoposide treatments.[133] Unlike Nek5-proficient cells, Nek5-depleted cells failed to activate the G2/M checkpoint and were unable to repair etoposide-induced DNA damages within a recovery time of 6 h. Since DNA repair was measured only indirectly with an alkaline comet assay, these data are not sufficient to attribute the observed repair defect in Nek5-depleted HEK cells to the role of Nek5 in HR demonstrated in the last section.[133] Moreover, it would contradict the data presented in this work which demonstrated that embryonic cells (MEF) are only affected in DNA repair via HR when depleted for both, Nek3 and Nek5.

Due to their poor characterization, it is furthermore not possible to draw similar conclusions for Nek3 and Nek5 as for Nek1 regarding potential developmental adaptations in functionality. However, the differential gene expression analysis performed in this work demonstrated that both corresponding genes are higher expressed in embryonic cells than in adult cells (Fig. 9), which could at least indicate an altered importance of the two kinases during development. Why embryonic cells employ two redundantly working kinases for the activation of Rad54 and adult cells only rely on one, cannot be discussed based on this data.

The general observation of Nek1, Nek3, and Nek5 dynamically functioning in HR-mediated repair during development is indeed interesting, how this can be translated into any benefit remains speculative. All three kinases are associated with cancerous diseases (Tab. 1), yet

only Nek1 sparked substantial interest as a target for novel therapeutic approaches as highlighted in the next chapter. Based on the finding that Nek3 and Nek5 function similarly to Nek1, at least in the context of HR-mediated DNA repair, but only in less differentiated cells, they might be targeted to fight a very specific population of cancer cells, namely cancer stem cells (CSCs). CSCs share many characteristics with “normal” stem cells including the ability to self-renew and differentiate into cell types that eventually ensure tumor stability and functionality.[134] Due to their stemness, CSCs are considered the main drivers of cancer progression and contribute to tumor reoccurrence as they resist many treatments employed in cancer therapy.[135] Assuming that CSCs suffer from genomic instability as a result of e.g., enhanced replicative stress caused by uncontrolled proliferation, they most likely require functional DSB repair via HR for survival. If Nek3 and Nek5 indeed regulate HR in CSCs, what has to be shown first, of course, inhibiting both might provide a useful strategy to sensitize CSCs to their endogenously arising DSBs but more importantly to DSBs induced by chemo- or radiotherapy. Moreover, therapies that include inhibitors against Nek1, Nek3 and Nek5 may prove to be particularly effective in this context since not only CSCs themselves but also their more differentiated descendants would lose their ability to repair therapy-induced DSBs via HR.

While similar protein-related adaptations in cellular signaling have been described in the field of developmental biology, they are mostly associated with pathways that coordinate the general assembly of organisms, such as the FGF signaling.[136] How and for what reason the HR pathway is differentially regulated during development should be the subject of further investigation, especially because of potential implications for cancer therapy.

3 Project 2: Nek1 as a molecular target for cancer therapy

3.1 Scope of the study

The previous chapters indicate that proliferating healthy cells need Nek1 to ensure tissue homeostasis during embryogenesis, probably by regulating ciliogenesis, and to maintain the integrity of differentiated cells by orchestrating DDR processes. However, several cancer entities have been found to overexpress Nek1 which has been associated with an adverse prognosis for patients with pancreatic cancer, glioma, or cervical carcinoma.[115,137–142]

Cancer generally arises when healthy cells transform and eventually evolve specific hallmarks, such as uncontrolled proliferation, apoptosis evasion, and metastasis. The transition from a healthy to cancerous state is mainly driven by genetic alterations, e.g., gain/loss of function mutations, deletions, and overexpression, in various oncogenes and tumor suppressors such as p53. While these broad genetic and thus metabolic alterations are accumulated by cancer cells to survive under normally deleterious conditions in the first place, they also contribute to an intrinsic resistance towards standard treatments such as radiotherapy.

This most likely also applies to Nek1, which most likely promotes cancer progression due to its key roles in the DDR allowing tumors to maintain DNA repair via HR while inhibiting apoptosis induction.[116] Although the exact mechanisms underlying the association of this kinase with the radiation response of cancer cells requires further characterization, Nek1 presents a potential target for the sensitization of tumors to radiation.

The Rödel lab thus conducted preclinical studies and demonstrated that depleting Nek1 in 3D-cultured HeLa and HCT-15 cancer cells significantly diminished their ability to form colonies following single-dose irradiation. Further assays confirmed that this radiosensitization was attributable to Nek1's roles in HR and apoptosis as reflected by a slightly, yet significantly increased number of residual γH2AX foci and a modest surge in apoptosis-inducing caspase 3/7 activity in both lines 24 h after irradiation. Surprisingly, cell cycle analyses indicated that Nek1-depleted, irradiated cancer cells were able to induce the G2/M cell cycle checkpoint. While this finding contradicted existing literature describing Nek1 as an essential factor for checkpoint activation after genotoxic stress, it also raised the question of whether fractionated irradiation could be beneficial for the treatment of Nek1-depleted cells.

Fractionation describes a commonly used technique in radiotherapy in which a total dose of radiation is applied to a tumor in multiple, small fractions over several weeks to damage malignant cells as much as possible while sparing the surrounding healthy tissues.[143] However, when each fractionated dose would be applied in a "timely correct" manner, meaning under consideration of the time cells need to progress through the cell cycle, fractionation could be used to induce DSBs in cells while capturing and enriching them in the G2 phase due to the activation of the G2/M checkpoint. With every applied fraction, the population of G2 phase cells would grow, as it is unable to continue cycling, and accumulate DSBs, which cannot be

repaired by HR in Nek1-depleted cells and thus eventually contribute to cell death. The following study, therefore, aimed to investigate the extent to which fractionated irradiation can reduce cancer cell survival by enriching cells in the G2 phase while causing irreparable damages in a growing population of Nek1-depleted, hence HR-deficient cells.

Accordingly, to identify the ideal time interval for G2 phase accumulation, cancer cell lines, HeLa shCtrl, HeLa shNek1, and HCT-15, should be subjected to three fractionation regimes (2 h, 6 h, or 24 h between each fraction) while analyzing their cycling behavior using a cytometric assay. Furthermore, clonogenic assays should be conducted to evaluate how these fractionation regimes affect the survival of Nek1-depleted cells compared to single-dose irradiations. Finally, *in vivo* xenograft studies were to be performed demonstrating the efficacy of a tumor treatment combining the depletion of Nek1 with fractionated irradiation. The following data as well as parts of the previously given information were published in the journal *Cells* in 2020.[142]

3.2 Materials

3.2.1 Devices

Device (**Type**)	**Supplier**
Basic shaker (IKA® KS 260)	IKA Labortechnik
Centrifuge (MEGA STAR 1.6R)	VWR
Centrifuge (MiniSpin®)	Eppendorf
Centrifuge (Universal 320R)	Hettich
Dual-mode Imaging System (Odyssey® Fc)	LI-COR Biosciences
Electrophoresis power supply (Power Pack P25T)	Biometra
Flow cytometer (CytoFLEX S)	Beckman Coulter
Gel casting glass plates (Mini-PROTEAN®)	Bio-Rad
Incubator (HERA cell 240i)	Thermo Fisher Scientific
Laminar flow hood (HERA safe)	Thermo Fisher Scientific
Linear accelerator (Synergy® FL)	Elekta
Magnetic stirrer with hotplate	VWR
Orbital shaker (ES-20)	BioSan
pH meter (765 Calimatic)	Knick
Photometer (Bio)	Eppendorf
Pipetus	Hirschmann-Laborgeräte
Plate reader (TECAN Infinite® M200 Pro)	TECAN
Precellys® homogenizer (24)	Bertin Instruments
Real-Time PCR System (QuantStudio™5)	Applied Biosystems
Scale (CP324S)	Sartorius
Scale (PRACTUM612-1S)	Sartorius
Semi-dry transfer system (Te70 Ecl)	Amersham Hoefer Ge
Shaker (IKA® MTS 4)	IKA Labortechnik

Small Animal Radiation Research Platform (SARRP)	XStrahl
Thermocycler (Primus 96 advanced®)	PEQLab Biotechnologie
Vertical Electrophoresis cell and accessories (Mini-PROTEAN ® Tetra)	Bio-Rad
Vortexer (Genie 2)	Scientific Industries
Waterbath (Type W/B5)	Gesellschaft für Labortechnik

3.2.2 Consumables

Consumable (**Type**)	**Supplier**
15/50 ml falcon tubes	Greiner Bio-One
6-/24-/96-well cell culture plates (CELLSTAR®)	Greiner Bio-One
96-Well qPCR Plate (MicroAmp™ Optical)	Applied Biosystems
Disposable Hematocytometer (C-Chip)	NanoEnTek
Disposable Polystyrene Serological Pipettes (Corning™ Stripette™)	FisherScientific
Filter paper	Whatman
Filter Top cell culture flasks (CELLSTAR®, T25/T75)	Greiner Bio-One
Glass beakers	Schott
Insulin syringes	B. Braun
Kim wipes	NeoLab
Nitrocellulose Membrane (Amersham™ Protran™ Premium, 0.2 µm)	GE Healthcare
PCR tubes (0.2 ml)	ThermoFisher Scientific
Pipette tips (TipOne® graduated)	Starlab
Polystyrene Round-Bottom tubes	Becton Dickinson
Reaction tubes (0.5 ml)	Eppendorf
Reaction tubes (1.5 ml, 2 ml)	Sarstedt
Reaction tubes with ceramic beads (Precellys®, 2 ml)	VWR
Sealing film (EASYseal™)	Greiner

3.2.3 Chemicals and premade buffers

Chemical (**Abbreviation**)	**Supplier**
7-AminoactinomycinD (7-AAD)	BD Biosciences
Agarose	Carl Roth
Ammonium persulfate (APS)	Carl Roth
Bovine serum albumin (BSA)	AppliChem
Bromophenol blue	AppliChem
Cultrex® Reduced Growth Factor Basement Membrane Matrix, Type 2 (BME 2)	Trevigen
CytoFLEX Sheath Fluid	Beckman Coulter
Deoxynucleotides (dNTP, 10 mM)	Thermo Fisher Scientific
Deoxycholic acid (DOC)	AppliChem
Dithiothreitol (DTT)	Sigma-Aldrich

Ethanol	Sigma-Aldrich
Glycerol	Carl Roth
Glycine	AppliChem
Halt™ Protease Inhibitor Cocktail (100x)	Thermo Fisher Scientific
Hydrochloric acid (HCl)	AppliChem
Isofluran	AbbVie
Isopropanol	Sigma-Aldrich
Methanol	Sigma-Aldrich
Nonidet P-40 (NP-40)	AppliChem
Phosphate-buffered saline (PBS), 1x	Thermo Fisher Scientific
SuperSignal™ West Femto Maximum Sensitivity Substrate	Thermo Fisher Scientific
PonceauS	AppliChem
Propidium iodide (PI)	Thermo Fisher Scientific
Random Hexamer Primers	Thermo Fisher Scientific
RNAse/DNase-free water	Thermo Fisher Scientific
Roti-Fect PLUS	Carl Roth
Rotiphoresis gel 30	Carl Roth
RT² SYBR Green qPCR Mastermix	Qiagen
Skim milk powder	Carl Roth
Sodium chloride (NaCl)	Sigma-Aldrich
Sodium fluoride (NaF)	Sigma-Aldrich
Sodium hydroxide (NaOH)	Sigma-Aldrich
Sodium lauryl sulfate (SDS) pellets	Carl Roth
Sodium orthovanadat (Na_3VO_4)	Sigma-Aldrich
Sucrose	Carl Roth
Tetramethylethylendiamine (TEMED)	Carl Roth
Trichloroacetic acid (TCA)	AppliChem
Tris(hydroxymethyl)aminomethane (TRIS)	Carl Roth
Triton X-100	AppliChem
Trypan Blue Stain 0.4%	Thermo Fisher Scientific
Trypsin/Ethylene diamine tetraacetic acid (EDTA, 0.25%)	Thermo Fisher Scientific
Tween® 20	AppliChem

3.2.4 Media, antibiotics, and supplements

Medium/Supplement	**Supplier**
Dulbecco's Modified Eagle's Medium (DMEM)	Thermo Fisher Scientific
Optimized Minimal Essential Medium I (OptiMEMI)	Thermo Fisher Scientific
Roswell Park Memorial Institute Medium (RPMI1640)	Thermo Fisher Scientific
Fetal bovine serum (FBS)	Thermo Fisher Scientific
Penicillin/Streptomycin (100,000 Units/10 mg/ml)	Sigma-Aldrich
Doxycycline (Dox)	AppliChem
Puromycin (Puro)	Sigma-Aldrich

3.2.5 Buffers and solutions

3.2.5.1 General Buffers

TRIS-buffered saline (TBS), pH 7.5	TRIS base	10 mM
	NaCl	150 mM
	Milli-Q water	
TRIS buffer (TRIS), pH 6.8 or 8.0 or pH 8.8	TRIS base	1 M or 1.5 M
	Milli-Q water	

3.2.5.2 (3D) Cell culture

HeLa culture medium	FBS	10% (v/v)
	Penicillin/Streptomycin	1% (v/v)
	Puromycin	0.2 µg/ml
	DMEM	
HCT-15 culture medium	FBS	10% (v/v)
	Penicillin/Streptomycin	1% (v/v)
	RPMI1640	
1% Agarose gel	Agarose	1% (w/v)
	Milli-Q water	

3.2.5.3 Cell lysis

Radio Immuno Precipitation Assay (RIPA) buffer	1.5 M TRIS, pH 8.0	50 mM
	NaCl	150 mM
	SDS	0.1% (w/v)
	DOC	0.5% (w/v)
	NP-40	1% (v/v)
	100x Halt™ Protease Inhibitor Cocktail	2% (v/v)
	Na_3VO_4, NaF	1 mM, 2 mM
	Milli-Q water	

3.2.5.4 SDS-PAGE

SDS running buffer, pH 8.8	TRIS base	25 mM
	SDS	3.5 mM
	Glycin	190 mM
	Milli-Q water	
6% Reducing loading buffer	1 M TRIS, pH 6.8	350 mM
	SDS	10.28% (w/v)
	Glycerol	50% (v/v)
	DTT	600 mM
	Bromophenol blue	0.05% (w/v)
	Milli-Q water	

5% SDS stacking gel	1 M TRIS, pH 6.8	125 mM
	30 % Acrylamide	5% (v/v)
	SDS	0.1 % (w/v)
	APS	0.15 % (w/v)
	TEMED	0.1 % (v/v)
	Milli-Q water	
8% SDS separation gel	1 M TRIS, pH 8.8	370 mM
	30 % Acrylamide	8% (v/v)
	SDS	0.1 % (w/v)
	APS	0.15 % (w/v)
	TEMED	0.11 % (v/v)
	Milli-Q water	

3.2.5.5 Immunoblotting

Transfer buffer	TRIS base	25 mM
pH 8.3	Glycine	190 mM
	Methanol	20% (v/v)
	Milli-Q water	
Membrane staining solution	PonceauS	0.2% (w/v)
	TCA	3% (v/v)
	Milli-Q water	
TBS-Tween (TBS-T)	Tween 20	0.1% (v/v)
	TBS	
Primary antibody dilution buffer	BSA	5% (w/v)
	TBS-T	
Blocking and secondary	Skim milk powder	5% (w/v)
antibody dilution buffer	TBS-T	

3.2.6 Kits

Kit	**Supplier**
NucleoSpin RNA Kit	Macherey-Nagel
Pierce™ Micro BCA Protein Assay Kit	ThermoFisher Scientific

3.2.7 Oligonucleotides

siRNA	**Sense sequence** (**5'- 3'**)	**Supplier**
AllStars Control (Ctrl)	-	Qiagen
Nek1	ggagagaaguugcaguauu	Eurofins Genomics GmbH

All primers were purchased from Eurofins Genomics GmbH (Ebersberg, Germany).

Primer	**Forward sequence** (**5'- 3'**)	**Reverse sequence** (**5'- 3'**)
Nek1	agaggatcagattttggact	gctctacagtactattaagaac

RPL37A	tgtggttcctgcatgaagaca	gtgacagcggaagtggtattgtac

3.2.8 Antibodies

Primary antibodies	Ordering no.	Supplier	Dilution
Rabbit anti-Nek1, polyclonal IgG	GTX130828	Biozol Diagnostika	1:1000
Mouse anti-β-Actin, monoclonal IgG	A5441	Sigma-Aldrich	1:10000
Secondary antibodies			
Goat anti-mouse-IgG-HRP	sc-2055	Santa Cruz Biotechnology	1:2000
Goat anti-rabbit-IgG-HRP	sc-2054	Santa Cruz Biotechnology	1:10000

3.2.9 Enzymes

Enzyme	Supplier
Moloney Murine Leukemia Virus (M-MLV) Reverse Transcriptase	Promega
RNaseA	Qiagen

3.2.10 Protein ladder

Ladder	Supplier
ProSieve QuadColor Protein Marker	Biozym

3.2.11 Cell lines

Cell line	Origin/Modification	Supplier
HCT15	Human colorectal carcinoma	American Type Culture Collection (ATCC)
HeLa shCtrl	Human cervical carcinoma with stably integrated, Dox-inducible unspecific shRNA expression cassette	Löbrich lab, TU Darmstadt
HeLa shNek1	Human cervical carcinoma with stably integrated, Dox-inducible Nek1-specific shRNA expression cassette	See [111]

3.2.12 Animals

Branded/Common name	Strain name	Breeder
NSG™	NOD.*Cg-Prkdc^{scid}Il2rg$^{tm1Wjl/}$SzJ*	The Jackson Laboratory

3.2.13 Software and internet resources

Software/Resource	Developer	Application
CytExpert Software	Beckman Coulter	Flow Cytometry data analysis
Excel 2010	Microsoft	Calculation and graph design
Image Studio™ Software	LI-COR Biosciences	Western Blot image aquisition

NCBI primer designing tool	National Institutes of Health	Primer design
Serial Cloner v2.6.1	SerialBasics	Primer design
QuantStudio5 Design and Analysis Software v1.5.1	Applied Biosystems	qPCR data analysis

3.3 Methods

3.3.1 Cell biology

3.3.1.1 Cell culture

HeLa shRNA cells or HCT-15 cells were passaged at a confluency of 90% in a ratio of 1/9 or 1/5, respectively. For this, cells were washed once with PBS, treated with Trypsin/EDTA solution for 5 min at 37°C, and resuspended in their respective culture medium (see section 3.2.5.2). The resulting suspensions were transferred into new culture flasks or seeded as listed in table 6 for the induction of shRNA synthesis or siRNA transfection. All cell lines were cultured at standard conditions (37°C, humidified atmosphere with 5% CO_2) until further use. The number of cells within the suspensions was determined using hemocytometers.

Tab. 6 Cell numbers seeded for doxycycline treatment or siRNA transfection

Cells	Pretreatment	Culture vessel	Amount of medium	Cell number per flask/well
HeLa shRNA	Induction of shRNA synthesis	T75	12 ml	0.9×10^5
HCT-15	siRNA transfection	6 well plate	2 ml	3.5×10^5

3.3.1.2 RNA interference-mediated Knockdown

HeLa shRNA cell lines were treated daily with 2 µg/ml Doxycycline (Dox) for 5 consecutive days to induce the synthesis of unspecific or Nek1-specific shRNA, respectively.

In the case of HCT-15 cells, Nek1 was depleted by conventional siRNA transfection using the Roti-Fect PLUS reagent. 24 h after seeding, HCT-15 cells were washed once with PBS and covered with 1 ml of Opti-MEMI medium. 25 nM of unspecific control or Nek1-specific siRNA (see section 3.2.7) and 5 µl of the Roti-Fect PLUS reagent were then combined in OptiMEMI medium, incubated for 20 min at RT, and added dropwise to the cells. After 8 h at standard conditions (37°C, humidified atmosphere with 5% CO_2), cells were supplemented with 1 ml of OptiMEMI medium containing 20% FBS and kept at standard conditions for 24 h.

3.3.1.3 3D culture and experimental seeding

Chemotherapeutics and radiation treatments are traditionally examined for their effects on cancer cells that are cultured as monolayers on the surface of culture dishes. However, this so-called 2D culture is afflicted with some shortcomings because monolayers of cells do not reflect the actual complexity of a three-dimensional tumor embedded in tissue.[144] Therefore, it is commonly observed that treatments with substantial success in 2D culture assays prove

ineffective when applied *in vivo*.[145] A more physiological environment for *in vitro* experiments can be created by seeding cancer cells into a laminin-rich extracellular matrix (lrECM), also called 3D culture, in which cells migrate and orientate according to their intrinsic nature. Consequently, tumor spheres form that consist of a heterogenous population with metabolisms individually adapted to oxygen availability, intercellular communication and matrix-cell interactions.[146] These adaptations influence various intracellular responses to for example radiation which is why 3D-cultured cells were applied for the following studies.[147]

First of all, the well bottoms of the used culture plates were covered with 1% agarose to restrict adherence of cells to the plate surface. Single-cell suspensions of HeLa shRNA and HCT-15 cells were prepared as described in section 3.3.1.1 on day 5 of the Dox treatment or 24 h after transfection, respectively. Cell numbers listed in table 7 were resuspended in respective amounts of ice-cold culture medium with or without Dox and mixed with 0.5 mg/ml Cultrex BME on ice. BME/Cell suspensions were transferred into wells and incubated at standard conditions (37°C, humidified atmosphere with 5% CO_2) until further use. BME/Cell suspension seeded into wells of a 96-well plate were covered with 100 µl of culture medium with or without Dox 1 h after seeding and kept at standard conditions. Shortly before irradiation, Dox was added to HeLa shRNA cells again. For the preparation of protein and RNA lysates, HeLa shRNA and HCT-15 cells were seeded into 2D cultures on day 5 of the Dox treatment or 24 h after transfection, respectively (Tab. 8).

Tab. 7 Cell numbers seeded for 3D experiments

Cells	Experiment	Culture plate	Amount of medium containing BME	Cell number per well
HeLa shRNA	Colony formation	96-well	0.1 ml (-/+ Dox)	400
	Cell cycle analysis	48-well	0.5 ml (-/+ Dox)	0.2 x 10^6
HCT-15	Colony formation	96-well	0.2 ml	750
	Cell cycle analysis	48-well	0.5 ml	0.1 x 10^6

-/+: with or without

Tab. 8 Cell numbers seeded for 2D experiments

Cells	Experiment	Culture plate	Amount of culture medium	Cell number per well
HeLa shRNA	qPCR and Immunoblotting	6-well	2 ml; with or without Dox	0.6 x 10^6
HCT-15	qPCR and Immunoblotting	6-well	2 ml	0.8 x 10^6

3.3.1.4 DNA damage induction

24 h after seeding into 3D cultures, HeLa shRNA and HCT-15 cells were irradiated with a 6 MV photon beam produced by a Synergy FL linear accelerator to induce DNA damage such as double-strand breaks. Cells were placed at a focus-to-isocenter distance of 100 cm and single doses of 2, 4, or 6 Gy were applied with a dose rate of 6 Gy/min. For fractionation schedules, cells were irradiated with a total dose of 6 Gy splitted into three doses of 2 Gy (3x2 Gy) applied every 2, 6, or 24 h. Cells were then cultured at standard conditions (37°C, humidified atmosphere with 5% CO_2) until further use.

3.3.1.5 Cell cycle analysis

The cell cycle distribution in Nek1-depleted cell populations was measured after fractionated irradiation in a flow cytometric assay using propidium iodide (PI) as DNA dye. For this, 3D cultured cells were taken up in PBS at timepoints indicated in the figures and centrifuged for 5 min at 200 x g and 4°C. The resulting pellet was digested with Trypsin/EDTA for 5 min at 37°C, resuspended with the respective culture medium, and centrifuged again. Cells were fixed and permeabilized with 1 ml of ice-cold ethanol (80%) under rigorous vortexing, incubated on ice for at least 10 min, and subsequently centrifuged. After the addition of 50 µl of PBS, cellular RNA was digested by addition of 10 µg of RNase A, and DNA was stained with 170 µg of PI for 30 min at 37°C in the dark. The suspensions were then analyzed in a flow cytometer where, first of all, histograms were generated to discriminate single cells from cell clumps by plotting the side scatter height (SSC-H) and forward scatter height (FSC-H). Single-cell events were then arranged in a second histogram according to their respective PI signal intensity (FL2: 585 nm). This allowed for the discrimination between G2 phase cells with a doubled DNA content and, thus, higher PI signal and G1 phase cells with a lower PI signal. S phase cells were defined as events that were positioned between the PI signal spikes for G1 and G2 cells.

3.3.1.6 Colony formation assay

The fact that 3D-cultured cells can grow into tumor spheres is utilized in the colony formation assay. This technique provides valuable information about the effectiveness of cytotoxic treatments since cells severely damaged following the exposure to IR potentially fail to form colonies due to the induction of senescence or cell death.[148]

After irradiation, HeLa shRNA and HCT-15 cells seeded in a 3D matrix as described in section 3.3.1.3 were cultured for 6 to 7 days at standard conditions. In the case of HeLa shRNA cells, Dox was added to the suspensions two days after irradiation to sustain the shRNA-mediated knockdown of *nek1*. Colonies consisting of at least 50 cells were counted followed by the calculation of plating efficiency and surviving fractions according to the following formulas.

$$\textbf{Plating efficiency (\%)} = \frac{\text{Formed colonies}}{\text{Plated single cells}}$$

$$\textbf{Surviving fraction (\%)} = \frac{\text{Formed colonies}}{\text{(Plated cells irradiated} \times \text{plating efficiency unirradiated cells)}}$$

3.3.2 Molecular biology

3.3.2.1 Quantitative Real-Time PCR

RNA lysates were prepared from HeLa shRNA and HCT-15 cells with the NucleoSpin RNA kit according to the manufacturer's instructions. 500 ng of RNA were then mixed with 0.5 µg of random hexamer primers in nuclease-free water and subjected to a denaturing step at 70°C for 15 min. 200 units of M-MLV reverse transcriptase were added and reverse transcription was run as follows: 25°C for 10 min, 37°C for 30 min, and 42°C for 30 min. The Nek1-specific primer pair for qPCR was designed with the NCBI primer design tool except for the primer pair against RPL37A which was kindly provided by Stephanie Hehlgans (see section 3.2.7). After cDNA synthesis, qPCR samples were set up containing 2.5 µl of undiluted cDNA, 0.2 µM of each forward and reverse primer, and RT² SYBR Green qPCR Mastermix. Samples were transferred into a QuantStudio 5 Real-Time light cycler and amplified under the following conditions: 95°C for 10 min, 40 cycles at 95 °C for 15 sec, and 60 °C for 60 sec. A melting curve was staged right after each amplification process to confirm the specificity of all primer pairs used. The resulting cycle thresholds served as a basis for the calculation of fold changes in *Nek1* expression in NEK1-depleted cells compared to control cells using the $2^{-\Delta\Delta Ct}$ method. *Rlp37A* values served as normalization for cDNA content.

3.3.3 Biochemistry

3.3.3.1 SDS-Page and Immunoblotting

For the isolation of total protein from HeLa shRNA and HCT-15 cells, cells were washed shortly with PBS and scraped from well bottoms in ice-cold radioimmunoprecipitation assay (RIPA) buffer at the timepoints indicated in the figures. After incubation on ice for 30 min, the lysate was cleared by centrifugation for 15 min at 4°C and 16,100 x g. The concentration was measured using the Pierce™ Micro BCA Protein Assay kit according to the manufacturer's instructions. Finally, protein extracts were subjected to sodium dodecyl sulfate-polyacrylamide gel electrophoresis (SDS-PAGE) and immunoblotting for analysis. First of all, 35 µg of protein were supplemented with 6x reducing loading buffer, denatured by heating for 10 min at 95°C, and subsequently loaded onto an SDS gel (5% stacking, 8% separation). Proteins were separated at 25 mA for at least 55 min. The SDS gel was then placed onto a nitrocellulose membrane surrounded by blotting paper both soaked in transfer buffer. The gel/membrane sandwich was placed onto a semi-dry transfer unit and covered with transfer buffer. Proteins were blotted onto the membrane with a current of 45 mA for 3.5 h. Before cutting at desired protein sizes, the membrane was stained with Ponceau S solution for 1 min and washed with MilliQ water. Unspecific antibody binding was prevented by blocking the membrane with

blocking solution for 1 h at RT before incubation overnight at 4°C with primary antibodies diluted in primary antibody dilution buffer as listed in section 3.2.8. Following washing with TBS-T three times for 10 min, the membrane was incubated for 1 h at RT with secondary antibodies diluted in blocking buffer and washed again with TBS-T three times for 10 min followed by a final wash with TBS for 10 min. Protein bands were visualized with the Odyssey Fc imaging system after incubation of the membrane with the SuperSignal™ West Femto Maximum Sensitivity Substrate for 5 min at RT.

3.3.4 Animal research

3.3.4.1 Murine xenograft model and in vivo irradiation

To finalize preclinical studies, it is vital to establish *in vivo* models to prove the fundamental concept behind a novel cancer treatment. Conventionally, this is accomplished by so-called xenograft models in which human cancer cells are implanted into immunodeficient mice subcutaneously. The resulting tumors can be treated with cytotoxic agents such as radiation and are monitored for their treatment response. The experiment described below was conducted with the approval of the government committee (Regierungspräsidium Darmstadt, FK/1098). Single-cell suspensions of untreated HeLa shNek1 or shCtrl cells were prepared as described in 3.3.1.1. 1 x 10^6 cells were resuspended in 100 µl of PBS, transferred into an insulin syringe, and injected subcutaneously into the left or right flank, respectively, of female 12- to 16-week-old NSG mice. Mice were treated with 2 mg/ml Dox provided in sweet drinking water (2 % (w/v) Sucrose) as soon as tumor nodes were visible. After 10 days of treatment, tumors were irradiated by image-guided-radiotherapy (IGRT) using a Small Animal Radiation Research Platform (SARRP) operated by Stephanie Hehlgans. Mice were anesthetized with 2.5% isoflurane and subjected to a Cone-Beam CT operating at 65 kV, 0.5 mA to visualize the tumor shape for exact irradiation. A total dose of 6 G was applied in three doses of 2 Gy every 6 hours (3x2 Gy) using a 10-mm collimated beam operating at 175 kV, 15 mA, and a 2 mm aluminum filter. Tumor size was measured daily using a caliper and volumes were calculated for the assessment of growth using the following formula: Volume (mm^3) = ($width^2$ × length)/2.[149] Mice were treated with Dox during the observation period and sacrificed either 12 days after irradiation or earlier when tumors reached a volume of 1 cm^3. Tumors were isolated and shredded in RNA lysis or RIPA buffer using a tissue homogenizer and bead tubes kindly provided by Adele Nicholas. RNA and protein isolation were then performed as described in sections 3.3.2.1 and 3.3.3.1.

3.3.5 Statistics

Experimental data were gathered from three experiments compiled in figures as mean values +/- standard deviations. In the case of the animal experiments, each tumor was defined as an

experimental setup. Statistics were calculated in Microsoft Excel using the student's T-test for independent samples and considered significant when reaching a p-value of at least 0.05.

3.4 Results

3.4.1 Fractionation decreases cancer cell survival in dependency of Nek1

The Rödel lab previously demonstrated that depleting Nek1 significantly reduced the clonogenic capacity of 3D-cultured cancer cells in response to single-dose irradiation. Considering Nek1's cell cycle-dependent function in HR, it was speculated that fractionated irradiation might affect the survival of Nek1-depleted cells even stronger when doses are administered in an interval that forces cells to accumulate in G2 phase while repeatedly inducing irreparable DSBs.

To test this hypothesis, 3D-cultured HeLa shNek1, and HCT-15 cells were depleted for Nek1 by either doxycycline (Dox)-mediated shRNA expression or siRNA transfection (Figs. 12A and 12D). Upon successful knockdown validation at both the mRNA (Figs. 12B and 12E) and protein (Figs. 12C and 12F) levels, cells were irradiated with a total dose of 6 Gy according to three fractionation regimes:

1. 2 h fractionation: 3 fractions of 2 Gy (3x2 Gy) applied every 2h (Fig. 13A and 14A)
2. 6 h fractionation: 3 fractions of 2 Gy (3x2 Gy) applied every 6 h (Fig. 13B and 14B)
3. 24 h fractionation: 3 fractions of 2 Gy (3x2 Gy) applied every 24 h (Fig. 13C and 14C)

Cell cycle distributions were then analyzed 2 h, 6 h, or 24 h after every fraction using a propidium iodide-based flow cytometry assay to evaluate the potential of each fractionation regime to enrich cells in the G2 phase. In the case of Dox-treated HeLa shRNA cells, unirradiated populations consisted of around 15-20% G2 phase cells, 5-10% S phase cells, and 70-80% G1 phase cells independently of their Nek1 status (Fig. 13D-I). This distribution remained unchanged following irradiation according to the 2 h (Fig. 13D and 13G) and 24 h (Fig. 13F and 13I) fractionation intervals. However, the 6 h fractionation regime gradually increased the proportion of G2 phase cells in both, control and Nek1-deficient populations to a total of 35% 6 h after the third fraction (Fig. 13E and 13H), while the amount of G1 phase cells decreased by 25%. These results were also obtained in untreated (-Dox) HeLa shRNA cells which are therefore not shown.

Subsequently, colony formation assays were conducted to examine how the fractionation regimes affect the clonogenic capacity of Nek1-depleted cells compared to Nek1-proficient control cells. The irradiation of Nek1-proficient HeLa cells (HeLa shCtrl) with a single-dose of 6 Gy (straight lines in black) reduced their clonogenic survival by a factor of 3 and, following the depletion of Nek1 (HeLa shNek1, straight lines in red), by a factor of 5 (Fig. 13J-L). Identical survival curves were obtained when cells were irradiated according to the 2 h fractionation interval (dashed lines, Fig. 13J). The daily application of 2 Gy fractions did not increase the

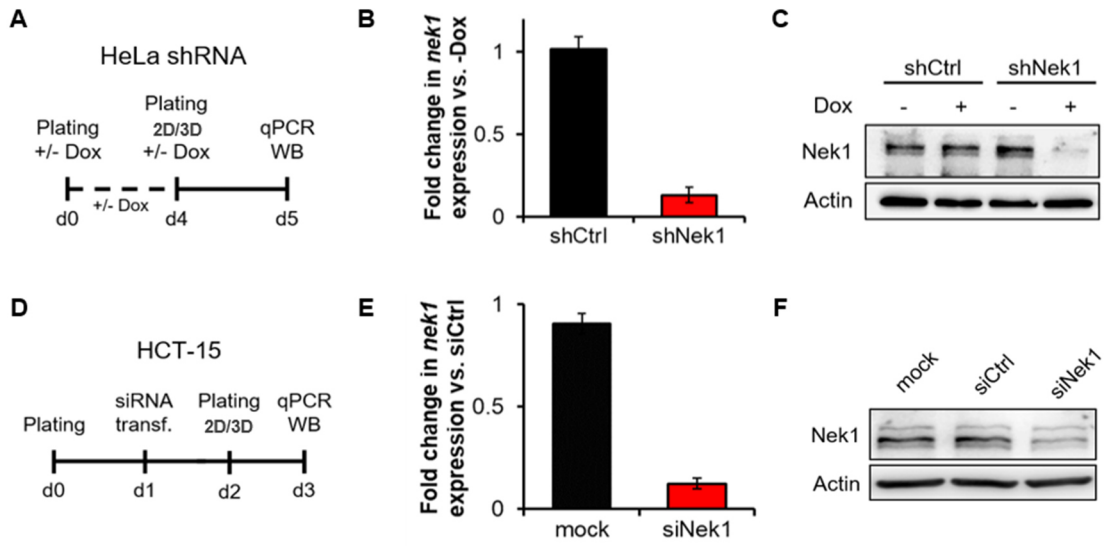

Fig. 12 Knockdown of Nek1 in HeLa shRNA and HCT-15 cells. A, **D** Schematic representation of knockdown induction in HeLa shRNA cells and HCT-15 cells. HeLa cells were treated with doxycycline (Dox) for four days prior to seeding into experiments (**A**) while HCT-15 cells were transfected with 25 nM unspecific control or Nek1-specific siRNA two days before seeding (**D**). RNA and protein lysates were prepared from HeLa shRNA cells after five days of Dox-treatment or from HCT-15 cells two days after siRNA transfection. **B**, **E** *nek1* expression analysis in HeLa shRNA cells and HCT-15 cells. Fold changes in expression were calculated with the $2^{-\Delta\Delta Ct}$ method using *RPL37A* as reference gene and normalizing the expression levels of *nek1* in cells treated with Dox (**B**) or Nek1-specific siRNA (**E**) to the respective level in untreated cells or siCtrl-treated cells. **C**, **F** Representative Western Blots showing the protein levels of Nek1 in HeLa shRNA (**C**) and HCT-15 (**F**) cells following Dox-treatment or siRNA transfection, respectively. Actin served as loading control. Data are shown as mean values ± SDM (n=3). Transf., transfection; WB, Western Blot

radiosensitivity of HeLa cells compared to single-dose irradiations and even slightly attenuated the radiosensitizing effect mediated by the Nek1 depletion (Fig. 13L). Strikingly, the survival of Nek1-deficient HeLa cells was significantly reduced in response to the 6 h interval compared to the respective single-dose irradiations, whereas control cells in the same context tolerated the fractionation better (Fig. 13K).

To further validate these findings, HCT-15 cells were subjected to the aforementioned experiments after siRNA-mediated depletion of Nek1 (Fig. 12D-E). After fractionated irradiation, cell cycle distributions were measured and, interestingly, HCT-15 cells behaved quite similarly to HeLa cells (Fig. 14D-I). While a dose fractionation according to the 2 h or 24 h interval did not alter the abundance of G2 phase cells in either control or Nek1-depleted populations (Fig. 14D, F, G, and I, mock population not shown), the 6 h interval was sufficient to gradually enrich cells in the G2 phase independently of their Nek1 status from approximately 25% in unirradiated samples to 40% after the third fraction (Figs. 6E and 6H). Irradiation with a single-dose of 6 Gy (straight lines) reduced the clonogenic survival of Nek1-depleted cells (black for mock treatment, grey for siCtrl-treated samples) by a factor of 10 whereas Nek1-proficient cells exhibited a decline in survival by a factor of 3 compared to unirradiated controls (Fig. 14J-L). The clonogenic survival was similarly affected in samples irradiated according to

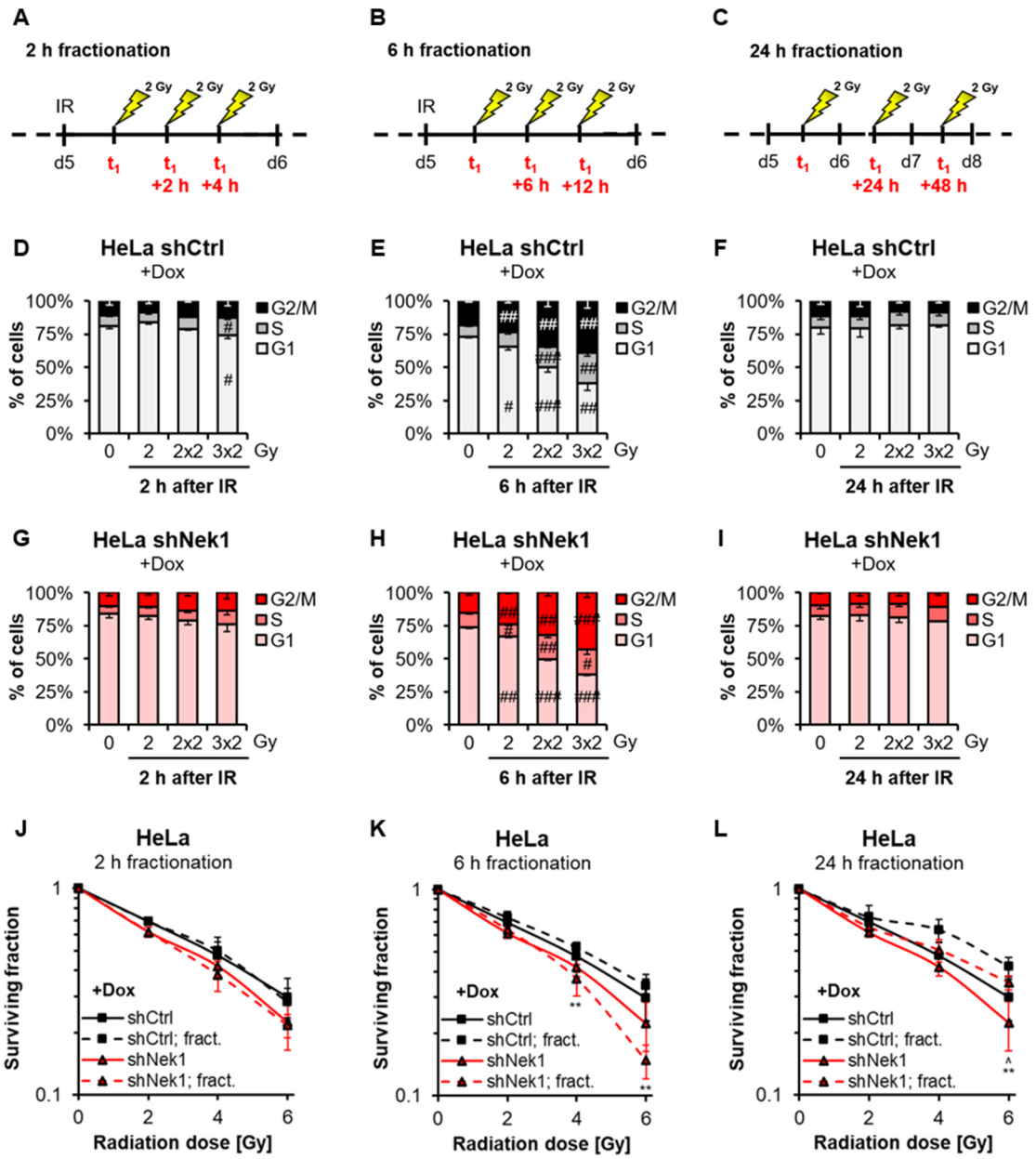

Fig. 13 Cell cycle analysis and survival measurements in Dox-treated HeLa shRNA cells following fractionated irradiation. A-C Schematic representation of fractionation regimes. HeLa cells were pretreated as depicted in figure 12 and then irradiated according to the 2 h (**A**), the 6 h (**B**) or the 24 h (**C**) fractionation interval. **D-I** Cell cycle distributions of doxycycline (Dox)-treated, Nek1-proficient HeLa shCtrl cells (**D-F**) and Nek1-depleted HeLa shNek1 cells (**G-I**) following fractionation with the 2 h (**D**, **G**), 6 h (**E**, **H**) or 24 h (**F**, **I**) interval. Cell cycle was analyzed at indicated timepoints after IR, e.g., 0 h after 0 Gy, 2 h after 2 Gy, 2 h after 2x2 Gy, 2 h after 3x2 Gy (**D**, **G**) or 0 h after 0 Gy, 6 h after 2 Gy, 6 h after 2x2 Gy, 6 h after 3x2 Gy (**E**, **H**). **J-K** Colony formation assay in Dox-treated HeLa shCtrl (black lines) and HeLa shNek1 cells (red lines) following single-dose irradiation with 2, 4, and 6 Gy (straight lines) or fractionated irradiation (dashed lines) according to the 2 h (**J**), the 6 h (**K**) or the 24 h (**L**) fractionation interval. Colonies (≥ 50 cells) were counted seven days after the last irradiation was applied (Triplets). Data are shown as mean values ± SDM (n=3). #, irradiation vs. 0 Gy; *, knockdown vs. control; ^, fractionation vs. single-dose; #,*,^ $p < 0.05$; ##,** $p < 0.01$; ### $p < 0.001$ (Student's T-test). IR, irradiation; fract., fractionation.

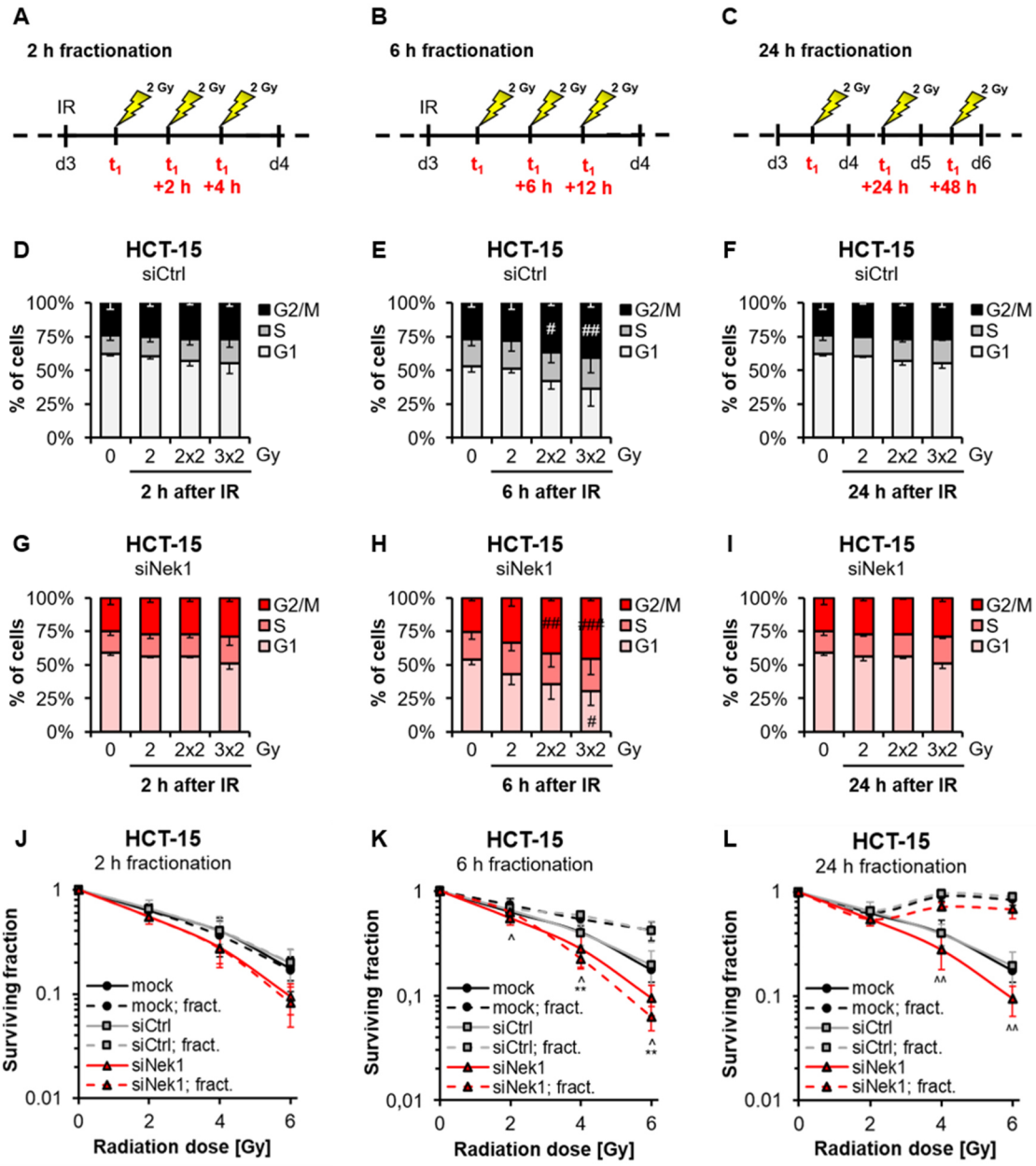

Fig. 14 Cell cycle analysis and survival measurements in siRNA-transfected HCT-15 cells following fractionated irradiation. A-C Schematic representation of fractionation regimes. HCT-15 cells were pretreated as depicted in **figure 12** and then irradiated according to the 2 h (**A**), the 6 h (**B**) or the 24 h (**C**) fractionation interval. **D-I** Cell cycle distributions of Nek1-proficient HCT-15 siCtrl (**D-F**) and Nek1-depleted HCT-15 siNek1 cells (**G-I**) following fractionation with the 2 h (**D**, **G**), 6 h (**E**, **H**) or 24 h (**F**, **I**) interval. Cell cycle was analyzed at indicated timepoints after IR, e.g., 0 h after 0 Gy, 2 h after 2 Gy, 2 h after 2x2 Gy, 2 h after 3x2 Gy (**D**, **G**) or 0 h after 0 Gy, 6 h after 2 Gy, 6 h after 2x2 Gy, 6 h after 3x2 Gy (**E**, **H**). **J-K** Colony formation assay in mock-treated (black lines), siCtrl-treated (grey lines) and siNek1-treated (red lines) HCT-15 cells following single-dose irradiation with 2, 4, and 6 Gy (straight lines) or fractionated irradiation (dashed lines) according to the 2 h (**J**), the 6 h (**K**) or the 24 h (**L**) fractionation interval. Colonies (≥ 50 cells) were counted six days after the last irradiation was applied (Triplets). Data are shown as mean values ± SDM (n=3). #, irradiation vs. 0 Gy; *, knockdown vs. control; ^, fractionation vs. single-dose; #,^ $p < 0.05$; ##,**, ^^ $p < 0.01$; ###,***$p < 0.001$ (Student's T-test). IR, irradiation; fract., fractionation.

the 2 h fractionation interval (dashed lines, Fig. 14J). The application of the 24 h fractionation interval did not impair the clonogenic survival and resulted instead in a severely enhanced radiation resistance in both, Nek1-proficient and -depleted populations (Fig. 14L) compared to the respective single doses. HCT-15 cells treated according to the 6 h fractionation interval were sensitized to radiation beyond the level observed for the respective single-doses when depleted for Nek1, but were less affected by fractionation when proficient for Nek1 (Fig. 14K). In summary, the collected data demonstrate that the Nek1-mediated radiosensitization of both employed cancer cells lines is most pronounced when combined with a 6 h fractionation interval as it allows the enrichment of cells in the G2 phase and the repeated induction of DSBs which are unrepairable in the Nek1-depleted, thus HR-defective population.

3.4.2 Depletion of Nek1 sensitizes xenograft tumors to radiation

The previously shown data demonstrated that targeting Nek1 has tremendous potential for the treatment of cancer using radiotherapy. However, there is no evidence so far that the Nek1-mediated effects on cellular survival observed *in vitro* are also relevant for fully-developed tumors *in vivo*. It was therefore of substantial interest to establish xenograft models through subcutaneous injection of HeLa shRNA cells into immunocompromised NSG mice and to examine how the resulting solid tumors respond to fractionated irradiation (6 h interval) when depleted for Nek1.

In a preliminary experiment, mice were treated with drinking water supplemented with doxycycline for 5 or 10 days as soon as tumor nodes were visible. The resulting tumors were isolated, processed, and analyzed in qPCR and immunoblotting assays, both demonstrating that a 10-day treatment sufficiently reduced Nek1 mRNA and protein levels in the tumor tissue (Fig. 15A and 15B). HeLa shCtrl and shNek1 tumors were consequently treated with doxycycline for 10 days before irradiation according to the 6 h fractionation interval and then monitored by calculating tumor volumes (Fig. 15C).

Within 5 days after irradiation, Nek1-depleted tumors lost around two-thirds of their volume and exhibited a significant delay in growth compared to unirradiated tumors (Fig. 15G). The growth of Nek1-proficient control tumors, however, was not or only marginally altered by irradiation (Fig. 15D, E, F).

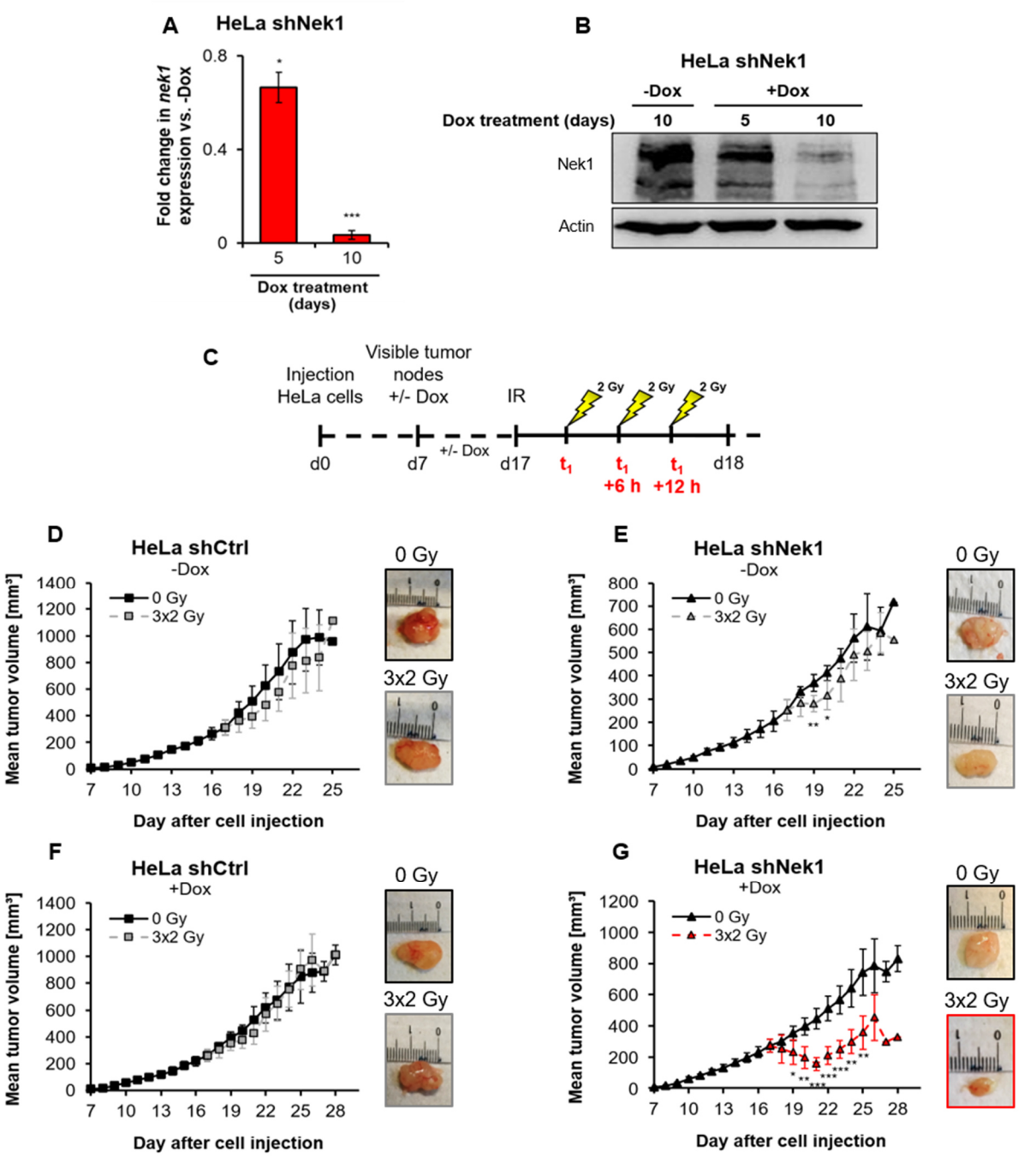

Fig. 15 Analysis of subcutaneous xenograft tumor growth following fractionated irradiation. A, **B** HeLa shRNA cells were subcutaneously injected into female NSG mice. After detection of tumor nodes, mice were treated with doxycycline in drinking water for 5 or 10 days. Tumors were then subjected to Nek1 gene expression analysis in **A**. Fold changes in expression were calculated with the $2^{-\Delta\Delta Ct}$ method using *RPL37A* as reference gene and normalizing the expression levels of *nek1* in Dox-treated tumors to the level in untreated tumors. Representative Western Blots of Nek1 protein levels in HeLa shRNA tumors are shown in **B**. Actin served as loading control. **C** Schematic representation of the Xenograft experiment. Following a 10-day Dox treatment, tumors were irradiated according to the 6 h fractionation interval. **D**-**G** Tumor growth curves for untreated (**D**, **E**) and Dox-treated HeLa shRNA (**F**, **G**) tumors as measured by using calipers. Representative images of tumors that were isolated at the end of the experiment are depicted on the right site of the respective graph. Data are shown as mean values of two (**A**, **B**) or five (**D**-**G**) tumors per condition ± SDM. *, irradiation vs. 0 Gy; * $p < 0.05$; ** $p < 0.01$; *** $p < 0.001$ (Student's T-test). D, day; IR, irradiation.

3.5 Discussion

Since its implementation in the 1930s, fractionated radiotherapy has become the most prominent strategy for the treatment of cancer. The primary goal of fractionation is to create a therapeutic window by exploiting the differences in the radiobiological responses of the tumor and normal tissue.[150] However, standard fractionation regimes are regarded as less potent compared to single-dose irradiations exactly because lower radiation doses are administered between long intervals, providing recovery time not only for normal but also for cancer cells.[143] Together with the intrinsic radioresistance of many tumors due to adaptations in their DDR signaling pathways, it is necessary to find ways to improve the efficiency of radiotherapy, e.g., by selectively interfering with factors that confer resistance in cancer cells and are thus essential for their survival.[151]

The previously described data demonstrate that HeLa and HCT-15 cells can be further sensitized to standard fractionation intervals (24 h) when depleted for Nek1. Since these effects were, as expected, considerably weaker compared to the corresponding single-dose irradiations, a hyperfractionation regime (6 h) was established, taking the cycling rate of cancer cells, but also the cell cycle-dependent function of Nek1 as a DNA repair factor into account. In this way, the radiosensitivity of Nek1-depleted HeLa and HCT-15 cells was tremendously increased, as cells were enriched and damaged in the G2 phase when they depend on Nek1 for proper DSB repair via HR. In combination with the defective G1/M checkpoint in HeLa and HCT-15 cells, the observed decrease in cellular survival may have resulted from two major events:

a) With the first fraction of 2 Gy, irreparable DSBs are generated in the existing population of S and G2 phase cells resulting in the activation of the G2/M checkpoint at which cells are eventually trapped and further damaged by the second fraction.

b) G1 phase cells also acquire DNA damage following the first fraction and directly transition to S phase during which they accumulate additional DSBs caused by radiation-induced replication stress. Cells will stop cell cycle progression at the activated G2/M checkpoint and subsequently hit with the next fraction.

Each applied fraction therefore potentially contributed to the accumulation of unresolvable DNA damage in a growing population of HR-defective G2 phase cells.

The importance of combining a Nek1 interference with "properly timed" fractionation regimes is particularly evident from the results obtained for the 2 h and 24 h intervals, which, although generally benefiting from the depletion of Nek1, proved much less efficient than the 6 h interval. Considering the cell cycle data in the case of the 2 h interval, cells simply did not have enough time to progress through the cell cycle. All three fractions of 2 Gy were therefore applied to the same population of G2 phase cells resulting in cellular survival rates similar to those of the

corresponding populations after single-dose irradiation with 6 Gy. In contrast, the 24 h interval most likely provided too much time between fractions, and, thus, allowed cellular recovery manifesting in an increased survival rate of both, Nek1-depleted and -proficient cancer cells compared to respective single-dose-irradiated populations.

The enormous potential that a pharmacological inactivation of Nek1 provides for cancer therapy is further highlighted by the results obtained in the xenograft studies. Tumors depleted for Nek1 lost a huge part of their volume in response to fractionated irradiation. Notably, control tumors were only slightly, if at all, affected by irradiation confirming that Nek1 was the crucial factor to make tumor cells susceptible to radiation in the first place.

However, two noteworthy aspects complicate or might even prevent the realization of a Nek1 interference in the clinics.

First of all, finding specific and potent inhibitors seems to be a challenging task as there is none commercially available despite Nek1's frequent association with cancerous diseases over the last decades. Only one very recent publication presents a small molecule that could serve as a tool compound for further optimization.[152]

Secondly, the multifunctional nature of Nek1 is not restricted to tumor cells and is important for the homeostasis of proliferating normal cells as well. Chen *et al*. reported for example that depleting Nek1 in human renal tubular epithelial cells (HK2) led to a substantial reduction in survival within 72-96 h, even without the application of genotoxic stressors such as IR.[112] Another study demonstrated furthermore that human embryonic kidney cells (Hek293) overexpressing a hypoactive Nek1 variant (T141A) lost 90% of their clonogenic ability after a two-day treatment with doxorubicin.[114] Given the potential side effects on both, irradiated and non-irradiated proliferating normal tissues, it remains to be elucidated whether a systemic inhibition of Nek1 can substantially improve the therapeutic outcome currently achieved with radiotherapy alone.

Assuming that Nek1 inhibitors are established but prove inefficient, it would be good to know whether targeting other HR-specific, yet less multifunctional factors similarly enhances the efficacy of hyperfractionation regimes like a Nek1 interference and, thus, might present a more feasible alternative. The previously conducted studies should therefore be repeated with an available Rad51 inhibitor (CYT-0851), which is currently tested in patients with B-cell malignancies and advanced solid tumors by Cyteir Therapeutics, USA.[153] Irrespective of the availability of HR-specific inhibitors, there are patients which potentially benefit from hyperfractionated radiotherapy as they suffer from tumor entities such as breast, ovarian, and pancreatic cancers that are inherently HR-deficient due to mutations in, for example, BRCA1 or BRCA2.[154]

Although hyperfractionation regimes are certainly employed in clinical practice, it remains controversial whether a "real" advantage over conventional schedules exists. For example, a

meta-analysis of data collected from patients with lung cancer revealed that hyperfractionation (2-3 fractions per day) indeed leads to improved overall survival rates compared to standard radiotherapy but also increases the risk of acute esophageal toxicity.[155] Considering the presented data, however, it is reasonable to assume that the performance of hyperfractionation can be significantly enhanced by targeting HR-specific factors. Since the 6 h interval may not yield optimal results when treating slow-growing or highly-proliferative tumors, the time interval between fractions should be adjusted to the cycling speed of the targeted cancer cells to ensure enrichment of G2 phase cells and, thus, maximize the associated effects described previously.

4 Concluding remarks

This thesis highlights the potential of a pharmacological inactivation of Nek1 for treating cancer. More importantly, though, it is the first to demonstrate that Nek1's function in DNA repair is regulated in a development-dependent manner. Accordingly, future studies should focus on the identification of potent and specific Nek1 inhibitors, keeping in mind that the resulting compounds will have to be tested in adult cells or animal models to reliably determine their efficacy. On top of that, Nek3 and Nek5 have been identified as novel components of the HR signaling pathway that seem to underlie a similar developmental regulation as Nek1. Considering that both kinases fully replace Nek1 with regards to DNA repair, could they also take over other DDR-related functions of Nek1 in embryonic cells e.g., cell cycle regulation and apoptosis induction? Since this would be of tremendous significance for future cancer treatments, further studies should rigorously characterize the functional range of Nek3 and Nek5.

The mammalian Nek family has received little attention, as indicated by the number of publications on PubMed, and most family members are therefore largely uncharacterized. However, in light of this work, it should not be ruled out that many of these kinases have a far more important role in cellular signaling than previously appreciated. Do other Neks also acquire distinct functions during development and for what reason is this beneficial for cells? How are Neks generally integrated into the cellular signaling network? Numerous questions remain unanswered, and this is very unfortunate considering that Neks could not only serve as new targets in cancer therapy but could also offer insights into unknown developmental processes.

5 References

1. Shahbazi-Gahrouei D, Setayandeh S, Gholami M. A review on natural background radiation. *Adv Biomed Res*. 2013; 2:65. <https://doi.org/10.4103/2277-9175.115821>.
2. Dartnell LR. Ionizing Radiation and Life. *Astrobiology*. 2011; 11:551-582. <https://doi.org/10.1089/ast.2010.0528>.
3. Reisz JA, Bansal N, Qian J, Zhao W, Furdui CM. Effects of Ionizing Radiation on Biological Molecules—Mechanisms of Damage and Emerging Methods of Detection. *Antioxid Redox Signal*. 2014; 21:260-292. <https://doi.org/10.1089/ars.2013.5489>.
4. Jeggo P, Löbrich M. Radiation-induced DNA damage responses. *Radiat Prot Dosimetry*. 2006; 122:124-127. <https://doi.org/10.1093/rpd/ncl495>.
5. Minchin S, Lodge J. Understanding biochemistry: structure and function of nucleic acids. *Essays Biochem*. 2019; 63:433-456. <https://doi.org/10.1042/EBC20180038>.
6. Roots R, Kraft G, Gosschalk E. The formation of radiation-induced dna breaks: The ratio of double-strand breaks to single-strand breaks. *Int J Radiat Oncol*. 1985; 11:259-265. <https://doi.org/10.1016/0360-3016(85)90147-6>.
7. Durante M, Bedford JS, Chen DJ, Conrad S, Cornforth MN, Natarajan AT, van Gent DC, Obe G. From DNA damage to chromosome aberrations: Joining the break. *Mutat Res Toxicol Environ Mutagen*. 2013; 756:5-13. <https://doi.org/10.1016/j.mrgentox.2013.05.014>.
8. Donya M, Radford M, ElGuindy A, Firmin D, Yacoub MH. Radiation in medicine: Origins, risks and aspirations. *Glob Cardiol Sci Pract*. 2014; 2014:57. <https://doi.org/10.5339/gcsp.2014.57>.
9. Mu H, Sun J, Li L, Yin J, Hu N, Zhao W, Ding D, Yi L. Ionizing radiation exposure: hazards, prevention, and biomarker screening. *Environ Sci Pollut Res*. 2018; 25:15294-15306. <https://doi.org/10.1007/s11356-018-2097-9>.
10. Bundesamt für Strahlenschutz. Bekanntmachung der aktualisierten diagnostischen Referenzwerte für diagnostische und interventionelle Röntgenanwendungen. June 2016.
11. Biau J, Chautard E, Verrelle P, Dutreix M. Altering DNA Repair to Improve Radiation Therapy: Specific and Multiple Pathway Targeting. *Front Oncol*. 2019; 9:1009. <https://doi.org/10.3389/fonc.2019.01009>.
12. Lomax ME, Folkes LK, O'Neill P. Biological Consequences of Radiation-induced DNA Damage: Relevance to Radiotherapy. *Clin Oncol*. 2013; 25:578-585. <https://doi.org/10.1016/j.clon.2013.06.007>.
13. Chandra RA, Keane FK, Voncken FEM, Thomas CR. Contemporary radiotherapy: present and future. *The Lancet*. 2021; 398:171-184. <https://doi.org/10.1016/S0140-6736(21)00233-6>.
14. Baskar R, Lee KA, Yeo R, Yeoh K-W. Cancer and Radiation Therapy: Current Advances and Future Directions. *Int J Med Sci*. 2012; 9:193-199. <https://doi.org/10.7150/ijms.3635>.
15. Vítor AC, Huertas P, Legube G, de Almeida SF. Studying DNA Double-Strand Break Repair: An Ever-Growing Toolbox. *Front Mol Biosci*. 2020; 7:24. <https://doi.org/10.3389/fmolb.2020.00024>.
16. Barnes JL, Zubair M, John K, Poirier MC, Martin FL. Carcinogens and DNA damage. *Biochem Soc Trans*. 2018; 46:1213-1224. <https://doi.org/10.1042/BST20180519>.
17. Zeman MK, Cimprich KA. Causes and consequences of replication stress. *Nat Cell Biol*. 2014; 16:2-9. <https://doi.org/10.1038/ncb2897>.
18. Nitiss JL. DNA topoisomerase II and its growing repertoire of biological functions. *Nat Rev Cancer*. 2009; 9:327-337. <https://doi.org/10.1038/nrc2608>.

19. Mehta A, Haber JE. Sources of DNA Double-Strand Breaks and Models of Recombinational DNA Repair. *Cold Spring Harb Perspect Biol*. 2014; 6:a016428-a016428. <https://doi.org/10.1101/cshperspect.a016428>.
20. Ciccia A, Elledge SJ. The DNA Damage Response: Making It Safe to Play with Knives. *Mol Cell*. 2010; 40:179-204. <https://doi.org/10.1016/j.molcel.2010.09.019>.
21. Jackson SP, Bartek J. The DNA-damage response in human biology and disease. *Nature*. 2009; 461:1071-1078. <https://doi.org/10.1038/nature08467>.
22. Wang J. DNA damage and apoptosis. *Cell Death Differ*. 2001; 8:1047-1048. <https://doi.org/10.1038/sj.cdd.4400938>.
23. Sia J, Szmyd R, Hau E, Gee HE. Molecular Mechanisms of Radiation-Induced Cancer Cell Death: A Primer. *Front Cell Dev Biol*. 2020; 8:41. <https://doi.org/10.3389/fcell.2020.00041>.
24. Uziel T. Requirement of the MRN complex for ATM activation by DNA damage. *EMBO J*. 2003; 22:5612-5621. <https://doi.org/10.1093/emboj/cdg541>.
25. Lavin MF. ATM and the Mre11 complex combine to recognize and signal DNA double-strand breaks. *Oncogene*. 2007; 26:7749-7758. <https://doi.org/10.1038/sj.onc.1210880>.
26. Deckbar D, Jeggo PA, Löbrich M. Understanding the limitations of radiation-induced cell cycle checkpoints. *Crit Rev Biochem Mol Biol*. 2011; 46:271-283. <https://doi.org/10.3109/10409238.2011.575764>.
27. Iliakis G, Wang Y, Guan J, Wang H. DNA damage checkpoint control in cells exposed to ionizing radiation. *Oncogene*. 2003; 22:5834-5847. <https://doi.org/10.1038/sj.onc.1206682>.
28. Liu K, Zheng M, Lu R, Du J, Zhao Q, Li Z, Li Y, Zhang S. The role of CDC25C in cell cycle regulation and clinical cancer therapy: a systematic review. *Cancer Cell Int*. 2020; 20:213. <https://doi.org/10.1186/s12935-020-01304-w>.
29. Abbas T, Dutta A. p21 in cancer: intricate networks and multiple activities. *Nat Rev Cancer*. 2009; 9:400-414. <https://doi.org/10.1038/nrc2657>.
30. Kondratova A, Watanabe T, Marotta M, Cannon M, Segall AM, Serre D, Tanaka H. Replication fork integrity and intra-S phase checkpoint suppress gene amplification. *Nucleic Acids Res*. 2015; 43:2678-2690. <https://doi.org/10.1093/nar/gkv084>.
31. Iyer D, Rhind N. The Intra-S Checkpoint Responses to DNA Damage. *Genes*. 2017; 8:74. <https://doi.org/10.3390/genes8020074>.
32. Burma S, Chen BP, Murphy M, Kurimasa A, Chen DJ. ATM Phosphorylates Histone H2AX in Response to DNA Double-strand Breaks. *J Biol Chem*. 2001; 276:42462-42467. <https://doi.org/10.1074/jbc.C100466200>.
33. Stucki M, Clapperton JA, Mohammad D, Yaffe MB, Smerdon SJ, Jackson SP. MDC1 Directly Binds Phosphorylated Histone H2AX to Regulate Cellular Responses to DNA Double-Strand Breaks. *Cell*. 2005; 123:1213-1226. <https://doi.org/10.1016/j.cell.2005.09.038>.
34. Lou Z, Minter-Dykhouse K, Franco S, Gostissa M, Rivera MA, Celeste A, Manis JP, van Deursen J, Nussenzweig A, Paull TT, Alt FW, Chen J. MDC1 Maintains Genomic Stability by Participating in the Amplification of ATM-Dependent DNA Damage Signals. *Mol Cell*. 2006; 21:187-200. <https://doi.org/10.1016/j.molcel.2005.11.025>.
35. Chatterjee N, Walker GC. Mechanisms of DNA damage, repair, and mutagenesis: DNA Damage and Repair. *Environ Mol Mutagen*. 2017; 58:235-263. <https://doi.org/10.1002/em.22087>.
36. van Gent DC, Hoeijmakers JHJ, Kanaar R. Chromosomal stability and the DNA double-stranded break connection. *Nat Rev Genet*. 2001; 2:196-206. <https://doi.org/10.1038/35056049>.
37. Lieber MR. The Mechanism of Human Nonhomologous DNA End Joining. *J Biol Chem*. 2008; 283:1-5. <https://doi.org/10.1074/jbc.R700039200>.

38. Sonoda E, Sasaki MS, Morrison C, Yamaguchi-Iwai Y, Takata M, Takeda S. Sister Chromatid Exchanges Are Mediated by Homologous Recombination in Vertebrate Cells. *Mol Cell Biol*. 1999; 19:5166-5169. <https://doi.org/10.1128/MCB.19.7.5166>.
39. San Filippo J, Sung P, Klein H. Mechanism of Eukaryotic Homologous Recombination. *Annu Rev Biochem*. 2008; 77:229-257. <https://doi.org/10.1146/annurev.biochem.77.061306.125255>.
40. Sung P, Klein H. Mechanism of homologous recombination: mediators and helicases take on regulatory functions. *Nat Rev Mol Cell Biol*. 2006; 7:739-750. <https://doi.org/10.1038/nrm2008>.
41. Sartori AA, Lukas C, Coates J, Mistrik M, Fu S, Bartek J, Baer R, Lukas J, Jackson SP. Human CtIP promotes DNA end resection. *Nature*. 2007; 450:509-514. <https://doi.org/10.1038/nature06337>.
42. Huertas P. DNA resection in eukaryotes: deciding how to fix the break. *Nat Struct Mol Biol*. 2010; 17:11-16. <https://doi.org/10.1038/nsmb.1710>.
43. Ma CJ, Gibb B, Kwon Y, Sung P, Greene EC. Protein dynamics of human RPA and RAD51 on ssDNA during assembly and disassembly of the RAD51 filament. *Nucleic Acids Res*. 2017; 45:749-761. <https://doi.org/10.1093/nar/gkw1125>.
44. Krejci L, Altmannova V, Spirek M, Zhao X. Homologous recombination and its regulation. *Nucleic Acids Res*. 2012; 40:5795-5818. <https://doi.org/10.1093/nar/gks270>.
45. Wright WD, Shah SS, Heyer W-D. Homologous recombination and the repair of DNA double-strand breaks. *J Biol Chem*. 2018; 293:10524-10535. <https://doi.org/10.1074/jbc.TM118.000372>.
46. Wright WD, Heyer W-D. Rad54 Functions as a Heteroduplex DNA Pump Modulated by Its DNA Substrates and Rad51 during D Loop Formation. *Mol Cell*. 2014; 53:420-432. <https://doi.org/10.1016/j.molcel.2013.12.027>.
47. Solinger JA, Lutz G, Sugiyama T, Kowalczykowski SC, Heyer W-D. Rad54 protein stimulates heteroduplex DNA formation in the synaptic phase of DNA strand exchange via specific interactions with the presynaptic Rad51 nucleoprotein filament11Edited by M. Belfort. *J Mol Biol*. 2001; 307:1207-1221. <https://doi.org/10.1006/jmbi.2001.4555>.
48. Mazin AV, Alexeev AA, Kowalczykowski SC. A Novel Function of Rad54 Protein. *J Biol Chem*. 2003; 278:14029-14036. <https://doi.org/10.1074/jbc.M212779200>.
49. Tavares EM, Wright WD, Heyer W-D, Le Cam E, Dupaigne P. In vitro role of Rad54 in Rad51-ssDNA filament-dependent homology search and synaptic complexes formation. *Nat Commun*. 2019; 10:4058. <https://doi.org/10.1038/s41467-019-12082-z>.
50. Goyal N, Rossi MJ, Mazina OM, Chi Y, Moritz RL, Clurman BE, Mazin AV. RAD54 N-terminal domain is a DNA sensor that couples ATP hydrolysis with branch migration of Holliday junctions. *Nat Commun*. 2018; 9:34. <https://doi.org/10.1038/s41467-017-02497-x>.
51. Maloisel L, Fabre F, Gangloff S. DNA Polymerase δ Is Preferentially Recruited during Homologous Recombination To Promote Heteroduplex DNA Extension. *Mol Cell Biol*. 2008; 28:1373-1382. <https://doi.org/10.1128/MCB.01651-07>.
52. Chen XJ. Mechanism of Homologous Recombination and Implications for Aging-Related Deletions in Mitochondrial DNA. *Microbiol Mol Biol Rev*. 2013; 77:476-496. <https://doi.org/10.1128/MMBR.00007-13>.
53. Elbakry A, Löbrich M. Homologous Recombination Subpathways: A Tangle to Resolve. *Front Genet*. 2021; 12:723847. <https://doi.org/10.3389/fgene.2021.723847>.
54. Bizard AH, Hickson ID. The Dissolution of Double Holliday Junctions. *Cold Spring Harb Perspect Biol*. 2014; 6:a016477-a016477. <https://doi.org/10.1101/cshperspect.a016477>.
55. McMahill MS, Sham CW, Bishop DK. Synthesis-Dependent Strand Annealing in Meiosis. Lichten M, ed. *PLoS Biol*. 2007; 5:e299. <https://doi.org/10.1371/journal.pbio.0050299>.

56. Bensimon A, Aebersold R, Shiloh Y. Beyond ATM: The protein kinase landscape of the DNA damage response. *FEBS Lett*. 2011; 585:1625-1639. <https://doi.org/10.1016/j.febslet.2011.05.013>.
57. Lu KP, Hunter T. The NIMA kinase: A mitotic regulator in Aspergillus nidulans and vertebrate cells. In: Meijer L, Guidet S, Tung HYL, eds. Progress in Cell Cycle Research. Boston, MA, Springer US, 1995, pp 187-205.
58. Fry AM, O'Regan L, Sabir SR, Bayliss R. Cell cycle regulation by the NEK family of protein kinases. *J Cell Sci*. January 2012:jcs.111195. <https://doi.org/10.1242/jcs.111195>.
59. Parker JDK, Bradley BA, Mooers AO, Quarmby LM. Phylogenetic Analysis of the Neks Reveals Early Diversification of Ciliary-Cell Cycle Kinases. Redfield R, ed. *PLoS ONE*. 2007; 2:e1076. <https://doi.org/10.1371/journal.pone.0001076>.
60. Moniz L, Dutt P, Haider N, Stambolic V. Nek family of kinases in cell cycle, checkpoint control and cancer. *Cell Div*. 2011; 6:18. <https://doi.org/10.1186/1747-1028-6-18>.
61. Meirelles GV, Silva JC, Mendonça Y de A, Ramos CH, Torriani IL, Kobarg J. Human Nek6 is a monomeric mostly globular kinase with an unfolded short N-terminal domain. *BMC Struct Biol*. 2011; 11:12. <https://doi.org/10.1186/1472-6807-11-12>.
62. de Souza EE, Meirelles GV, Godoy BB, Perez AM, Smetana JHC, Doxsey SJ, McComb ME, Costello CE, Whelan SA, Kobarg J. Characterization of the Human NEK7 Interactome Suggests Catalytic and Regulatory Properties Distinct from Those of NEK6. *J Proteome Res*. 2014; 13:4074-4090. <https://doi.org/10.1021/pr500437x>.
63. Fry AM, Bayliss R, Roig J. Mitotic Regulation by NEK Kinase Networks. *Front Cell Dev Biol*. 2017; 5:102. <https://doi.org/10.3389/fcell.2017.00102>.
64. Pavan ICB, Peres de Oliveira A, Dias PRF, Basei FL, Issayama LK, Ferezin C de C, Silva FR, Rodrigues de Oliveira AL, Alves dos Reis Moura L, Martins MB, Simabuco FM, Kobarg J. On Broken Ne(c)ks and Broken DNA: The Role of Human NEKs in the DNA Damage Response. *Cells*. 2021; 10:507. <https://doi.org/10.3390/cells10030507>.
65. Nguyen CL, Possemato R, Bauerlein EL, Xie A, Scully R, Hahn WC. Nek4 Regulates Entry into Replicative Senescence and the Response to DNA Damage in Human Fibroblasts. *Mol Cell Biol*. 2012; 32:3963-3977. <https://doi.org/10.1128/MCB.00436-12>.
66. Melixetian M, Klein DK, Sørensen CS, Helin K. NEK11 regulates CDC25A degradation and the IR-induced G2/M checkpoint. *Nat Cell Biol*. 2009; 11:1247-1253. <https://doi.org/10.1038/ncb1969>.
67. Peres de Oliveira A, Kazuo Issayama L, Betim Pavan IC, Riback Silva F, Diniz Melo-Hanchuk T, Moreira Simabuco F, Kobarg J. Checking NEKs: Overcoming a Bottleneck in Human Diseases. *Molecules*. 2020; 25:1778. <https://doi.org/10.3390/molecules25081778>.
68. Letwin K, Mizzen L, Motro B, Ben-David Y, Bernstein A, Pawson T. A mammalian dual specificity protein kinase, Nek1, is related to the NIMA cell cycle regulator and highly expressed in meiotic germ cells. *EMBO J*. 1992; 11:3521-3531. <https://doi.org/10.1002/j.1460-2075.1992.tb05435.x>.
69. Melo-Hanchuk TD, Slepicka PF, Meirelles GV, Basei FL, Lovato DV, Granato DC, Pauletti BA, Domingues RR, Leme AFP, Pelegrini AL, Lenz G, Knapp S, Elkins JM, Kobarg J. NEK1 kinase domain structure and its dynamic protein interactome after exposure to Cisplatin. *Sci Rep*. 2017; 7:5445. <https://doi.org/10.1038/s41598-017-05325-w>.
70. Feige E, Shalom O, Tsuriel S, Yissachar N, Motro B. Nek1 shares structural and functional similarities with NIMA kinase. *Biochim Biophys Acta BBA - Mol Cell Res*. 2006; 1763:272-281. <https://doi.org/10.1016/j.bbamcr.2006.01.009>.
71. van de Kooij B, Creixell P, van Vlimmeren A, Joughin BA, Miller CJ, Haider N, Simpson CD, Linding R, Stambolic V, Turk BE, Yaffe MB. Comprehensive substrate specificity profiling of the human Nek kinome reveals unexpected signaling outputs. *eLife*. 2019; 8:e44635. <https://doi.org/10.7554/eLife.44635>.
72. Janaswami PM, Birkenmeier EH, Cook SA, Rowe LB, Bronson RT, Davisson MT.

Identification and Genetic Mapping of a New Polycystic Kidney Disease on Mouse Chromosome 8. *Genomics*. 1997; 40:101-107. <https://doi.org/10.1006/geno.1996.4567>.

73. Upadhya P, Birkenmeier EH, Birkenmeier CS, Barker JE. Mutations in a NIMA-related kinase gene, Nek1, cause pleiotropic effects including a progressive polycystic kidney disease in mice. *Proc Natl Acad Sci*. 2000; 97:217-221. <https://doi.org/10.1073/pnas.97.1.217>.
74. Vogler C, Homan S, Pung A, Thorpe C, Barker J, Birkenmeier EH, Upadhya P. Clinical and Pathologic Findings in Two New Allelic Murine Models of Polycystic Kidney Disease. *J Am Soc Nephrol*. 1999; 10:2534-2539. <https://doi.org/10.1681/ASN.V10122534>.
75. Thiel C, Kessler K, Giessl A, Dimmler A, Shalev SA, von der Haar S, Zenker M, Zahnleiter D, Stöss H, Beinder E, Abou Jamra R, Ekici AB, Schröder-Kreß N, Aigner T, Kirchner T, Reis A, Brandstätter JH, Rauch A. NEK1 Mutations Cause Short-Rib Polydactyly Syndrome Type Majewski. *Am J Hum Genet*. 2011; 88:106-114. <https://doi.org/10.1016/j.ajhg.2010.12.004>.
76. Monroe GR, Kappen IF, Stokman MF, Terhal PA, van den Boogaard M-JH, Savelberg SM, van der Veken LT, van Es RJ, Lens SM, Hengeveld RC, Creton MA, Janssen NG, Mink van der Molen AB, Ebbeling MB, Giles RH, Knoers NV, van Haaften G. Compound heterozygous NEK1 variants in two siblings with oral-facial-digital syndrome type II (Mohr syndrome). *Eur J Hum Genet*. 2016; 24:1752-1760. <https://doi.org/10.1038/ejhg.2016.103>.
77. Chen C-P, Chang T-Y, Chen C-Y, Wang T-Y, Tsai F-J, Wu P-C, Chern S-R, Wang W. Short rib-polydactyly syndrome type II (Majewski): Prenatal diagnosis, perinatal imaging findings and molecular analysis of the NEK1 gene. *Taiwan J Obstet Gynecol*. 2012; 51:100-105. <https://doi.org/10.1016/j.tjog.2012.01.020>.
78. Toriello HV. Are the oral-facial-digital syndromes ciliopathies? *Am J Med Genet A*. 2009; 149A:1089-1095. <https://doi.org/10.1002/ajmg.a.32799>.
79. McConnachie DJ, Stow JL, Mallett AJ. Ciliopathies and the Kidney: A Review. *Am J Kidney Dis*. 2021; 77:410-419. <https://doi.org/10.1053/j.ajkd.2020.08.012>.
80. Malicki JJ, Johnson CA. The Cilium: Cellular Antenna and Central Processing Unit. *Trends Cell Biol*. 2017; 27:126-140. <https://doi.org/10.1016/j.tcb.2016.08.002>.
81. Wheway G, Nazlamova L, Hancock JT. Signaling through the Primary Cilium. *Front Cell Dev Biol*. 2018; 6:8. <https://doi.org/10.3389/fcell.2018.00008>.
82. Shalom O, Shalva N, Altschuler Y, Motro B. The mammalian Nek1 kinase is involved in primary cilium formation. *FEBS Lett*. 2008; 582:1465-1470. <https://doi.org/10.1016/j.febslet.2008.03.036>.
83. Chen Y, Chiang H-C, Litchfield P, Pena M, Juang C, Riley DJ. Expression of Nek1 during kidney development and cyst formation in multiple nephron segments in the Nek1-deficient kat2J mouse model of polycystic kidney disease. *J Biomed Sci*. 2014; 21:63. <https://doi.org/10.1186/s12929-014-0063-5>.
84. Surpili MJ, Delben TM, Kobarg J. Identification of Proteins That Interact with the Central Coiled-Coil Region of the Human Protein Kinase NEK1. *Biochemistry*. 2003; 42:15369-15376. <https://doi.org/10.1021/bi034575v>.
85. Lin F, Hiesberger T, Cordes K, Sinclair AM, Goldstein LSB, Somlo S, Igarashi P. Kidney-specific inactivation of the KIF3A subunit of kinesin-II inhibits renal ciliogenesis and produces polycystic kidney disease. *Proc Natl Acad Sci*. 2003; 100:5286-5291. <https://doi.org/10.1073/pnas.0836980100>.
86. Kleymenova E, Ibraghimov-Beskrovnaya O, Kugoh H, Everitt J, Xu H, Kiguchi K, Landes G, Harris P, Walker C. Tuberin-Dependent Membrane Localization of Polycystin-1. *Mol Cell*. 2001; 7:823-832. <https://doi.org/10.1016/S1097-2765(01)00226-X>.
87. White MC, Quarmby LM. The NIMA-family kinase, Nek1 affects the stability of centrosomes and ciliogenesis. *BMC Cell Biol*. 2008; 9:29. <https://doi.org/10.1186/1471-2121-9-29>.

88. Al-Jassar C, Andreeva A, Barnabas DD, McLaughlin SH, Johnson CM, Yu M, van Breugel M. The Ciliopathy-Associated Cep104 Protein Interacts with Tubulin and Nek1 Kinase. *Structure*. 2017; 25:146-156. <https://doi.org/10.1016/j.str.2016.11.014>.

89. Yim H, Sung CK, You J, Tian Y, Benjamin T. Nek1 and TAZ Interact to Maintain Normal Levels of Polycystin 2. *J Am Soc Nephrol*. 2011; 22:832-837. <https://doi.org/10.1681/ASN.2010090992>.

90. Dutcher SK, Lin H. Tying TAZ and Nek1 into Polycystic Kidney Disease through Polycystin 2 Levels. *J Am Soc Nephrol*. 2011; 22:791-793. <https://doi.org/10.1681/ASN.2011030256>.

91. Winokurow N, Schumacher S. A role for polycystin-1 and polycystin-2 in neural progenitor cell differentiation. *Cell Mol Life Sci*. 2019; 76:2851-2869. <https://doi.org/10.1007/s00018-019-03072-x>.

92. Marston AL, Amon A. Meiosis: cell-cycle controls shuffle and deal. *Nat Rev Mol Cell Biol*. 2004; 5:983-997. <https://doi.org/10.1038/nrm1526>.

93. Brieño-Enríquez MA, Moak SL, Toledo M, Filter JJ, Gray S, Barbero JL, Cohen PE, Holloway JK. Cohesin Removal along the Chromosome Arms during the First Meiotic Division Depends on a NEK1-PP1γ-WAPL Axis in the Mouse. *Cell Rep*. 2016; 17:977-986. <https://doi.org/10.1016/j.celrep.2016.09.059>.

94. Holloway K, Roberson EC, Corbett KL, Kolas NK, Nieves E, Cohen PE. NEK1 Facilitates Cohesin Removal during Mammalian Spermatogenesis. *Genes*. 2011; 2:260-279. <https://doi.org/10.3390/genes2010260>.

95. Guo W, Vandoorne T, Steyaert J, Staats KA, Van Den Bosch L. The multifaceted role of kinases in amyotrophic lateral sclerosis: genetic, pathological and therapeutic implications. *Brain*. 2020; 143:1651-1673. <https://doi.org/10.1093/brain/awaa022>.

96. Ferrante RJ, Browne SE, Shinobu LA, Bowling AC, Baik MJ, MacGarvey U, Kowall NW, Brown RH, Beal MF. Evidence of Increased Oxidative Damage in Both Sporadic and Familial Amyotrophic Lateral Sclerosis. *J Neurochem*. 2002; 69:2064-2074. <https://doi.org/10.1046/j.1471-4159.1997.69052064.x>.

97. Fitzmaurice PS, Shaw IC, Kleiner HE, Miller RT, Monks TJ, Lau SS, Mitchell JD, Lynch PG. Evidence for DNA damage in amyotrophic lateral sclerosis. *Muscle Nerve*. 1996; 19:797-798.

98. Sun Y, Curle AJ, Haider AM, Balmus G. The role of DNA damage response in amyotrophic lateral sclerosis. Wu Q, ed. *Essays Biochem*. 2020; 64:847-861. <https://doi.org/10.1042/EBC20200002>.

99. Cirulli ET, Lasseigne BN, Petrovski S, Sapp PC, Dion PA, Leblond CS, Couthouis J, Lu Y-F, Wang Q, Krueger BJ, Ren Z, Keebler J, Han Y, Levy SE, Boone BE, Wimbish JR, Waite LL, Jones AL, Carulli JP, Day-Williams AG, Staropoli JF, Xin WW, Chesi A, Raphael AR, McKenna-Yasek D, Cady J, Vianney de Jong JMB, Kenna KP, Smith BN, Topp S, Miller J, Gkazi A, FALS Sequencing Consortium, Al-Chalabi A, van den Berg LH, Veldink J, Silani V, Ticozzi N, Shaw CE, Baloh RH, Appel S, Simpson E, Lagier-Tourenne C, Pulst SM, Gibson S, Trojanowski JQ, Elman L, McCluskey L, Grossman M, Shneider NA, Chung WK, Ravits JM, Glass JD, Sims KB, Van Deerlin VM, Maniatis T, Hayes SD, Ordureau A, Swarup S, Landers J, Baas F, Allen AS, Bedlack RS, Harper JW, Gitler AD, Rouleau GA, Brown R, Harms MB, Cooper GM, Harris T, Myers RM, Goldstein DB. Exome sequencing in amyotrophic lateral sclerosis identifies risk genes and pathways. *Science*. 2015; 347:1436-1441. <https://doi.org/10.1126/science.aaa3650>.

100. Sohn E. Fundraising: The Ice Bucket Challenge delivers. *Nature*. 2017; 550:S113-S114. <https://doi.org/10.1038/550S113a>.

101. Brenner D, Müller K, Wieland T, Weydt P, Böhm S, Lulé D, Hübers A, Neuwirth C, Weber M, Borck G, Wahlqvist M, Danzer KM, Volk AE, Meitinger T, Strom TM, Otto M, Kassubek J, Ludolph AC, Andersen PM, Weishaupt JH. *NEK1* mutations in familial amyotrophic lateral sclerosis. *Brain*. 2016; 139:e28-e28. <https://doi.org/10.1093/brain/aww033>.

102. SLAGEN Consortium, Kenna KP, van Doormaal PTC, Dekker AM, Ticozzi N, Kenna BJ, Diekstra FP, van Rheenen W, van Eijk KR, Jones AR, Keagle P, Shatunov A, Sproviero W, Smith BN, van Es MA, Topp SD, Kenna A, Miller JW, Fallini C, Tiloca C, McLaughlin RL, Vance C, Troakes C, Colombrita C, Mora G, Calvo A, Verde F, Al-Sarraj S, King A, Calini D, de Belleroche J, Baas F, van der Kooi AJ, de Visser M, ten Asbroek ALMA, Sapp PC, McKenna-Yasek D, Polak M, Asress S, Muñoz-Blanco JL, Strom TM, Meitinger T, Morrison KE, Lauria G, Williams KL, Leigh PN, Nicholson GA, Blair IP, Leblond CS, Dion PA, Rouleau GA, Pall H, Shaw PJ, Turner MR, Talbot K, Taroni F, Boylan KB, Van Blitterswijk M, Rademakers R, Esteban-Pérez J, García-Redondo A, Van Damme P, Robberecht W, Chio A, Gellera C, Drepper C, Sendtner M, Ratti A, Glass JD, Mora JS, Basak NA, Hardiman O, Ludolph AC, Andersen PM, Weishaupt JH, Brown RH, Al-Chalabi A, Silani V, Shaw CE, van den Berg LH, Veldink JH, Landers JE. NEK1 variants confer susceptibility to amyotrophic lateral sclerosis. *Nat Genet*. 2016; 48:1037-1042. <https://doi.org/10.1038/ng.3626>.

103. Higelin J, Catanese A, Semelink-Sedlacek LL, Oeztuerk S, Lutz A-K, Bausinger J, Barbi G, Speit G, Andersen PM, Ludolph AC, Demestre M, Boeckers TM. NEK1 loss-of-function mutation induces DNA damage accumulation in ALS patient-derived motoneurons. *Stem Cell Res*. 2018; 30:150-162. <https://doi.org/10.1016/j.scr.2018.06.005>.

104. Polci R, Peng A, Chen P-L, Riley DJ, Chen Y. NIMA-Related Protein Kinase 1 Is Involved Early in the Ionizing Radiation-Induced DNA Damage Response. *Cancer Res*. 2004; 64:8800-8803. <https://doi.org/10.1158/0008-5472.CAN-04-2243>.

105. Chen Y, Chen P-L, Chen C-F, Jiang X, Riley DJ. Never-in-mitosis related Kinase 1 functions in DNA damage response and checkpoint control. *Cell Cycle*. 2008; 7:3194-3201. <https://doi.org/10.4161/cc.7.20.6815>.

106. Pelegrini AL, Moura DJ, Brenner BL, Ledur PF, Maques GP, Henriques JAP, Saffi J, Lenz G. Nek1 silencing slows down DNA repair and blocks DNA damage-induced cell cycle arrest. *Mutagenesis*. 2010; 25:447-454.<https://doi.org/10.1093/mutage/geq026>.

107. Grudzenski S, Raths A, Conrad S, Rübe CE, Löbrich M. Inducible response required for repair of low-dose radiation damage in human fibroblasts. *Proc Natl Acad Sci*. 2010; 107:14205-14210. <https://doi.org/10.1073/pnas.1002213107>.

108. Liu S, Ho CK, Ouyang J, Zou L. Nek1 kinase associates with ATR-ATRIP and primes ATR for efficient DNA damage signaling. *Proc Natl Acad Sci*. 2013; 110:2175-2180. <https://doi.org/10.1073/pnas.1217781110>.

109. Chen Y, Chen C-F, Riley DJ, Chen P-L. Nek1 kinase functions in DNA damage response and checkpoint control through a pathway independent of ATM and ATR. *Cell Cycle*. 2011; 10:655-663. <https://doi.org/10.4161/cc.10.4.14814>.

110. Chen Y, Chen C-F, Chiang H-C, Pena M, Polci R, Wei RL, Edwards RA, Hansel DE, Chen P-L, Riley DJ. Mutation of NIMA-related kinase 1 (NEK1) leads to chromosome instability. *Mol Cancer*. 2011; 10:5. <https://doi.org/10.1186/1476-4598-10-5>.

111. Spies J, Waizenegger A, Barton O, Sürder M, Wright WD, Heyer W-D, Löbrich M. Nek1 Regulates Rad54 to Orchestrate Homologous Recombination and Replication Fork Stability. *Mol Cell*. 2016; 62:903-917. <https://doi.org/10.1016/j.molcel.2016.04.032>.

112. Chen Y, Craigen WJ, Riley DJ. Nek1 regulates cell death and mitochondrial membrane permeability through phosphorylation of VDAC1. *Cell Cycle*. 2009; 8:257-267. <https://doi.org/10.4161/cc.8.2.7551>.

113. Martins MB, Perez AM, Bohr VA, Wilson DM, Kobarg J. NEK1 deficiency affects mitochondrial functions and the transcriptome of key DNA repair pathways. *Mutagenesis*. 2021; 36:223-236. <https://doi.org/10.1093/mutage/geab011>.

114. Singh V, Khalil MI, De Benedetti A. The TLK1/Nek1 axis contributes to mitochondrial integrity and apoptosis prevention via phosphorylation of VDAC1. *Cell Cycle*. 2020; 19:363-375. <https://doi.org/10.1080/15384101.2019.1711317>.

115. Chen Y, Chen C-F, Polci R, Wei R, Riley DJ, Chen P-L. Increased Nek1 expression in Renal Cell Carcinoma cells is associated with decreased sensitivity to DNA-damaging treatment. *Oncotarget*. 2014; 5:4283-4294.<https://doi.org/10.18632/oncotarget.2005>.

116. Chen Y. NEK1 Protein Kinase as a Target for Anticancer Therapeutics. *Chemother Open Access*. 2012; 01. <https://doi.org/10.4172/2167-7700.1000e118>.

117. Essers J, Hendriks RW, Swagemakers SMA, Troelstra C, de Wit J, Bootsma D, Hoeijmakers JHJ, Kanaar R. Disruption of Mouse RAD54 Reduces Ionizing Radiation Resistance and Homologous Recombination. *Cell*. 1997; 89:195-204. <https://doi.org/10.1016/S0092-8674(00)80199-3>.

118. Behringer R, Gertsenstein M, Nagy KV, Nagy A. Selecting Female Mice in Estrus and Checking Plugs. *Cold Spring Harb Protoc*. 2016; 2016:pdb.prot092387. <https://doi.org/10.1101/pdb.prot092387>.

119. Durkin ME, Qian X, Popescu NC, Lowy DR. Isolation of Mouse Embryo Fibroblasts. *Bio-Protoc*. 2013; 3:e908. <https://doi.org/10.21769/bioprotoc.908>.

120. Khan M, Gasser S. Generating Primary Fibroblast Cultures from Mouse Ear and Tail Tissues. *J Vis Exp*. 2016:53565. <https://doi.org/10.3791/53565>.

121. Hayflick L. THE LIMITED IN VITRO LIFETIME OF HUMAN DIPLOID CELL STRAINS. *Exp Cell Res*. 1965; 37:614-636. <https://doi.org/10.1016/0014-4827(65)90211-9>.

122. Tolstonog GV, Belichenko-Weitzmann IV, Lu J-P, Hartig R, Shoeman RL, Taub U, Traub P. Spontaneously Immortalized Mouse Embryo Fibroblasts: Growth Behavior of Wild-Type and Vimentin-Deficient Cells in Relation to Mitochondrial Structure and Activity. *DNA Cell Biol*. 2005; 24:680-709. <https://doi.org/10.1089/dna.2005.24.680>.

123. Amand MM, Hanover JA, Shiloach J. A comparison of strategies for immortalizing mouse embryonic fibroblasts. *J Biol Methods*. 2016; 3:e41. <https://doi.org/10.14440/jbm.2016.110>.

124. Xu J. Preparation, culture, and immortalization of mouse embryonic fibroblasts. *Curr Protoc Mol Biol*. 2005; Chapter 28:Unit 28.1. <https://doi.org/10.1002/0471142727.mb2801s70>.

125. Kegel P, Riballo E, Kühne M, Jeggo PA, Löbrich M. X-irradiation of cells on glass slides has a dose doubling impact. *DNA Repair*. 2007; 6:1692-1697. <https://doi.org/10.1016/j.dnarep.2007.05.013>.

126. Durfee T, Nelson R, Baldwin S, Plunkett G, Burland V, Mau B, Petrosino JF, Qin X, Muzny DM, Ayele M, Gibbs RA, Csörgő B, Pósfai G, Weinstock GM, Blattner FR. The Complete Genome Sequence of *Escherichia coli* DH10B: Insights into the Biology of a Laboratory Workhorse. *J Bacteriol*. 2008; 190:2597-2606. <https://doi.org/10.1128/JB.01695-07>.

127. Edelheit O, Hanukoglu A, Hanukoglu I. Simple and efficient site-directed mutagenesis using two single-primer reactions in parallel to generate mutants for protein structure-function studies. *BMC Biotechnol*. 2009; 9:61. <https://doi.org/10.1186/1472-6750-9-61>.

128. Loonstra A, Vooijs M, Beverloo HB, Allak BA, van Drunen E, Kanaar R, Berns A, Jonkers J. Growth inhibition and DNA damage induced by Cre recombinase in mammalian cells. *Proc Natl Acad Sci*. 2001; 98:9209-9214. <https://doi.org/10.1073/pnas.161269798>.

129. Baralle FE, Giudice J. Alternative splicing as a regulator of development and tissue identity. *Nat Rev Mol Cell Biol*. 2017; 18:437-451. <https://doi.org/10.1038/nrm.2017.27>.

130. Park J, Farris S. Spatiotemporal Regulation of Transcript Isoform Expression in the Hippocampus. *Front Mol Neurosci*. 2021; 14:694234. <https://doi.org/10.3389/fnmol.2021.694234>.

131. Tondeleir D, Vandamme D, Vandekerckhove J, Ampe C, Lambrechts A. Actin isoform expression patterns during mammalian development and in pathology: Insights from mouse models. *Cell Motil Cytoskeleton*. 2009; 66:798-815. <https://doi.org/10.1002/cm.20350>.

132. Cardoso VB, Hanchuk T, de Souza E, Papa P, Meirelles G, Kobarg J. Identification of NEK3 interacting proteins and functional characterization of its signaling mechanisms. *JIOMICS*. 2017. <https://doi.org/10.5584/jiomics.v7i1.195>.

133. Melo-Hanchuk TD, Slepicka PF, Pelegrini AL, Menck CFM, Kobarg J. NEK5 interacts with topoisomerase IIβ and is involved in the DNA damage response induced by etoposide. *J Cell Biochem*. 2019; 120:16853-16866. <https://doi.org/10.1002/jcb.28943>.

134. Nassar D, Blanpain C. Cancer Stem Cells: Basic Concepts and Therapeutic Implications. *Annu Rev Pathol Mech Dis*. 2016; 11:47-76. <https://doi.org/10.1146/annurev-pathol-012615-044438>.

135. Atashzar MR, Baharlou R, Karami J, Abdollahi H, Rezaei R, Pourramezan F, Zoljalali Moghaddam SH. Cancer stem cells: A review from origin to therapeutic implications. *J Cell Physiol*. 2020; 235:790-803. <https://doi.org/10.1002/jcp.29044>.

136. Ornitz DM, Marie PJ. Fibroblast growth factor signaling in skeletal development and disease. *Genes Dev*. 2015; 29:1463-1486. <https://doi.org/10.1101/gad.266551.115>.

137. Zhu J, Cai Y, Liu P, Zhao W. Frequent Nek1 overexpression in human gliomas. *Biochem Biophys Res Commun*. 2016; 476:522-527. <https://doi.org/10.1016/j.bbrc.2016.05.156>.

138. Singh V, Jaiswal PK, Ghosh I, Koul HK, Yu X, De Benedetti A. The TLK1-Nek1 axis promotes prostate cancer progression. *Cancer Lett*. 2019; 453:131-141. <https://doi.org/10.1016/j.canlet.2019.03.041>.

139. Melo-Hanchuk TD, Martins MB, Cunha LL, Soares FA, Ward LS, Vassallo J, Kobarg J. Expression of the NEK family in normal and cancer tissue: an immunohistochemical study. *BMC Cancer*. 2020; 20:23. <https://doi.org/10.1186/s12885-019-6408-4>.

140. Dyrskjøt L, Reinert T, Algaba F, Christensen E, Nieboer D, Hermann GG, Mogensen K, Beukers W, Marquez M, Segersten U, Høyer S, Ulhøi BP, Hartmann A, Stöhr R, Wach S, Nawroth R, Schwamborn K, Tulic C, Simic T, Junker K, Harving N, Petersen AC, Jensen JB, Keck B, Grimm M-O, Horstmann M, Maurer T, Steyerberg EW, Zwarthoff EC, Real FX, Malats N, Malmström P-U, Ørntoft TF. Prognostic Impact of a 12-gene Progression Score in Non–muscle-invasive Bladder Cancer: A Prospective Multicentre Validation Study. *Eur Urol*. 2017; 72:461-469. <https://doi.org/10.1016/j.eururo.2017.05.040>.

141. Smith AL, Alirezaie N, Connor A, Chan-Seng-Yue M, Grant R, Selander I, Bascuñana C, Borgida A, Hall A, Whelan T, Holter S, McPherson T, Cleary S, Petersen GM, Omeroglu A, Saloustros E, McPherson J, Stein LD, Foulkes WD, Majewski J, Gallinger S, Zogopoulos G. Candidate DNA repair susceptibility genes identified by exome sequencing in high-risk pancreatic cancer. *Cancer Lett*. 2016; 370:302-312. <https://doi.org/10.1016/j.canlet.2015.10.030>.

142. Freund I, Hehlgans S, Martin D, Ensminger M, Fokas E, Rödel C, Löbrich M, Rödel F. Fractionation-Dependent Radiosensitization by Molecular Targeting of Nek1. *Cells*. 2020; 9:1235. <https://doi.org/10.3390/cells9051235>.

143. Saberian F, Ghate A, Kim M. Optimal fractionation in radiotherapy with multiple normal tissues. *Math Med Biol*. 2016; 33:211-252. <https://doi.org/10.1093/imammb/dqv015>.

144. Jensen C, Teng Y. Is It Time to Start Transitioning From 2D to 3D Cell Culture? *Front Mol Biosci*. 2020; 7:33. <https://doi.org/10.3389/fmolb.2020.00033>.

145. Lv D, Hu Z, Lu L, Lu H, Xu X. Three-dimensional cell culture: A powerful tool in tumor research and drug discovery (Review). *Oncol Lett*. October 2017. <https://doi.org/10.3892/ol.2017.7134>.

146. Langhans SA. Three-Dimensional in Vitro Cell Culture Models in Drug Discovery and Drug Repositioning. *Front Pharmacol*. 2018; 9:6. <https://doi.org/10.3389/fphar.2018.00006>.

147. Storch K, Eke I, Borgmann K, Krause M, Richter C, Becker K, Schröck E, Cordes N. Three-Dimensional Cell Growth Confers Radioresistance by Chromatin Density Modification. *Cancer Res*. 2010; 70:3925-3934. <https://doi.org/10.1158/0008-5472.CAN-09-3848>.

148. Bahmad HF, Cheaito K, Chalhoub RM, Hadadeh O, Monzer A, Ballout F, El-Hajj A, Mukherji D, Liu Y-N, Daoud G, Abou-Kheir W. Sphere-Formation Assay: Three-Dimensional in vitro Culturing of Prostate Cancer Stem/Progenitor Sphere-Forming Cells. *Front Oncol*. 2018; 8:347. <https://doi.org/10.3389/fonc.2018.00347>.

149. Kersemans V, Cornelissen B, Allen PD, Beech JS, Smart SC. Subcutaneous tumor volume measurement in the awake, manually restrained mouse using MRI. *J Magn Reson Imaging*. 2013; 37:1499-1504. <https://doi.org/10.1002/jmri.23829>.

150. Billena C, Khan AJ. A Current Review of Spatial Fractionation: Back to the Future? *Int J Radiat Oncol*. 2019; 104:177-187. <https://doi.org/10.1016/j.ijrobp.2019.01.073>.

151. Hanahan D, Weinberg RA. Hallmarks of Cancer: The Next Generation. *Cell*. 2011; 144:646-674. <https://doi.org/10.1016/j.cell.2011.02.013>.

152. Baumann G, Meckel T, Böhm K, Shih Y-H, Dickhaut M, Reichardt T, Pilakowski J, Pehl U, Schmidt B. Illuminating a Dark Kinase: Structure-Guided Design, Synthesis, and Evaluation of a Potent Nek1 Inhibitor and Its Effects on the Embryonic Zebrafish Pronephros. *J Med Chem*. 2022; 65:1265-1282. <https://doi.org/10.1021/acs.jmedchem.0c02118>.

153. Cyteir Therapeutics. A Phase 1/2 Study of CYT-0851, an Oral RAD51 Inhibitor, in B-Cell Malignancies and Advanced Solid Tumors. *Natl Institue Health Clin Trials*. <https://clinicaltrials.gov/ct2/show/NCT03997968?id=NCT03997968&draw=2&rank=1&load=cart>.

154. Toh M, Ngeow J. Homologous Recombination Deficiency: Cancer Predispositions and Treatment Implications. *The Oncologist*. 2021; 26:e1526-e1537. <https://doi.org/10.1002/onco.13829>.

155. Mauguen A, Le Péchoux C, Saunders MI, Schild SE, Turrisi AT, Baumann M, Sause WT, Ball D, Belani CP, Bonner JA, Zajusz A, Dahlberg SE, Nankivell M, Mandrekar SJ, Paulus R, Behrendt K, Koch R, Bishop JF, Dische S, Arriagada R, De Ruysscher D, Pignon J-P. Hyperfractionated or Accelerated Radiotherapy in Lung Cancer: An Individual Patient Data Meta-Analysis. *J Clin Oncol*. 2012; 30:2788-2797. <https://doi.org/10.1200/JCO.2012.41.6677>.

6 Abbreviations

°C	Degree Celsius
µl/ml	Microliter/Milliliter
act	Active
ALS	Amyotrophic lateral sclerosis
ATM	Ataxia telangiectasia-mutated
ATR	Ataxia telangiectasia and Rad3-related protein
Blm	Bloom syndrome protein
BMBF	Bundesministerium für Bildung und Forschung
Brca1	Breast cancer 1, early-onset
Brca2	Breast cancer type 2 substantial protein
Cdc25a	Cell division cycle 25a
Cdk	Cyclin-dependent kinase
cDNA	Complementary DNA
Cep104	Centrosomal protein 104 kda
Chk2	Checkpoint kinase 2
CO_2	Carbon dioxide
CT	Computer tomography
Ct	Cycle threshold
CtIP	C-terminal-binding protein-interacting protein
CytC	Cytochrome C
d	Day
DDR	DNA damage response
dHj	Double Holliday junction
DNA	Deoxyribonucleic acid
Dna2	DNA replication helicase/nuclease 2
DNA-PKcs	DNA-dependent protein kinase catalytic subunit
DSB	Double-strand break
E. coli	*Escherichia coli*
Engl.	Englisch
e.g.	Exempli Gratia
et al.	*Et alii*
Exo1	Exonuclease 1
Fig.	Figure
Gy/mGy	Gray/milliGray
h	Hour
H2AX	Histone 2AX
HR	Homologous recombination
IR	Ionizing radiation
KI	Knock-In
Kif3A	Kinesin-like protein 3A
KO	Knock-Out
kV	Kilovolt

LigIV	DNA ligase IV
LC-MS	Liquid chromatography-mass spectrometry
mA	Milliampere
Mbp	Mega-base-pair
MCS	Mohr-Claussen syndrome
Mdc1	Mediator of DNA damage checkpoint protein 1
MEF	Murine embryonic fibroblasts
min	Minutes
Mm	Millimeter
MPF	Murine postnatal fibroblasts
Mre11	Meiotic recombination 11
Nbs1	Nijmegen breakage syndrome 1
ng/µg	Nanogram/microgram
NHEJ	Non-Homologous End Joining
NIMA	Never in mitosis-gene A
Nek	NIMA-related kinase
P21, P53	Tumor suppressor protein 21
PC-2	Polycystin-2
PCNA	Proliferating cell nuclear antigen
PCR/qPCR	Polymerase chain reaction/quantitative PCR
PDGF	Platelet-derived growth factor
PEST	Proline-glutamate-serine-threonine
pH3	Phospho-Histone 3
PIKK	Phosphatidylinositol 3-kinase-related kinases
PKD	Polycystic kidney disease
Rad	Radiation repair protein
Rcc1	Regulator of chromosome condensation 1
RNA	Ribonucleic acid
ROS	Reactive oxygen species
RPA	Replication protein A
RT	Room temperature
SDSA	Synthesis-dependent strand annealing
sec	Seconds
Smc3	Structural Maintenance of Chromosomes protein 3
SRPS	Short rib polydactyly syndrome
ssDNA	Single-stranded DNA
Tab.	Table
Taz	Transcriptional co-activator with PDZ-binding motif
Vdac1	Voltage-dependent anion-selective channel protein 1
Wapl	Wings apart-like homolog
WT	Wildtype
Xrcc4	X-ray repair cross-complementing 4

7 List of Figures and Tables

7.1 Figures

7.2 Tables

8 Appendix

8.1 Curriculum Vitae

Personal data

Name	Isabel Freund
Date of Birth	14.12.1992

Education

01.2018 - 04.2022	**Dr. rer. nat. Radiation Biology and DNA Repair** Technical University Darmstadt, Germany University Hospital Frankfurt a.M., Germany Thesis: *Nek1 - developmental involvement in DNA repair and role as target in radiotherapy*
10.2015 - 10.2017	**Master of science Technische Biologie** Technical University Darmstadt, Germany Sanofi-Aventis, Frankfurt a.M., Germany Thesis: *In vitro characterization of novel small-molecule activators of AMP-activated protein kinase for the treatment of type II diabetes*
10.2012 - 09.2015	**Bachelor of science Biologie** Technical University Darmstadt, Germany Thesis: *Cloning and heterologous expression of esterases from Olea europaea*
06.2012	**Abitur** Sankt-Angela School, Königstein im Taunus, Germany

Internships/Secondments

09.2017 - 12.2017	Secondment to the Mast4Health program (mast4health.eu) Harokopio University, Athens, Greece
09.2016 - 12.2016	Research internship Kolmar lab (Biochemistry), Technical University Darmstadt
04.2015 - 05.2015	Research internship Schmoll lab, Sanofi-Aventis, Frankfurt a.M.

Achievements

09.2019	Poster prize at the 22nd Annual Meeting of the German Society for Biological Radiation Research
02.2018	Scholarship for Ph.D. studies at the graduate school 1657

8.2 Publications

Freund I, Hehlgans S, Martin D, Ensminger M, Fokas E, Rödel C, Löbrich M, Rödel F.
Fractionation-Dependent Radiosensitization by Molecular Targeting of Nek1
Cells 2020; 9(5); 1235; DOI: 10.3390/cells9051235

Acknowledged in

Amerikanou C, Papada E, Gioxari A, Smyrnioudis I, Kleftaki SA, Valsamidou E, Bruns V, Banerjee R, Trivella MG, Milic N, Medić-Stojanoska M, Gastaldelli A, Kannt A, MAST4HEALTH, Dedoussis GV, Kaliora AC.
Mastiha has efficacy in immune-mediated inflammatory diseases through a microRNA-155 Th17 dependent action
Pharmacol Res. 2021; 171:105753. DOI: 10.1016/j.phrs.2021.105753.

8.3 Conference Contributions

5th German-French DNA Repair Meeting 2020
Online, 11/2020
Regulation of Homologous Recombination during development (Poster in cooperation with Holly Thomas)

22nd Annual Meeting of the German Society for Biological Radiation Research (**DeGBS**)
Mannheim; Germany, 09/2019
Silencing of Never-in-mitosis A-related kinase 1 (Nek1) decreases radiation survival of cervix and colorectal carcinoma cells in vitro and in vivo (Poster)

25th Annual Meeting of the German Society for Radiation Oncology (**DEGRO**)
Münster, Germany, 06/2019
Silencing of Never-in-mitosis A-related kinase 1 (Nek1) decreases radiation survival of cervix and colorectal carcinoma cells after single-dose and fractionated irradiation (Poster)

Frankfurt Cancer Conference (**FCC**)
Frankfurt am Main, Germany, 09/2018
Knockdown of Never-in-mitosis A-related kinase 1 (Nek1) decreases radiation survival of 3D-grown cervix and colorectal carcinoma cells (Poster)

8.4 Danksagung

Mein Dank gilt in erster Linie Herrn Prof. Dr. Markus Löbrich und Prof. Dr. Franz Rödel für die Aufnahme ins Graduiertenkolleg und die Möglichkeit, Projekte in beiden Arbeitsgruppen zu bearbeiten. Vielen Dank für die zahlreichen Eindrücke, die ich in dieser Zeit sammeln durfte, sowie Ihre umfassende Förderung und Unterstützung, ohne die unsere Veröffentlichung, mein Posterpreis und vor allem diese Thesis nie möglich gewesen wären.

Ein besonderer Dank gilt auch den Mitgliedern beider Arbeitsgruppen, die mir meinen Alltag durch die angenehme Atmosphäre und die Hilfsbereitschaft ungemein erleichtert haben. Ich bedanke mich besonders bei Stephanie, Melanie, Michi, Ratna und Ann-Charlotte nicht nur für ihre wissenschaftliche Unterstützung, sondern auch für die Momente, in denen sie immer ein offenes Ohr für mich hatten und auch mein Gezeter gelassen ertragen haben…
Ein großes Dankeschön geht hier aber explizit an Michi für die Korrektur meiner Thesis!

Vielen Dank auch an die Mitarbeiter der Strahlentherapeutischen Abteilung am Universitätsklinikum Frankfurt, die die Bestrahlungen am LINAC jederzeit ermöglicht haben. Den TAs Julius, Conny, Christel und Bettina möchte ich für das großartige Labormanagement danken, das maßgeblich zum reibungslosen Durchführen von Experimenten beigetragen hat.

Ich möchte mich schließlich ganz besonders bei meiner Familie für ihre Unterstützung während meines gesamten Studiums bedanken. Dies gilt vor allem für meinen Papa, der nie an meinen Fähigkeiten zweifelte und mir immer den Rücken freigehalten hat. Und natürlich auch Patrick, der seit nun 8 Jahren an meiner Seite steht und vor allem in den letzten 4 Jahren nie die Geduld mit mir verlor, immer für mich da war und ermutigende Worte fand. Ohne euch wäre ich mit Sicherheit komplett verzweifelt!